GROUND-WATER HYDROLOGY AND HYDROCHEMISTRY OF EAGLE FLAT AND SURROUNDING AREA

by

Bruce K. Darling and Barry J. Hibbs

Final Report

Prepared for

Texas Low-Level Radioactive Waste Disposal Authority
under Interagency Contract Number IAC(92-93)-0910

Bureau of Economic Geology
W.L. Fisher, Director
The University of Texas at Austin
Austin, Texas 78713-7508

December 1993

QAe7693

CONTENTS

Figures

Tables

EXECUTIVE SUMMARY

This report presents the results of the Bureau of Economic Geology's investigation of the saturated-zone hydrology and hydrochemistry of Eagle Flat, Red Light Draw, and surrounding areas of southern Hudspeth County, Texas. Boundaries of the study area are the Rio Grande and Quitman Mountains to the south and west, the Van Horn and Carrizo Mountains to the east, and the Diablo Plateau to the north. Total land area is about 1,200 mi^2 (3,110 km^2).

The Bureau of Economic Geology initiated this study in July 1991 at the request of the Texas Low-Level Radioactive Waste Disposal Authority (TLLRWDA). The objective of the investigation was to ascertain whether northwest Eagle Flat may be considered a suitable location for disposal of low-level radioactive waste.

Methods of investigation included standard hydrological and hydrochemical techniques, including installation of observation wells, water quality sampling, aquifer testing, stream gauging, and measurement of water levels. The study relied upon well-established hydrochemical and isotopic methods to trace local, intermediate, and regional flowpaths, to describe the distribution of ground-water facies, and to account for ground-water origins. Basic physical and chemical hydrologic data were used to develop a conceptual model of ground-water flow in the study region. A numerical model was developed to test hypotheses regarding flow and to estimate flowpaths, residence times, and ground-water velocities. Study results are as follows:

1. The study area is sparsely populated. Sierra Blanca, the largest community in the study area, had a population of 700 in 1990. Sierra Blanca formerly depended upon local wells to satisfy municipal water needs but currently has most of its water piped in from Van Horn. Van Horn derives its water supplies from basin fill at Wild Horse Flat, a bolson aquifer east of the study area. In rural areas, water use is mainly limited to domestic and livestock consumption. A small number of low-capacity wells satisfy the needs of the local population and livestock industry.

2. The study area is divided into three basins, based on surface-water, ground-water drainage, and ground-water chemistry. The area within the Eagle Flat Draw watershed is referred to as southeast Eagle Flat. The area within the

Blanca Draw watershed is northwest Eagle Flat. Red Light Draw includes everything within the Red Light Draw watershed, including Indian Hot Springs.

3. Ground water occurs in unconfined, leaky confined, and confined aquifers in the study area. In mountainous areas, ground-water typically is unconfined. In parts of Red Light Draw, flowing artesian wells in bolson aquifers indicate confinement. Aquifer pump tests and associated hydrogeologic investigations indicate leaky confined aquifers in northwest Eagle Flat and unconfined to leaky confined aquifers in southeast Eagle Flat.

4. Recharge is limited to areas with exposures of bedrock, or where bedrock is covered by thin basin fill. Recently recharged waters have low total dissolved solids, ^{14}C signatures between 60 to 100 PMC (percent modern carbon), and tritium ranging from 1.5 to 8.0 TU (tritium units). The Streeruwitz, Bean, and Millican Hills, which lie south of the Diablo Plateau, constitute the most significant recharge zone. The Eagle Mountains constitute the second major recharge area, but within short distances of the mountain front, low carbon-14 values and tritium levels that are indistinguishable from background suggest very slow rates of ground-water drainage. There is no evidence of recharge through the basin floors.

5. Depths to water typically vary between 667 and 920 ft (203.5 and 280.5 m) in northwest Eagle Flat (between 667 and 751 ft [203.5 and 229 m] at Faskin Ranch), and between 160 and 700 ft (49 and 213.5 m) in southeast Eagle Flat. Depths to water in Red Light Draw vary from only a few feet in the Rio Grande alluvium to over 450 ft (137 m) in the northwestern part of the draw. Depths to water in the mountains typically are variable, as little as 15 to 20 ft (4.5 to 6 m) on the Eagle Mountains and Steeruwitz Hills, and as great as 1,130 ft (344.5 m) on the flanks of Sierra Blanca Mountain.

6. Local flow systems originate in mountains and along mountain fronts and replenish the aquifers in the low-lying draws and flats. Regional ground-water flow paths are oriented along a ground-water trough, northwest-southeast from the Diablo Plateau, across northwest Eagle Flat and Red Light Draw where ground-water probably discharges in very small amounts to low-lying areas

along the Rio Grande. Waters to the east of the Eagle Flat ground-water divide probably move via interbasin flow through Scott's Crossing to Lobo Valley.

7. Hydraulic gradients vary between 0.066 in the mountains and 0.0005 in the flats and draws. The Rio Grande is the apparent aquifer discharge area for waters in northwest Eagle Flat and Red Light Draw. A low-relief ground-water divide separates northwest and southeast Eagle Flat into two separate aquifers. Very small to moderate fluctuations in head (e.g., 1 to 10 ft [0.3 to 3 m]) over a 30-yr period with no consistent patterns are shown in aquifer hydrographs that compare historical with recent water-level data.

8. Aquifer test results from five well tests in northwest Eagle Flat indicate leaky confined aquifers of very low to moderately low yield. Transmissivity values in northwest Eagle Flat vary from 2.4 to 68 ft^2/day (0.2 to 6.5 m^2/day; using Hantush-Jacob [1955] type curve matches). Approximate hydraulic conductivity values vary from 0.007 to 0.3 ft/day (0.002 to 0.09 m/day). Within the footprint of Faskin Ranch, transmissivities and approximate hydraulic conductivities vary from 2.4 to 10.2 ft^2/day (0.2 to 0.95 m^2/day), and from 0.007 to 0.12 ft/day (0.002 to 0.035 m/day), respectively. In southeast Eagle Flat, a pump test provided a transmissivity estimate of about 270 ft^2/day (25 m^2/day) using the modified Theis (1935) equation for unconfined aquifers (modification discussed in Kruseman and De Ridder, 1979). The approximate hydraulic conductivity estimated from the pump test in southeast Eagle Flat was 5.2 ft/day (1.6 m/day). Calibrated transmissivity estimates from nine specific capacity tests in wells completed in bedrock aquifers varied from 0.40 to 20,499 ft^2/day (0.04 to 1,904 m^2/day). Approximate hydraulic conductivity values estimated from transmissivity calculations varied from 0.00094 to 539 ft/day (0.00029 to 164 m/day). The median transmissivity value for the nine specific capacity tests was 891.27 ft^2/day (82.80 m^2/day).

9. The hydrochemical composition of ground water southern Hudspeth County varies significantly from one basin to another. In southeast Eagle Flat, ground water is mixed-HCO_3 in composition, with total dissolved solids less than 500 mg/l. In northwest Eagle Flat, most wells produce water that is Na-Cl to Na-SO_4-Cl, with total dissolved solids between 1500 and 4000 mg/L. The more dilute waters from this area range from Ca-HCO_3 to Na-SO_4-HCO_3 in

composition. Ground water in the northeastern part of Red Light Draw is mixed-HCO_3 with total dissolved solids less than 500 mg/L. The southwestern part of the draw is dominated by Na-HCO_3-SO_4 to Na-SO_4-HCO_3 ground water, with total dissolved solids between 600 to 1,200 mg/L. A zone of high-TDS Na-Cl ground water is found along the Rio Grande, in the area between Indian Hot Springs and the southeastern corner of Red Light Draw. Cl/Br ratios, stable isotopes, and unstable isotopes indicate that upwelling of high-TDS water is the primary source of salinity in lower Red Light Draw and at Indian Hot Springs (figs. 14 to 16). This water mixes with the low-TDS water draining from Red Light Draw. The chemistry of the mixture is dominated by the high-TDS water.

10. The ^{14}C values range from 107 to less than 1.5 percent modern carbon (PMC), with most falling within the 0 to 20 PMC range (fig. 21). Highest ^{14}C values are associated with recently recharged waters of southeast Eagle Flat, where ^{14}C is typically between 107 and 40 PMC. In northwest Eagle Flat and Red Light Draw, ^{14}C is generally much lower (table 5), indicating very slow rates of ground-water drainage. With the exception of one monitor well at Devil Ridge, ^{14}C values in southeast Eagle Flat are less than 7 PMC, and as low as 1.5 PMC in samples drawn from monitor wells near the northern boundary of the proposed low-level radioactive waste disposal site. Tritium values are zero, indicating no recent recharge through the basin floor.

11. The δ^2H vs. $\delta^{18}O$ compositions all lie along the global meteoric water line, but vary in amount of depletion of the heavy isotopes (fig. 24). The most depleted values of deuterium and oxygen-18 are associated with the lowest percent modern carbon levels. This association, interpreted to indicate paleoclimatic labeling of stable isotopes, is supported by comparison of ground-water δ-values with the range of $\delta^{18}O$ from nearly 500 samples of precipitation from West Texas and southeast New Mexico (fig. 28A-B). With few exceptions, $\delta^{18}O$ of ground water with less than 20 PMC is more depleted in oxygen-18, compared with average values of recent rainfall. Lambert and Harvey (1987) reached similar conclusions in their study of ground water in the confined aquifers of southeastern New Mexico. This hypothesis is supported by the $\delta^{18}O$ map, which shows the most isotopically depleted waters lying along the central parts of basins and draws (fig. 25).

12. A two-dimensional, cross-sectional (profile) ground-water flow model was developed to estimate and predict flowpaths, residence times, and ground-water velocities between the Diablo Plateau and the Rio Grande (53.98 mile profile). In four model simulations, the simulated hydraulic gradient was matched with the measured hydraulic gradient by varying rock hydraulic conductivities and recharge rates within limits provided by field measurements and published literature values. In the first three model scenarios, the average recharge rate to the Diablo Plateau was specified as 0.0966 in/yr (0.24 cm/yr; or 0.8 percent of mean annual precipitation). This rate is consistent with the estimated recharge rate of 0.5 to 3 percent of the available precipitation falling on mountain drainage areas (Kelly and Hearne, 1976; Orr and Risser, 1992). Horizontal hydraulic conductivity values included: Precambrian rocks, 0.006 ft/day (0.002 m/day), basin fill, 0.25 ft/day (0.076 m/day), Permian and Cretaceous carbonate and siliciclastic rocks, 0.0091 to 3.2 ft/day (0.0028 to 1.0 m/day). These hydraulic conductivity values were selected from aquifer tests, specific capacity tests, and published literature values (e.g., Bedinger and others, 1976). Combinations of isotropy, anisotropy, and heterogeneity were simulated. Ground-water travel times between the Diablo Plateau and the Rio Grande were 60,178; 97,789; and 101,820 years in the three model scenarios. Travel times between Faskin Ranch and the Rio Grande varied from 19,134 to 43,619 years.

13. In the fourth model scenario, horizontal and vertical hydraulic conductivities were increased by one order of magnitude to test the sensitivity of the model to higher hydraulic conductivity values. Travel time between the Diablo Plateau and the Rio Grande was 8,054 years in the model (2,995 years from Faskin Ranch to the Rio Grande). Recharge rates in the Diablo Plateau had to be increased to 1.23 inches/yr (3.12 cm/yr; 10.3 percent mean annual precipitation) to match the simulated hydraulic gradient with the measured hydraulic gradient. The shorter residence times in the final model scenario were inconsistent with ground-water ages determined by ground-water isotopes. The recharge rate of 10.3 percent of mean annual precipitation on mountain drainage areas was much higher than the accepted 0.5 to 3 percent for recharge areas in Trans-Pecos aquifers (Kelly and Hearne, 1976; Orr and Risser, 1992). Model simulations in model scenario 4 implied that hydraulic conductivity values are closer to values specified in model scenarios 1 through 3.

14. Circuitous, three-dimensional flow components, fracture and double porosity flow, hydrochemically distinct "pockets" of water formed by successions of permeable and low-permeability rock and poorly consolidated strata, and areal transitions between unconfined, confined, and leaky confined aquifers mark some of the complexities of the regional ground-water flow system. Hydrochemical and isotopic data provide many insights on the ground-water flow system and allow testing of hypotheses regarding ground-water flow.

INTRODUCTION

Objective of Study

The Bureau of Economic Geology initiated this study of the ground-water hydrology and hydrochemistry of southern Hudspeth County in 1991 at the request of the Texas Low-Level Radioactive Waste Disposal Authority (TLLRWDA). The objective of this investigation was to ascertain whether Eagle Flat may be considered a suitable location for disposal of low-level radioactive waste. The study relies upon well-established hydrological, hydrochemical, and isotopic methods to delineate the boundaries of the ground-water system, to trace local, intermediate, and regional flowpaths, to describe the distribution of ground-water facies, and to account for ground-water origins.

Location of Study Area

The area encompassed by this study lies between north latitudes 30° 37′ 30″ and 31° 15' 22", and west longitudes 104° 52' 30" and 105° 30' 00" in southern Hudspeth County, Texas (fig. 1). The village of Sierra Blanca lies in the northwestern part of the study area, approximately 90 mi (144 km) east of El Paso, and 33 mi (53 km) west of the city of Van Horn, along Interstate Highway 10.

As part of the Basin and Range physiographic province, the area encompasses all of Eagle Flat, and the sections of Red Light Draw and Green River Valley north of the Rio Grande (fig. 2). Major topographic features are Sierra Blanca Mountain in the northwest, the Diablo Plateau to the north, the Streeruwitz, Bean, and Millican hills to the northeast, the Carrizo Mountains and the Van Horn Mountains along the east, and the Quitman Mountains along the southwest. The Rio Grande forms the southern boundary. Devil Ridge, Love Hogback, the Eagle Mountains, and the Indio Mountains bisect the area from northwest to southeast.

Sharp differences in relief are common throughout the area. The highest point is in the Eagle Mountains at 7,510 ft (2,290 m). At opposite ends of Eagle Flat are Sierra Blanca and Allamoore, both at 4,500 ft (1,372 m). Grayton Lake lies in the center of Eagle Flat at 4,270 ft (1,300 m). The Carrizo and Van Horn Mountains rise to more than 5,200 ft (1,585 m), and the Quitman Mountains are at least 6,200 ft (1,890 m). Along its southeasterly course, the elevation of the Rio

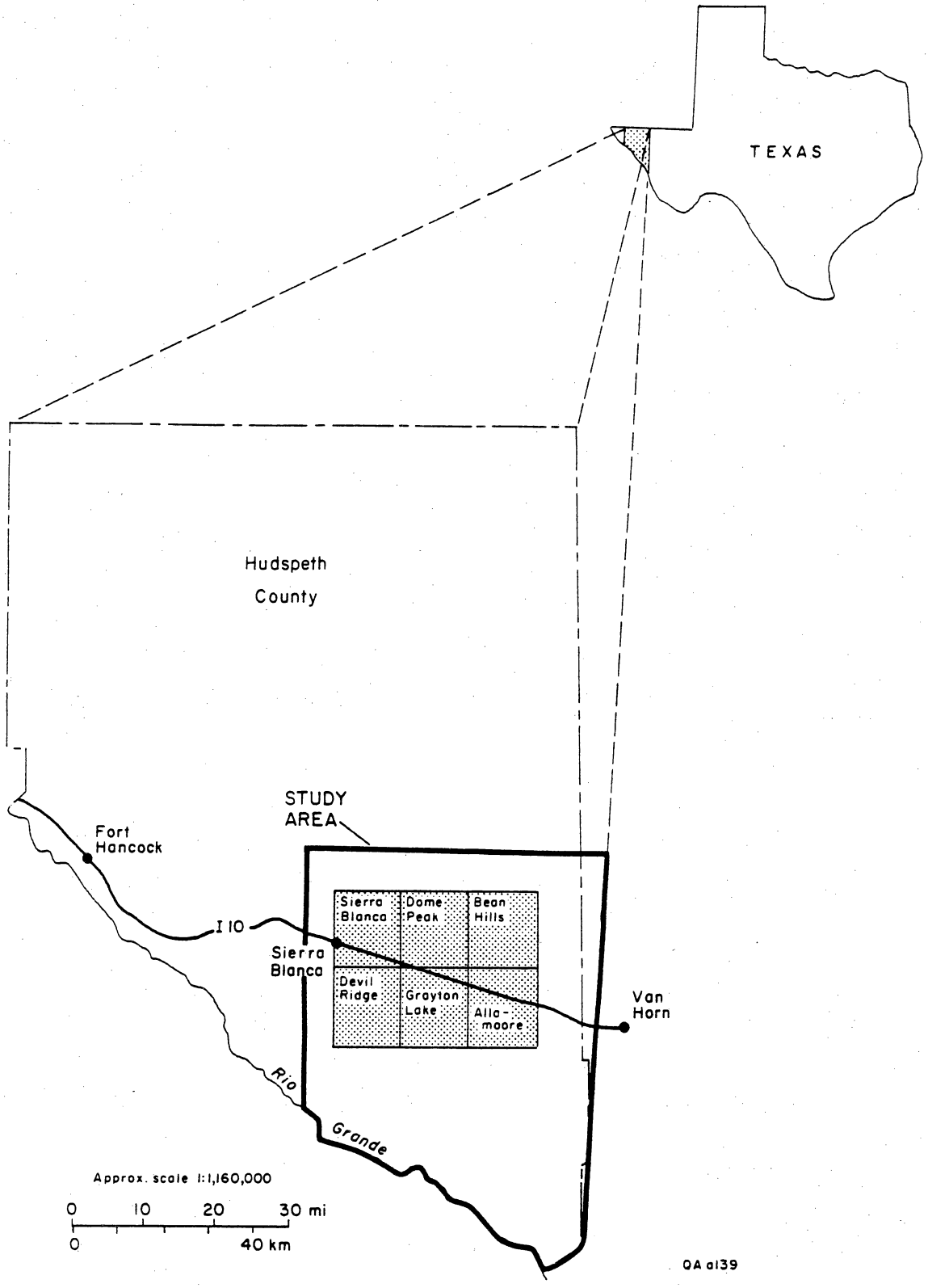

Figure 1. Location of the study area.

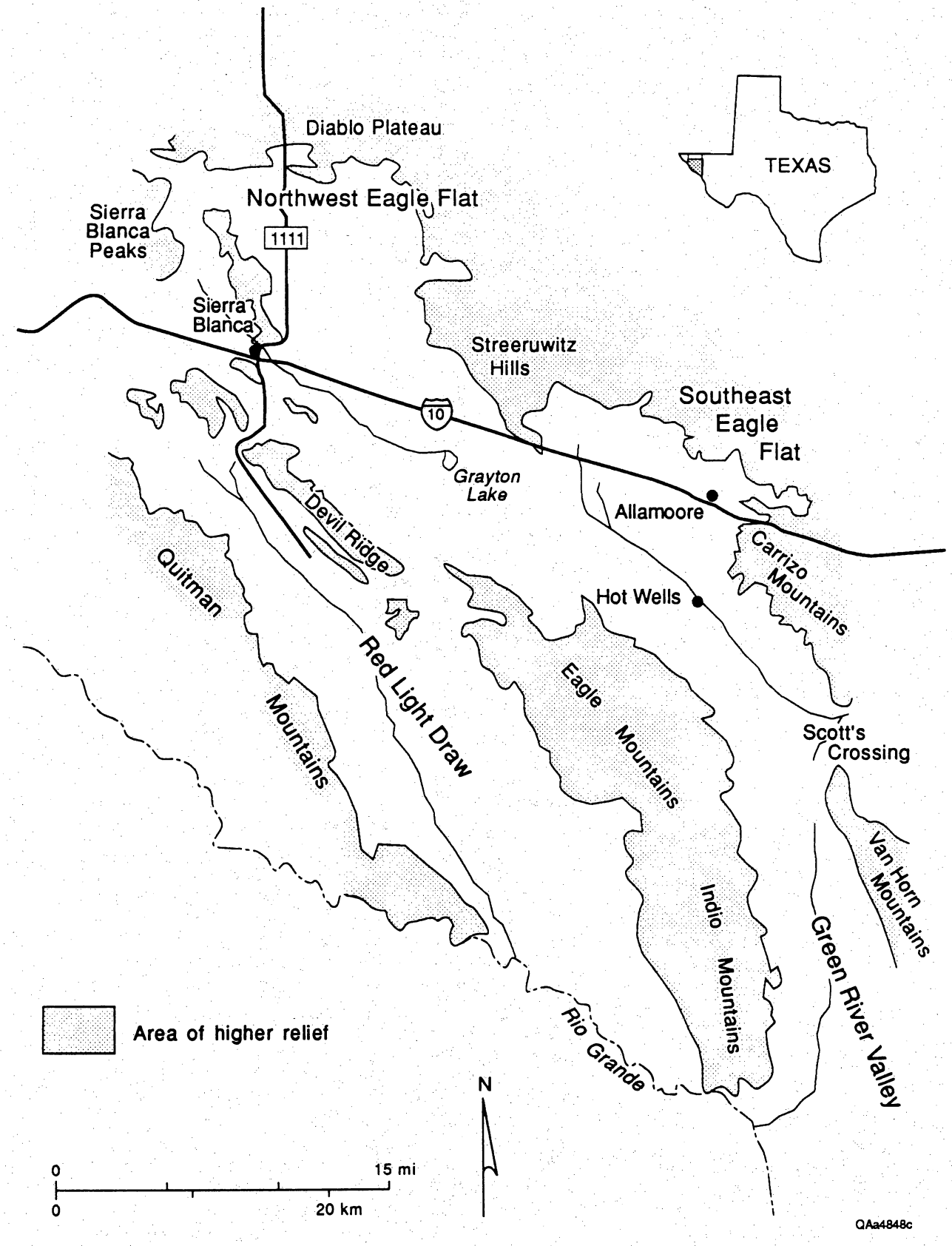

Figure 2. Prominent physiographic features in the study area.

Grande decreases from 3,300 ft (1,006 m) near Indian Hot Springs to less than 3,200 ft (975 m) at the southeastern corner of Green River Valley.

This report divides the study area into three basins, based on surface-water flow and differences in ground-water chemistry. The area defined by the boundaries of the Eagle Flat Draw watershed is identified as **southeast Eagle Flat**. The area within the Blanca Draw watershed is referred to as **northwest Eagle Flat. Red Light Draw** includes everything within the Red Light Draw catchment, including wells drilled into the Rio Grande Alluvium. Indian Hot Springs and Red Bull Spring, although within the Hueco Bolson, are included with Red Light Draw for ease of discussion.

Well-Numbering System

With few exceptions, all wells are referenced according to the numbering system adopted by the Texas Water Development Board, as summarized by White and others (1980) below:

> Under this system, each 1-degree quadrangle in the State is given a number consisting of two digits from 01 to 89. These are the first two digits in the well number. Each 1-degree quadrangle is divided into 7.50-minute quadrangles that are given two-digit numbers from 01 to 65. These are the third and fourth digits of the well number. Each 7.50-minute quadrangle is divided into nine 2.50-minute quadrangles that are given a single-digit number from 1 to 9. This is the fifth digit of the well number. Each well within a 2.50-minute quadrangle is given a two-digit number number in the order in which it is inventoried. These are the last two digits of the well number.

Exceptions are monitor wells and stratigraphic tests drilled by the Bureau of Economic Geology, all of which are given a designation such as "YM-xy," where "YM" refers to Yucca Mesa (a prominent landmark in the study area), and "xy" is a two-digit number from 01 to 64. These wells and bore holes were drilled south of Interstate Highway 10 in four U.S. Geological Survey 7.50-minute quadrangles: Sierra Blanca, Bean Hills, Devil Ridge, and Grayton Lake.

Another exception consists of wells not included in the data base of the Texas Water Development Board, and one exploratory well drilled in the Allamoore Quadrangle by the Bureau of Economic Geology. These wells are designated by four numbers followed by three capital letters. The four digits are

consistent with the Texas Water Development Board's numbering system, as described above. The three letters are based on a prominent local landmark, or the surname of the landowner (i.e., 48-64-BTH). Locations of wells and springs are shown in figure 3.

Structural Geology

The tectonic history of southern Hudspeth County includes two episodes of thrust faulting in the late Precambrian and one in the early Tertiary, followed by igneous activity and extensional faulting. The extensional faulting superimposed a series of northwest-trending fault blocks and intermontane basins on the previously deformed strata (King and Flawn, 1953; Underwood, 1962; Albritton and Smith, 1965; Henry and others, 1983; Raney and Collins, 1993).

Precambrian metasedimentary rocks ranging from greenschist to amphibolite facies of the Carrizo Mountain Group, and low-grade greenschist facies of the Allamoore Formation (Raney and Collins, 1993) predominate in the northern and easternmost areas of east Eagle Flat. Extensive outcrops are found in the Streeruwitz, Bean, and Millican hills to the north and in the Carrizo Mountains to the east.

Marine Cretaceous rocks averaging 7,000 ft (2,135) in thickness and ranging in age from Late Aptian to Late Turonian were deposited on a platform margin and in adjoining areas of the Chihuahua trough, with the carbonate and siliciclastic rocks displaying cyclic alternation throughout the section (Underwood, 1963). The Cretaceous rocks were deformed by regional compression in Late Cretaceous–Early Tertiary time (Underwood, 1963; Albritton and Smith, 1965). Thrust faults and folds are the dominant structural features, with repeated sections at Devil Ridge, Love Hogback, the Eagle Mountains, the Indio Mountains, and the Quitman Mountains (Underwood, 1962; Albritton and Smith, 1965; Raney and Collins, 1993).

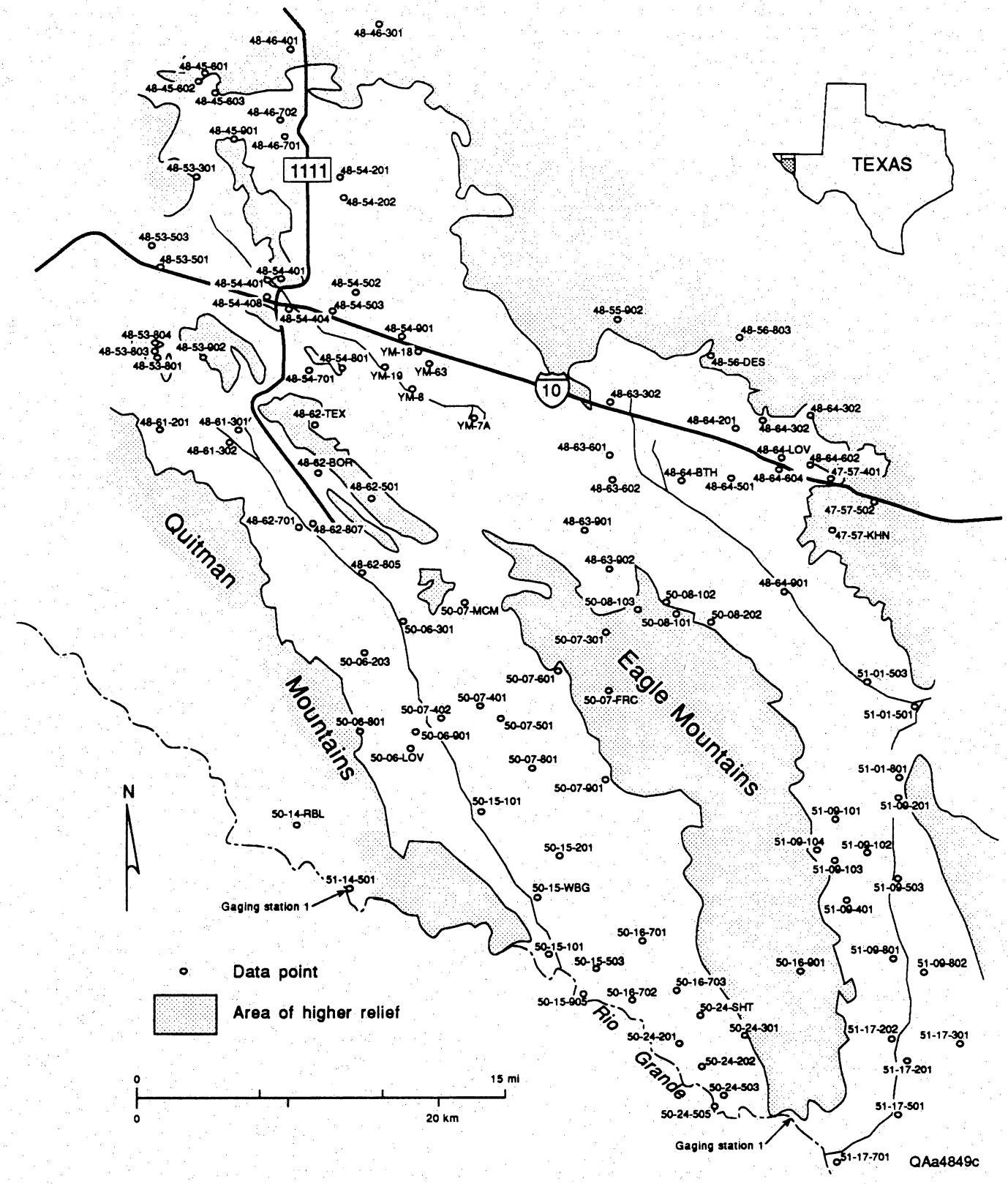

Figure 3. Locations of wells and springs.

Basin Fill

The basins are filled with Miocene, Pliocene, and early Pleistocene deposits of alluvial fan, fluvial, and playa depositional facies, and Quaternary wind-blown sediments (King and Flawn, 1953; Underwood, 1962; Albritton and Smith, 1965; Groat, 1972; Gustavson, 1991; Langford, 1993; Jackson and others, 1993). The thickness of the fill varies greatly among and within the basins (fig. 2 in Collins and Raney, 1993) (Albritton and Smith, 1965; Gates and White, 1976; Gates and others, 1980), as indicated by resistivity profiles, cores, well logs, and drillers' logs. Monitor wells, core holes, and geophysical surveys in northwest Eagle Flat, 5 to 7 mi (8 to 11.2 km) east of Sierra Blanca, show that the basin fill increases from less than 100 ft (30.5 m) to more than 700 ft (214 m) over a distance of 3 mi (4.8 km). Along the axis of southeast Eagle Flat, the fill increases from nearly 700 ft (214 m) at well 48-63-601 to more than 2,200 ft (670 m) at 50-01-504 near Scott's Crossing (Gates and others, 1980), over a distance of 13 mi (21 km). Well 48-64-BTH was completed in fine-grained basin fill at a depth of 1,050 ft (320 m). Based on the original basin fill isopach map of Gates and others (1980), bedrock was expected to be encountered between 700 to 800 ft (213 to 244 m). Basin fill is less than 500 ft (152 m) thick in northern Red Light Draw, increasing to more than 2,000 ft (610 m) along the Rio Grande.

Water-Bearing Units

Precambrian rocks form the principal aquifer in the northern and eastern areas of southeast Eagle Flat. Well depths range from 80 to 480 ft (24 to 146 m), with water depths of 20 to 230 ft (6 to 70 m). In other areas of southeast Eagle Flat, wells that are as much as 1,000 ft (305 m) in depth produce water from basin fill. Only well 48-63-601 is reported to have pumped water from an unspecified unit of the Cretaceous system (White and others, 1980).

The Cox Sandstone is the primary water-bearing unit in northwest Eagle Flat, especially north of Interstate Highway 10 (Albritton and Smith, 1965). Albritton and Smith (1965) describe the formation as "a heterogeneous body of sandstone and associated clastic rocks which is varied in detail and not entirely of the same age from place to place." Outcrop exposures are generally fine- to coarse-grained, yellowish gray, quartzitic, cross-laminated, and ferruginous. Interbeds of silt, shale, and medium-gray, flaggy limestone with shell fragments

and chert pebbles are common (Underwood, 1962; Albritton and Smith, 1965). Cuttings and core from monitor wells south of the interstate highway (YM-7A, YM-19, and YM-63), show the Cox to be a white to reddish, fine- to coarse-grained sandstone, with interbeds of gray limestone, and green and yellow siltstone.

Two monitor wells (YM-8, and YM-18) produce water from the Finlay Limestone. In the Sierra Blanca area, exposures of the Finlay range from massive beds of gray, fossiliferous limestone to a medium-gray, pale-yellowish, brown-weathering, thin- to thick-bedded, finely crystalline, nodular limestone with a few thin beds of shale, siltstone, and very fine-grained quartz sandstone (Underwood, 1962; Albritton and Smith, 1965). The lower part of the formation is marly, often giving way to beds of white sandstone, 6 inches to 3 ft (15.2 cm to 91.4 cm) thick (Albritton and Smith, 1965). Cuttings from the two above-mentioned monitor wells indicate that the Finlay consists of yellow siltstone and gray limestone with thin beds of white sandstone. In both wells, clean, white sandstone occurs at the base of the formation. A well drilled to a depth of 1,300 ft (396 m) on the northeast side of Devil Ridge (48-62-TEX) (fig. 3) produces water from either the Bluff Mesa Formation or the underlying Yucca Formation.

In Red Light Draw, wells produce water from Cretaceous rocks, and basin-fill material. Cretaceous rocks make up the water-bearing unit in the northern part of the basin. Wells in the central and southern reaches of Red Light Draw produce water from basin fill. At Indian Hot Springs and Red Bull Spring, at the southern end of the Hueco Bolson, ground-water issues from faults cutting through lower Cretaceous rocks.

Surface Water

The Rio Grande is the only perennial stream in the study area. All other water courses flow only after heavy rainfall (Underwood, 1962). Surface flow in Red Light Draw and southern Green River Valley is toward the Rio Grande; but Eagle Flat Draw, which drains southeastern Eagle Flat, flows eastward toward Scott's Crossing. Northwestern Eagle Flat is an area of internal drainage. Runoff from this watershed collects in Grayton Lake, which is a desert playa (Motts, 1965). Grayton Lake is a topographic low with 45 ft (14 m) of closure. It is dry for extended periods of time (Underwood, 1962), and water accumulates in the playa only after exceptionally heavy rainfalls. The northwestern and southeastern

sections of Eagle Flat are separated by a surface-water divide about 6 mi (9.5 km) east of Grayton Lake. The divide extends southward from the Streeruwitz Hills to the Eagle Mountains. Another surface-water divide separates Green River Valley from southeastern Eagle Flat basin to the north.

Climate

The climate is subtropical arid (Larkin and Bomar, 1983). Average annual precipitation is 12 inches (30.5 cm), and mean annual evaporation is 84 inches (213 cm), based on measurements of lake-surface evaporation (Larkin and Bomar, 1983). Average annual low temperatures are nearly 8.9°C (48 °F), and average high temperatures are close to 26.7°C (80°F). Most precipitation occurs during the months of July through October (Larkin and Bomar, 1983; Bedinger and others, 1985) as widely scattered thunderstorms with moisture originating primarily in the Gulf Coast (Elliot, 1949; Nativ and Riggio, 1990). Because of the convective nature of thunderstorms, most summer precipitation in West Texas and southern New Mexico increases with elevation (Gile and others, 1981). Winter rainfall, which accounts for less than one-third of total precipitation (Larkin and Bomar, 1983), is associated with widespread Pacific frontal systems (Elliot, 1949; Nativ and Riggio, 1990), which do not display a significant orographic effect.

Population and Water Use

The study area is sparsely populated. Sierra Blanca, the largest community, had a population of 700 in 1990. The economic base of the community is sustained predominantly by the ranching industry, interstate travel, and some small industries. Sierra Blanca formerly depended upon local wells to satisfy municipal water needs but currently has most of its water piped in from Van Horn. Van Horn derives its water supplies from basin fill at Wild Horse Flat, a bolson aquifer east of the study area. In rural areas, water use is mostly limited to domestic and livestock consumption. A small number of low-capacity water wells satisfy the needs of the local population and livestock industry. A few springs issue from bedrock formations in the mountains and augment livestock water supplies.

SOURCES OF INFORMATION

Geologic Studies

There have been a number of geologic studies in Trans-Pecos Texas and southeastern New Mexico that, collectively, establish a coherent framework for understanding local and regional controls on ground-water flow in southern Hudspeth County. King and Flawn (1953) studied the geology and mineral deposits of Precambrian rocks of the Van Horn area; Underwood (1962) described the geology of the Eagle Mountains and surrounding area; Albritton and Smith (1965) conducted a detailed evaluation of the geology around Sierra Blanca and the northern Quitman Mountains; and Jones and Reaser (1970) compiled a geologic map of the Quitman Mountains. More recently, Raney and Collins (1993) conducted a field study of the regional geologic setting of the Eagle Flat area, and Collins and Raney (1993) mapped late Cenozoic faults of northwestern Trans-Pecos Texas.

Hydrological Studies

Although there have been many studies of ground-water hydrology in Trans-Pecos Texas, none has concentrated principally on southeast Eagle Flat, northwest Eagle Flat, and Red Light Draw. Richardson (1904) surveyed ground-water resources in Trans-Pecos Texas north of the Texas and Pacific Railway. In a joint program between the U.S. Geological Survey and the Texas Department of Water Resources, Gates and White (1976) conducted a drilling program for ground-water resources in Hudspeth, Culberson, and Presidio Counties. Subsequently, Gates and others (1980) completed a reconnaissance of the availability of potable water resources in the westernmost counties of Texas, and White and others (1980) compiled a data base of water depths and major-ion chemistry in Eagle Flat, Red Light Draw, Green River Valley, Lobo Valley, the Salt Basin, and Hueco Bolson. Henry (1979) studied the geologic setting and geochemistry of thermal waters in Trans-Pecos Texas and adjacent parts of Mexico, and Hoffer (1978) directed an exploratory evaluation of geothermal energy potential. Other studies of significance addressed the distribution of stable isotopes (δ^2H and $\delta^{18}O$) in precipitation and in ground water in West

Texas and southeastern New Mexico (Hoy and Gross, 1982; Chapman, 1986; Lambert and Harvey, 1987; Nativ and Riggio, 1987; Nativ and Guitierrez, 1988; Chapman and others, 1992).

Researchers with the Bureau of Economic Geology conducted ground-water studies in the Hueco Bolson, the Diablo and Culberson Plateaus, and the Salt Basin during an earlier effort by the Texas Low-Level Radioactive Waste Disposal Authority to evaluate potential repository sites in Hudspeth and Culberson Counties (Kreitler and others, 1986; Fisher and Mullican, 1990; Scanlon and others, 1991; Mullican and Senger, 1992). In addition to the standard major ions, ground-water and surface-water samples were analyzed for stable isotopes (δ^2H, $\delta^{18}O$, $\delta^{13}C$, $\delta^{34}S$), unstable isotopes (^3H and ^{14}C), and a wide range of trace elements.

FIELD AND ANALYTICAL METHODS

Methods used to characterize the regional flow system included: (A) measuring water levels in wells and gauging Rio Grande streamflow; (B) analysis of aquifer pump and specific capacity tests; (C) acquisition and interpretation of water quality and isotopic data; and (D) numerical flow modeling to test hypothesis regarding the regional ground-water flow regime.

Water-Level Measurements and Stream Gauging

Historical data were combined with recent water-level measurements from all hydrostratigraphic units to prepare a composite potentiometric surface map. Historical and recent water-level measurements were compared to determine if the system is at or near steady-state and what the degree of error is in implying historical data in one map. An electric probe was used to measure the depth to water relative to the measuring point, usually the top of well casing.

Water levels in observation wells drilled for hydrologic tests were measured with pressure transducers. Transducers were hung at a given depth in the water column and connected to a data logger. The data logger converts strain across the pressure transducers measured by electrical current to pressure of the water column overlying the transducers and stores the reading in internal memory. Stored pressure data were downloaded from the data logger and converted to water-level elevations. Pressure gauged in units of pounds per

square inch (psi) was converted to hydraulic head in units of feet of water (assuming specific weight of water to be 0.433 psi/ft). Water-level elevation was determined by subtracting depth to water from measuring-point elevation.

Stream discharge was gauged in the Rio Grande at Indian Hot Springs (gauge station 1) and at Green River Valley (gauge station 2). The objective of stream gauging was to determine if baseflow from Red Light Draw and other aquifers could be measured (fig. 3). Stream discharge was measured using an AA-type current meter. At each station, a straight stream reach with a relatively symmetrical channel cross section and shallow depth of flow (less than 2.5 ft [0.8 m]) was chosen. A cloth measuring tape strung across the stream perpendicular to the direction of flow was used to divide the stream into uniform increments of 2 to 2.5 ft (0.6 to 0.8 m). At the midpoint of each increment, the depth of water was measured and the bucket wheel of the current meter placed at 0.6 times the depth of flow. The number of revolutions of the bucket wheel was counted over an interval of time and recorded. A U.S. Geological Survey rating table was used to convert revolutions per unit time to flow velocity. The velocity was multiplied by the width and depth of the increment to arrive at a value of stream discharge for that increment. The sum of at least 20 incremental discharges gave the total stream discharge for the stream reach.

Several discharge measurements were made at Indian Hot Springs (gauge station 1) on March 18. The following day, several measurements were performed at Green River Valley (gauge station 2). These measurements were arithmetically averaged to provide an average daily stream discharge.

Aquifer Testing

Aquifer tests were performed to estimate transmissivity and degree of aquifer confinement. Single well pump tests were performed in six wells for periods varying from 22 to 68 hours. Qualitative and quantitative methods were used to evaluate aquifer test data. Qualitative examination of the drawdown curves helped to distinguish between confined, leaky confined, and unconfined aquifers (fig. 4). Quantitative interpretations were provided with the curve matching program AQTESOLV (Duffield and Rumbaugh, 1989). Where appropriate, drawdown curves were matched using (1) the modified Theis (1935) method (discussed in Kruseman and De Ridder, 1979), for analysis of drawdown in an unconfined aquifer, (2) the Cooper-Jacob (1946) method for drawdown in a

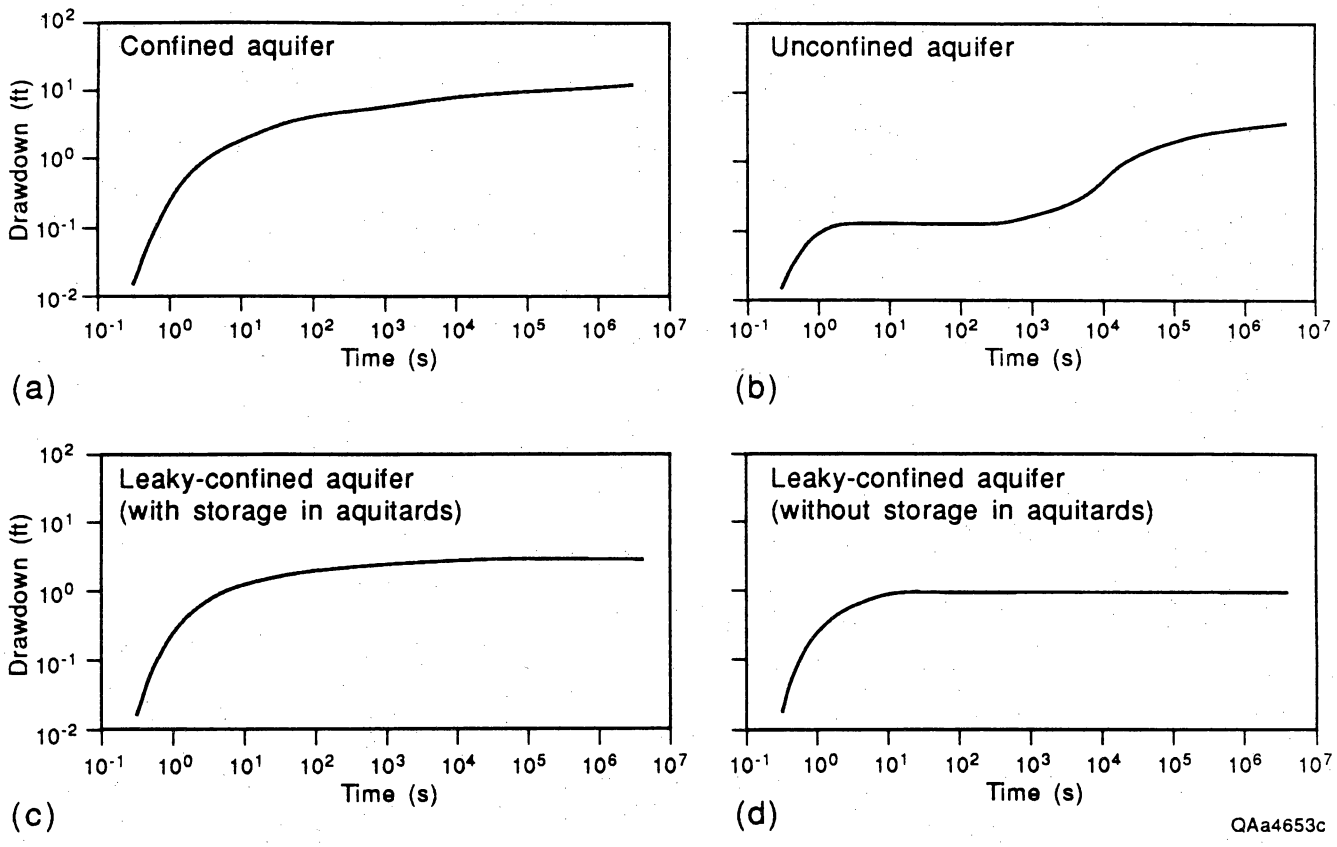

Figure 4. Representative time-drawdown curves for confined, leaky confined, and unconfined aquifers observed during aquifer testing. The nonequilibrium time-drawdown curve for a fully confined aquifer is a parabola (a). The time-drawdown curve for an unconfined aquifer often is an s-shaped curve (b). The time-drawdown curves for leaky confined aquifers (c and d) are suppressed parabolas because a leaky confined aquifer is replenished by vertical flow from lower permeability bounding strata.

confined aquifer, and (3) the Hantush (1960) and Hantush-Jacob (1955) methods for analysis of drawdown in leaky confined aquifers, with and without storage in confining layers. Recovery data were analyzed using the Theis (1935) recovery method.

Where aquifer test data of suitable quality were not available, specific capacity data were used to provide preliminary estimates of transmissivity. The modified nonleaky artesian formula (Walton, 1962) was used to relate the specific capacity of a well to the aquifer transmissivity:

$$\frac{Q}{s} = \frac{T}{[264 \log (Tt/2693\, r^2S) - 65.5]}$$

where

Q/s = specific capacity [L^2/T]
T = transmissivity [L^2/T]
S = storage coefficient (dimensionless)
r = well radius [L]
t = time since pumping started [T].

A graphical solution for transmissivity is obtained by plotting Q/s for various values of T on log-log paper while all other parameters are held constant. Storage coefficients of 0.14 (unconfined), and 0.0005 (confined) were used to bracket possible ranges where the degree of aquifer confinement was unknown. Specific capacity data were collated from files of the Texas Water Development Board.

With transmissivity known, the hydraulic conductivity was obtained by dividing transmissivity by the saturated thickness. For the purpose of analysis, wells were considered fully penetrating. Hydraulic conductivity was computed by dividing the transmissivity by the aquifer section occupied by the well.

Hydrochemical and Isotopic Sampling

Hydrochemical data were collected during a 2-year program of field work (September 1991 through August 1993), and were supplemented by data from White and others (1980). Fifty-nine wells and 2 springs were sampled in accordance with guidelines in Specific Work Instruction 3.1 of the Technical Program Manual of the Bureau of Economic Geology (1989). Samples were

analyzed at collection sites for unstable constituents (temperature, pH, Eh, alkalinity, and dissolved oxygen), and were prepared for laboratory analysis.

Before samples were collected for analysis of ionic constituents, wells were pumped until pH, Eh, and temperature stabilized. Measurements of pH, Eh, and temperature were made in flow cells, with electrodes calibrated with buffer solutions that had been equilibrated to sample temperature (Wood, 1976). The time required to reach equilibration varied substantially from well to well (20 to 120 minutes). Alkalinity calculations were based on potentiometric titrations of filtered samples to a pH of 3.5 to 3.0, with 1.60 N H_2SO_4; and dissolved oxygen was estimated by means of a modified Winkler titration method (Water Analysis Handbook 1988), with 0.20 N sodium thiosulfate and an indicator starch solution. Samples for analysis of cations and anions were collected in separate 500 ml polyethylene bottles after being run through a 0.45μ in-line flow filter. All cation samples were treated with 5 ml of 6 N HNO_3. The sample containers were sealed with parafilm and kept on ice. Samples that could not be filtered in the field were kept in ice-filled coolers until delivered to the laboratory, where they were filtered and the cation samples were treated with 6 N HNO_3.

Samples collected for analysis of stable isotopes (^2H and ^{18}O) and ^3H were stored in 500 ml and 1 L glass bottles, respectively, and sealed with parafilm to avoid contact with the atmosphere. The sampling procedure for carbon isotopes required three 50-L carboys filled with water, and 500 ml of ammoniacal strontium chloride, added to each carboy, to raise the pH above 11 and precipitate the dissolved carbon species as strontium carbonate. The precipitate from each carboy was transferred within 8 hours to a 1-qt jar through a collection valve designed to eliminate exposure to the atmosphere. The collection jars were then sealed with parafilm. The details of this procedure are reported by Dutton (1993).

Chemical analyses for cations and silica were performed by chemists at the Mineral Studies Laboratory of the Bureau of Economic Geology using inductively-coupled plasma-optical emission spectrometry (ICP-OES). Chloride, fluoride, sulfate, and nitrate were measured by ion chromatography; bromide was determined by spectrophotometry. In some cases, nitrate was measured by distillation-titration, and fluoride by an ion-selective electrode.

The δ^2H, and $\delta^{18}O$ measurements were made by means of gas-source mass spectrometry at the Mineral Studies Laboratory of the Bureau of Economic Geology. The δ-values are reported relative to SMOW. None of the $\delta^{18}O$

measurements required adjustment because of high ionic strength (Sofer and Gat, 1972). The ^{3}H activities were measured by low-level proportional counting of samples that had undergone electrolytic enrichment at the University of Miami Tritium Laboratory, Miami, Florida. Measurements of ^{14}C activity and $\delta^{13}C$ were made by scintillation counting and mass spectrometry at Beta Analytic, Inc., of Miami, Florida.

Mineral saturation states were computed by WATEQF, incorporated into the interactive geochemical reaction path modeling program NETPATH (Plummer and others, 1991). WATEQF calculates the equilibria between water and minerals, based on a comparison between the amount of dissolved species in solution and the amount that would be present if the water-solute system were at equilibrium with specific minerals at the sample temperature. The results, reported as saturation indices transformed to common logarithms (base 10), indicate whether the sample is undersaturated, oversaturated, or at equilibrium with respect to a given mineral. Equilibrium is indicated by a value of zero; negative values suggest undersaturation and positive values, oversaturation.

Numerical Flow Modeling

The U.S. Geological Survey modular flow model MODFLOW (McDonald and Harbaugh, 1988) and its associated particle-tracking routine MODPATH (Pollock, 1989b), were used to develop a two-dimensional cross-sectional model in the x-z plane (profile model). The profile model was developed to test hypotheses regarding flow and to estimate pathlines, residence times, and ground-water velocities. MODFLOW uses a finite-difference approximation to solve the steady-state, ground-water flow equation:

$$\partial/\partial x(K_{xx}\partial h/\partial x) + \partial/\partial y(K_{yy}\partial h/\partial y) + \partial/\partial z(K_{zz}\partial h/\partial z) = 0$$

where

> x, y, and z are cartesian coordinates aligned with the major axes of the flow system, with hydraulic conductivity tensors Kxx, Kyy, and Kzz and h is hydraulic head.

The fundamental simplifying assumptions used to construct and apply the model include:

1. Flow in the aquifer is in accordance with Darcy's law; that is, discharge is linearly related to hydraulic-head gradient.

2. Flow in the aquifer is two-dimensional in the vertical direction.

3. Density of the water is spatially and temporally constant.

4. Aquifer recharge, flow, and leakage are constant with time.

MODPATH is a post-processing package that develops pathlines based on steady-state output from the finite difference code MODFLOW. The processor assumes that each directional velocity component varies linearly within a model cell along a coordinate axis (Pollock, 1989a, 1989b). Pathlines are defined within a grid matrix by tracking a "particle" specified in a cell to a model boundary or user-specified zone. By computing the travel time along the flowpath, velocities and residence times are estimated.

RESULTS OF ANALYSES

Water-Level Measurements and Stream Gauging

Depths to water typically vary between 667 and 920 ft (203 and 280 m) in northwest Eagle Flat (between 667 and 751 ft [203 and 229 m] at Faskin Ranch), and between 160 and 700 ft (49 and 213 m) in southeast Eagle Flat. Depths to water in Red Light Draw vary from only a few feet in the Rio Grande alluvium to over 450 ft (137 m) in the northwestern part of the draw. Depths to water in the mountains are variable, as little as 15 to 20 ft (4.6 to 6.1 m) beneath the Eagle Mountains and Bean Hills, and as great at 1,130 ft (344 m) on the flanks of Sierra Blanca Mountain.

A potentiometric map (fig. 5) was constructed from water-depth measurements reported by White and others (1980) and measurements made at more than 30 wells during this investigation. Several wells were excluded because reliable measurements were not found in the archives of the Texas Water

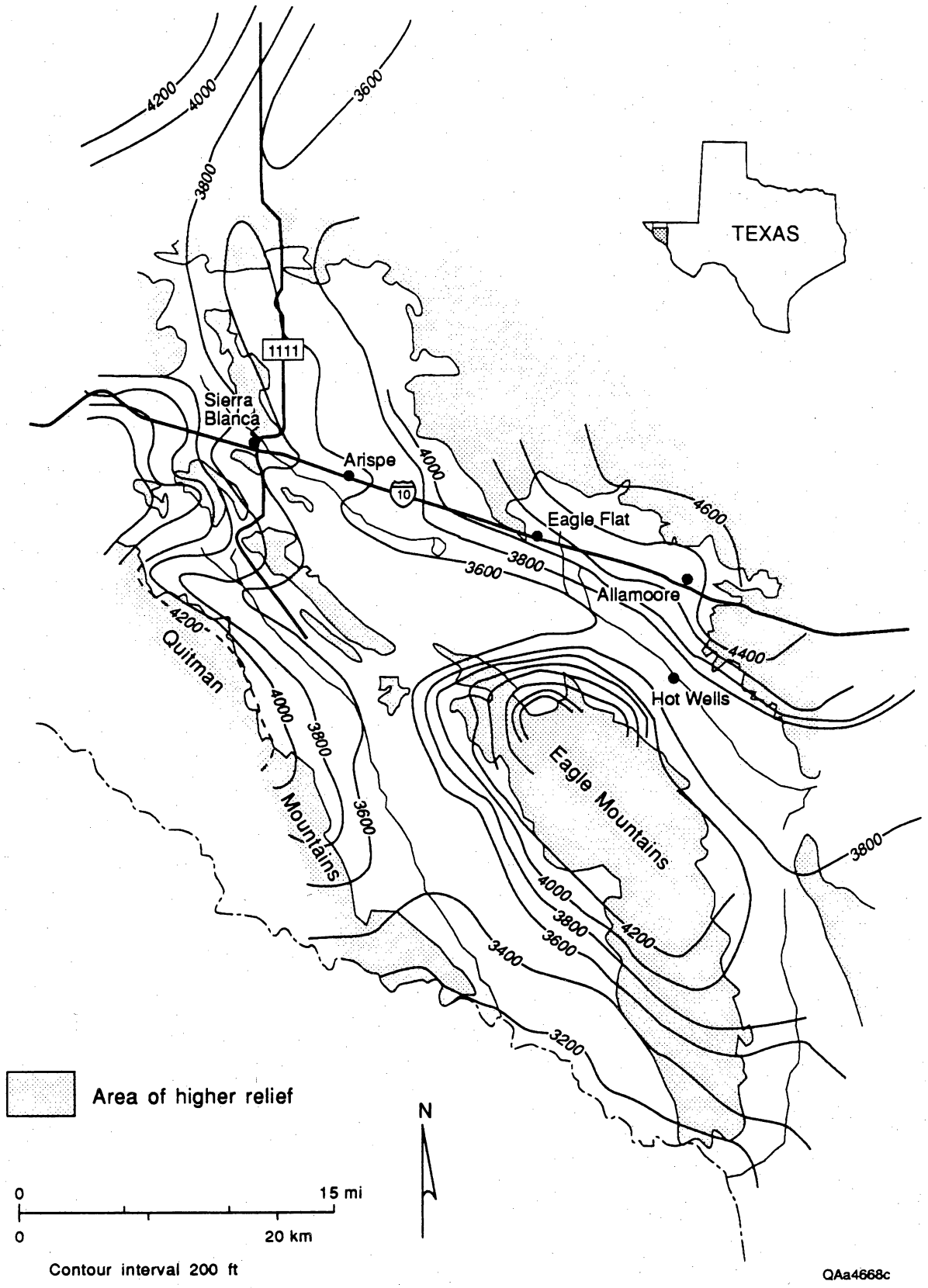

Figure 5. Composite potentiometric surface map generated with recent and historical water-level measurements in the study area. Quasi-steady flow in undeveloped aquifers suggests that historical measurements can be used with recent measurements to develop an acceptable potentiometric map (see fig. 6).

Development Board. Hydraulic gradients are as great as 0.066 in the mountains and as little as 0.005 in the flats and draws. A regional gradient is oriented northwest-southeast from the Diablo Plateau, across northwest Eagle Flat and Red Light Draw. This is the apparent regional ground-water flow direction. Along mountain axes, ground-water divides are created by prominent topography and recharge along mountain fronts. A low-relief ground-water divide separates the northwest and southeast Eagle Flat aquifers. Another divide that runs approximately subparallel to the Diablo Plateau escarpment separates the Diablo Plateau system in the north from the northwest Eagle Flat and southeast Eagle Flat systems to the south (Kreitler and others, 1990; Mullican and Fisher, 1990). The contoured head data suggest that the Rio Grande is the discharge area for waters in the northwest Eagle Flat - Red Light Draw flow systems. Ground waters in southeast Eagle Flat most likely flow through the Scott's Crossing area to Lobo Valley via interbasin flow.

Figure 6 presents selected hydrographs for wells in Eagle Flat, Blanca Draw, and Red Light Draw. Small to moderate fluctuations in head exist. The hydrograph for well 50-16-703 is atypical (fig. 7). Prior to 1980, pumping yields reportedly were very low in this well (e.g., 1 gallon per minute). Water levels rose nearly 150 ft (46 m) and well yields increased when the well was deepened (Mann Bramblett, personal communication, 1993). This indicates that the well was recompleted in basin-fill strata that are at higher pressure, which requires a confining layer to separate pressure zones, and implies permeable connection to a recharge zone to create higher pressure (see artesian zone in fig. 38).

Although ground-water discharge to the Rio Grande is inferred from aquifer head data (fig. 5), the stream gauging survey did not detect significant baseflow (table 1). Average stream discharge was 129.22 ft^3/s +/- 3.88 ft^3/s (3.66 m^3/s +/- 0.11 m^3/s) at Indian Hot Springs and 125.69 ft^3/s +/- 3.77 ft^3/s (3.56 m^3/s +/- 0.11 m^3/s) at Green River Valley. Although these data imply some stream loss, it is impossible to determine if real losses occurred because the measuring accuracy of the technique is at best +/- 3 percent. The preliminary conclusion offered by these limited data is that neither aquifer discharge nor recharge exceeded 10 ft^3/s (0.3 m^3/s) along the stream reach during steady streamflows.

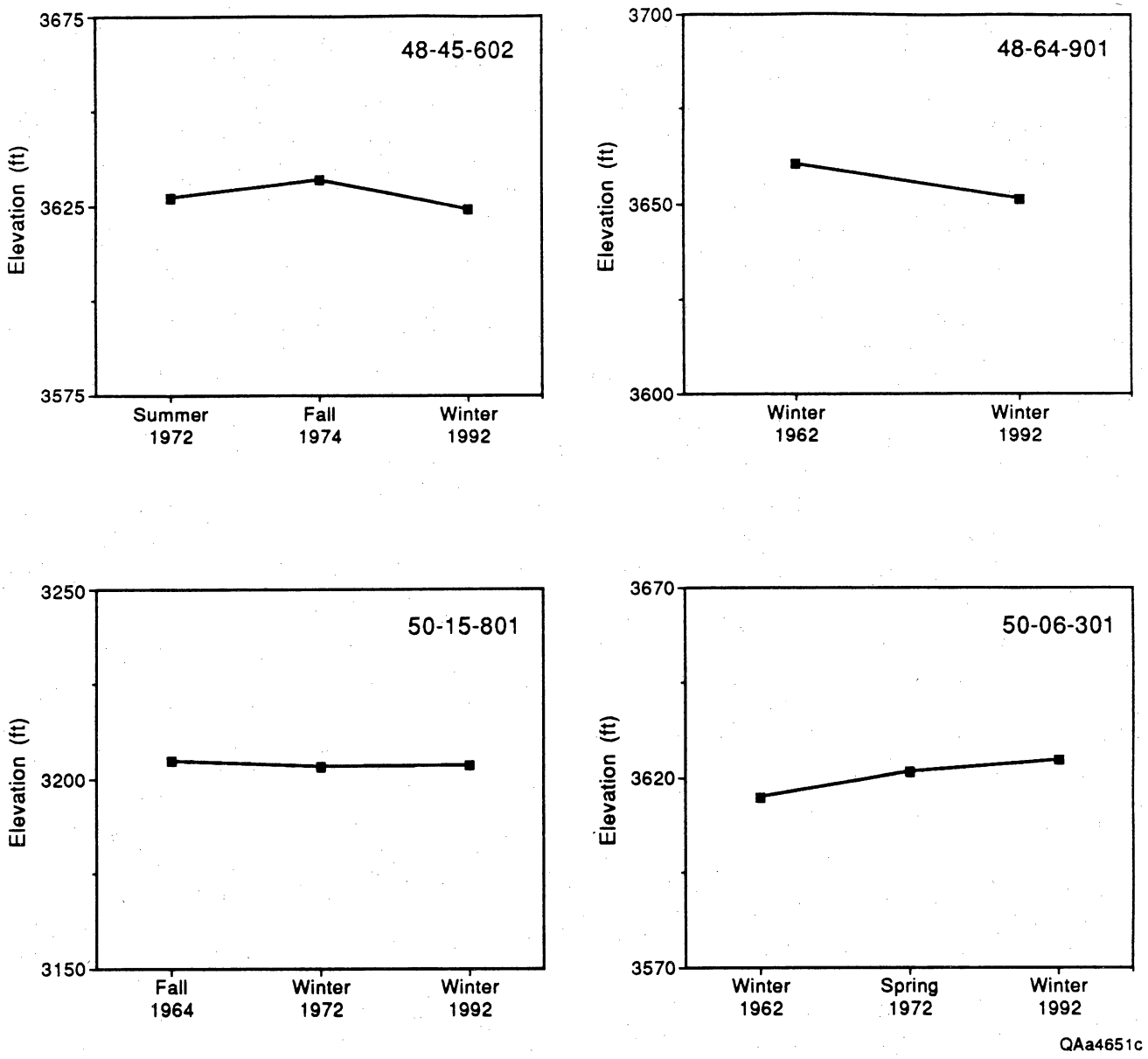

Figure 6. Hydrographs for wells in Eagle Flat, Red Light Draw, and Blanca Draw comparing historical and recent water-level measurements (1962–1992). Moderate to small water-level fluctuations (e.g., 1–10 ft) with no consistent patterns are shown.

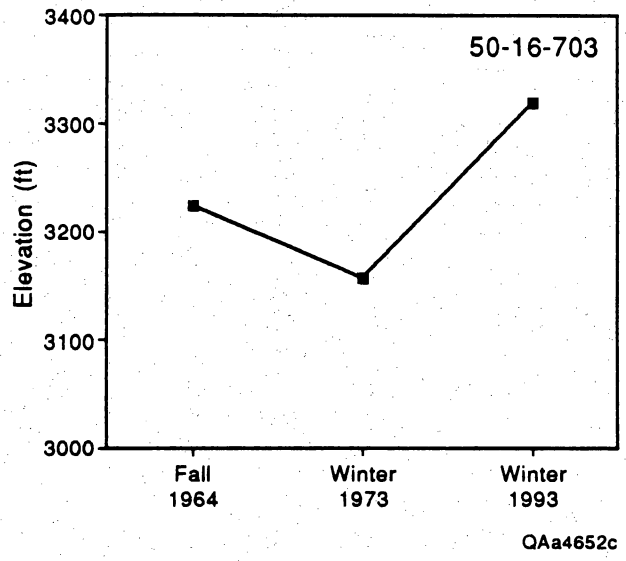

Figure 7. Hydrograph for well 50-16-703 in lower Red Light Draw, showing significant variation in water levels. Well yields in this well were very low initially (e.g., 1 gpm). In 1980 the well was deepened to increase its capacity. The well yield increased and the water-level rose when the well was recompleted in more permeable basin fill material. This indicates a confining layer to separate and preserve pressure, and implies a permeable connection to a recharge zone to create higher pressure.

Table 1. Results of stream gauging at station 1 (Indian Hot Springs) and station 2 (Green River Valley). Measurement error is +/- 3.9 cfs. Results indicate no significant gain or loss of flow between the two measuring segments.

Station #	Measurement #	Date	Time	Streamflow (cfs)
1 *Indian Hot Springs*	1	3/18/93	10:35	129.262
	2	3/18/93	11:52	129.359
	3	3/18/93	13:10	131.006
	4	3/18/93	14:23	129.718
	5	3/18/93	15:40	126.96
	6	3/18/93	17:20	129.034
Average streamflow (cfs)				129.223
2 *Green River Valley*	1	3/19/93	11:01	125.607
	2	3/19/93	13:20	127
	3	3/19/93	15:10	124.46
Average Streamflow (cfs)				125.689

Aquifer Test Results

Aquifer time-drawdown curves for single-well pump tests are presented in figure 8. Well locations are shown in figure 3. Curves in northwest Eagle Flat are representative of leaky-confined aquifers. Curve 48-64-BTH appears most representative of a leaky confined aquifer. Drilling data suggested that the aquifer may be slightly confined to unconfined at 48-64-BTH; therefore, both confined and unconfined curve matches are provided. Figure 9 and table 2 present the curve matches and parameter estimates for 48-64-BTH. Curve fits are good for all curves during late time drawdown. Curve fits during early time drawdown (1 to 50 seconds) are poor, probably because of wellbore storage effects.

Quantitative analysis of time-drawdown and recovery data for pump tests in northwest Eagle Flat are presented in table 2. For semi-log analysis, the Theis (1935) recovery method and the Cooper-Jacob (1946) method provide parameter estimates that had fair precision and accuracy (fig. 10). For log-log analysis, the Hantush-Jacob (1955) method for leaky aquifers with no storage in aquitards provided similar transmissivity estimates and, during late time drawdown, excellent curve fits (fig. 11; column 1). For early time-drawdown (first 10–500 seconds), curve fits are generally poor due to wellbore storage effects. The Hantush (1960) method for leakage with storage in aquitards usually provided a poor curve match for early and late-drawdown phases (fig. 10, column 2). Curve matches of time-drawdown data bolster qualitative analysis and suggest a leaky confined aquifer in northwest Eagle Flat.

Table 3 (columns 2 and 3) presents raw estimates from Walton's (1962) specific capacity analysis for wells with aquifer test data (e.g., YM-18, YM-19, etc.). In this study, results using Walton's (1962) method are generally between 140 and 500 percent higher than results using conventional methods (compare tables 2 and 3). The specific capacity analyses provided fair precision and moderate to somewhat poor accuracy. Because of its precision, Walton's (1962) method provides useful relative comparisons. A calibration factor is used to improve accuracy. The calibrated values (columns 4 and 5) are obtained by multiplying raw transmissivity values (columns 2 and 3) by 1/3, an average multiplier that accounts for overestimates in transmissivity. Estimates of aquifer parameters with specific capacity data for wells without aquifer tests are presented in table 3. Estimates in columns 2 and 3 (uncorrected) are multiplied

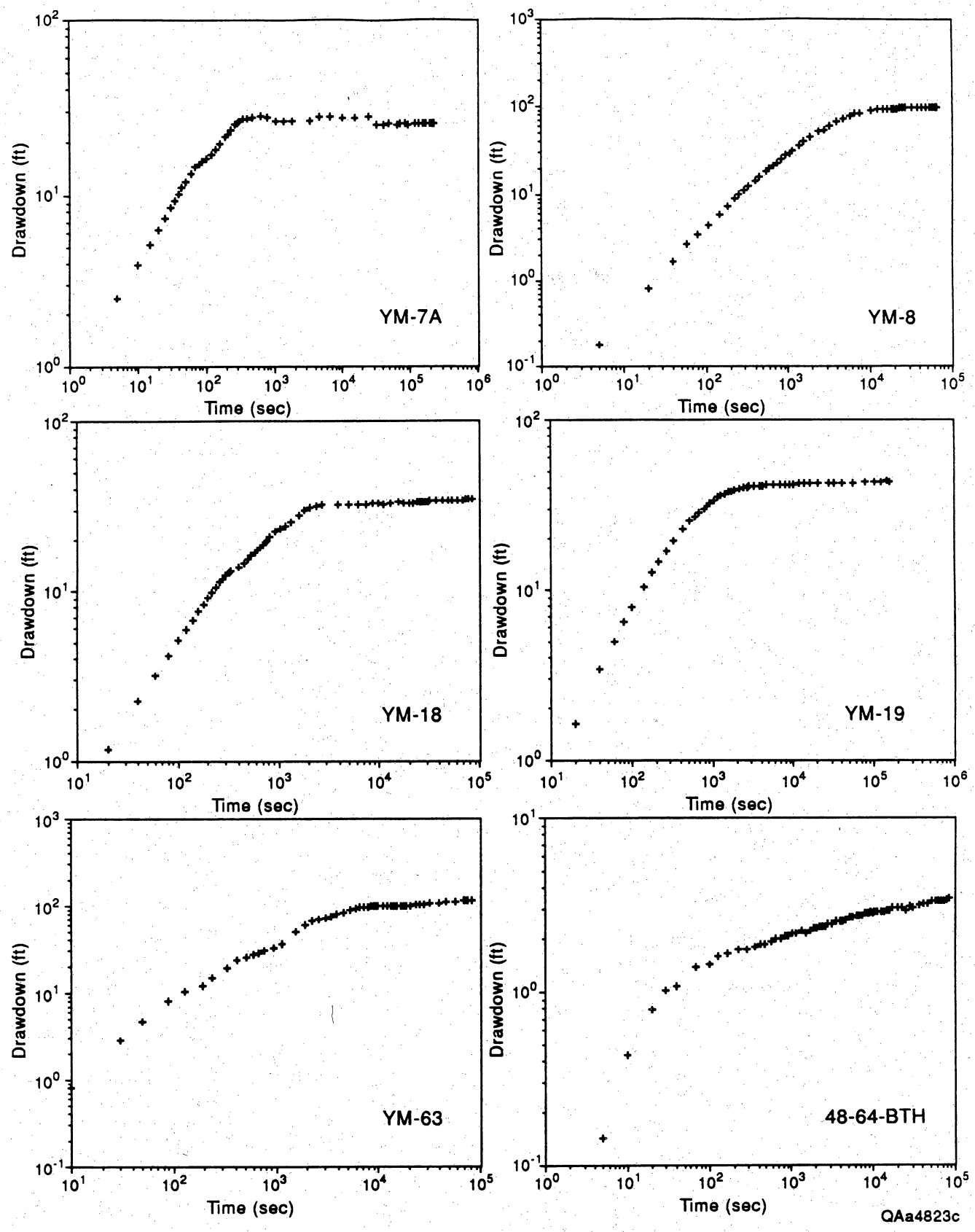

Figure 8. Time-drawdown curves for pump tests performed at Eagle Flat. All curves except 48-64-BTH are for bedrock aquifers in northwest Eagle Flat. Curve 48-64-BTH is for the bolson aquifer in southeast Eagle Flat. Time-drawdown curve shapes in northwest Eagle Flat are most representative of a leaky confined aquifer (see fig. 4). Drilling information and time-drawdown data indicate a locally unconfined to leaky confined aquifer at 48-64-BTH.

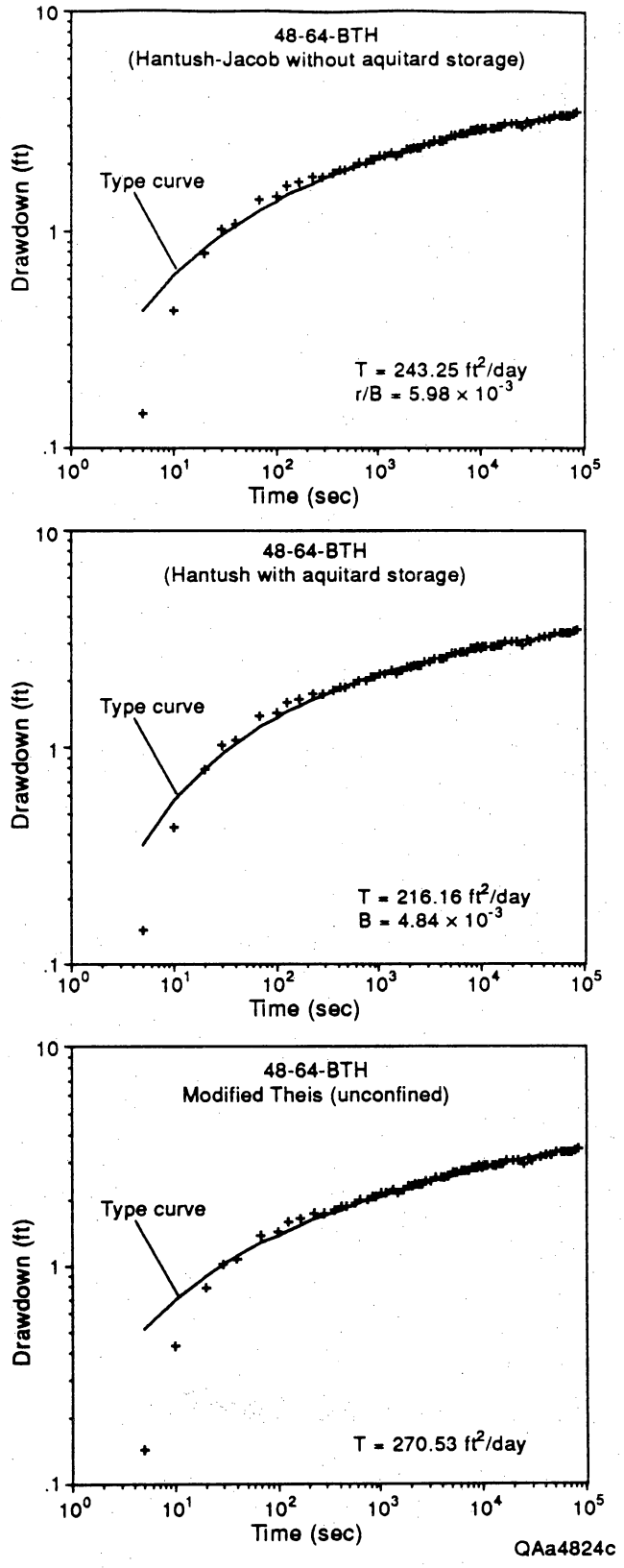

Figure 9. Aquifer test results for 48-64-BTH in southeast Eagle Flat. Curve matches provided by the Hantush-Jacob (1955) and Hantush (1960) methods for leaky confined aquifers, and the modified Theis method (discussed in Kruseman and De Ridder, 1979) for an unconfined aquifer. During early time drawdowns (e.g., the first 30 seconds) the curve fits are poor, probably due to wellbore storage effects. After early time drawdowns, the curve fits are good for all interpretive methods. Drilling information and time-drawdown data indicate a locally unconfined to leaky confined aquifer at 48-64-BTH.

Table 2. Aquifer test results for wells in northwest and southeast Eagle Flat. Hydraulic conductivity computed by dividing the transmissivity estimate by the saturated aquifer section occupied by the well. Such an approximation overestimates hydraulic conductivity if a well is partially penetrating.

TRANSMISSIVITY (FT-SQ./DAY)					
Well #	Hantush-Jacob (leaky confined)	Hantush (leaky confined)	Theis Recovery (confined)	Modified Theis (unconfined)	Cooper-Jacob (confined)
YM-7A	67.82	277.76	80.74	-	103.18
YM-8	2.40	3.19	2.50	-	3.12
YM-18	9.49	16.61	10.85	-	9.40
YM-19	10.23	23.48	10.19	-	15.00
YM-63	2.65	3.43	2.45	-	2.88
48-64-BTH	243.25	216.16	-	270.53	-

HYDRAULIC CONDUCTIVITY (FT/DAY)					
Well #	Hantush-Jacob (leaky confined)	Hantush (leaky confined)	Theis Recovery (confined)	Modified Theis (unconfined)	Cooper-Jacob (confined)
YM-7A	0.33	1.37	0.40	-	0.51
YM-8	0.0074	0.0099	0.0077	-	0.0097
YM-18	0.12	0.21	0.14	-	0.12
YM-19	0.11	0.25	0.11	-	0.16
YM-63	0.014	0.018	0.013	-	0.015
48-64-BTH	4.68	4.16	-	5.20	-

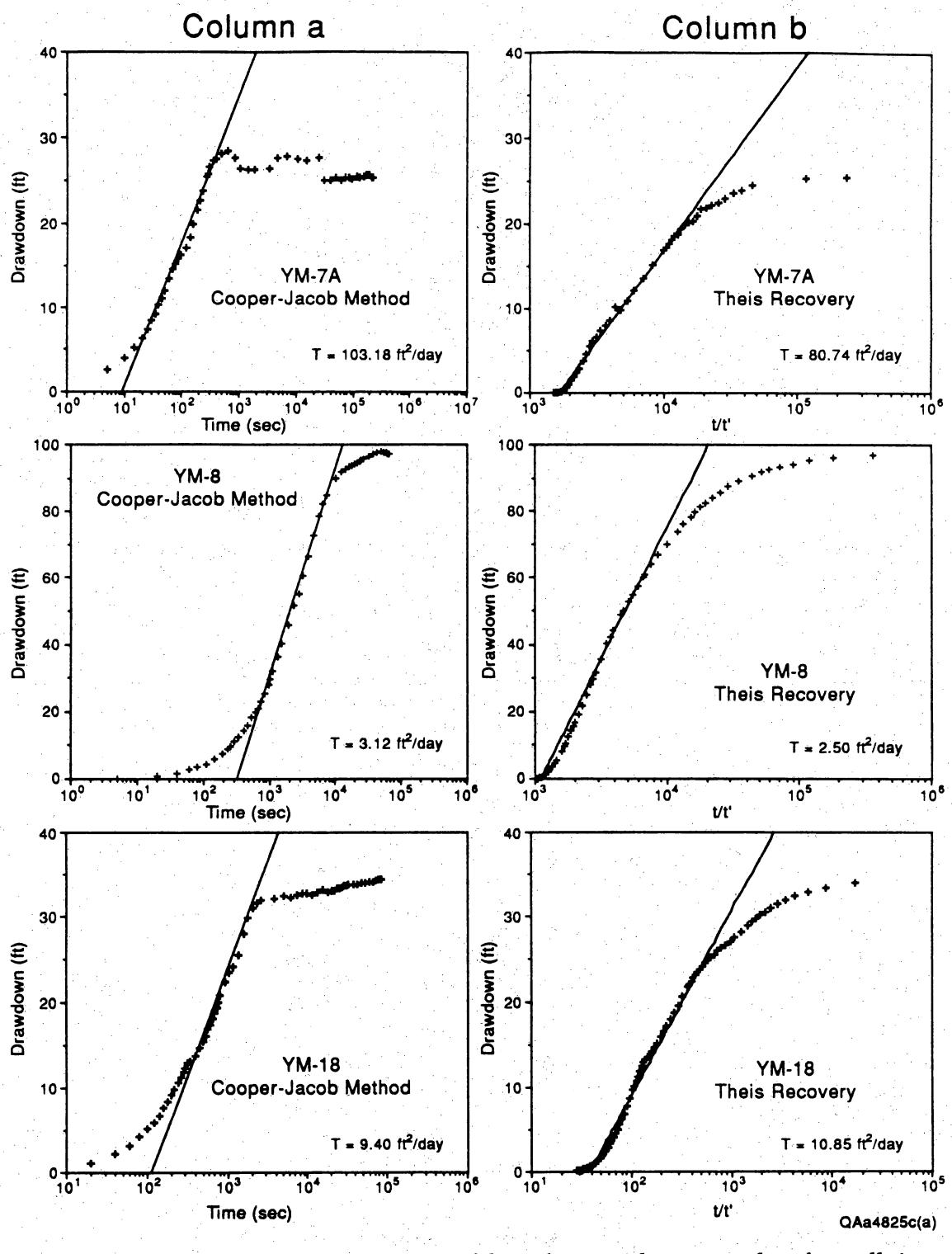

Figure 10. Semilog match of straight line segments of drawdown and recovery data for wells in northwest Eagle Flat. Semilog analysis provided by the Cooper-Jacob (1946) method (drawdown phase; column a) and the Theis (1935) recovery method (column b). For Cooper-Jacob (1946) interpretations, wellbore storage effects during early time drawdowns probably cause the nonlinear curve segment to drift to the left of the linear segment. The sharp inflection away from the linear segment during late time drawdowns is due to vertical leakage from the semipervious confining layers. The straight line segment matched during intermediate times represents the withdrawal of water from storage in the confined aquifer, no part of which was contributed from the semipervious confining layers (i.e., during intermediate times, all the water pumped comes from storage in the confined aquifer). After intermediate times, leakage from the semipervious units forms a significant part of the water pumped.

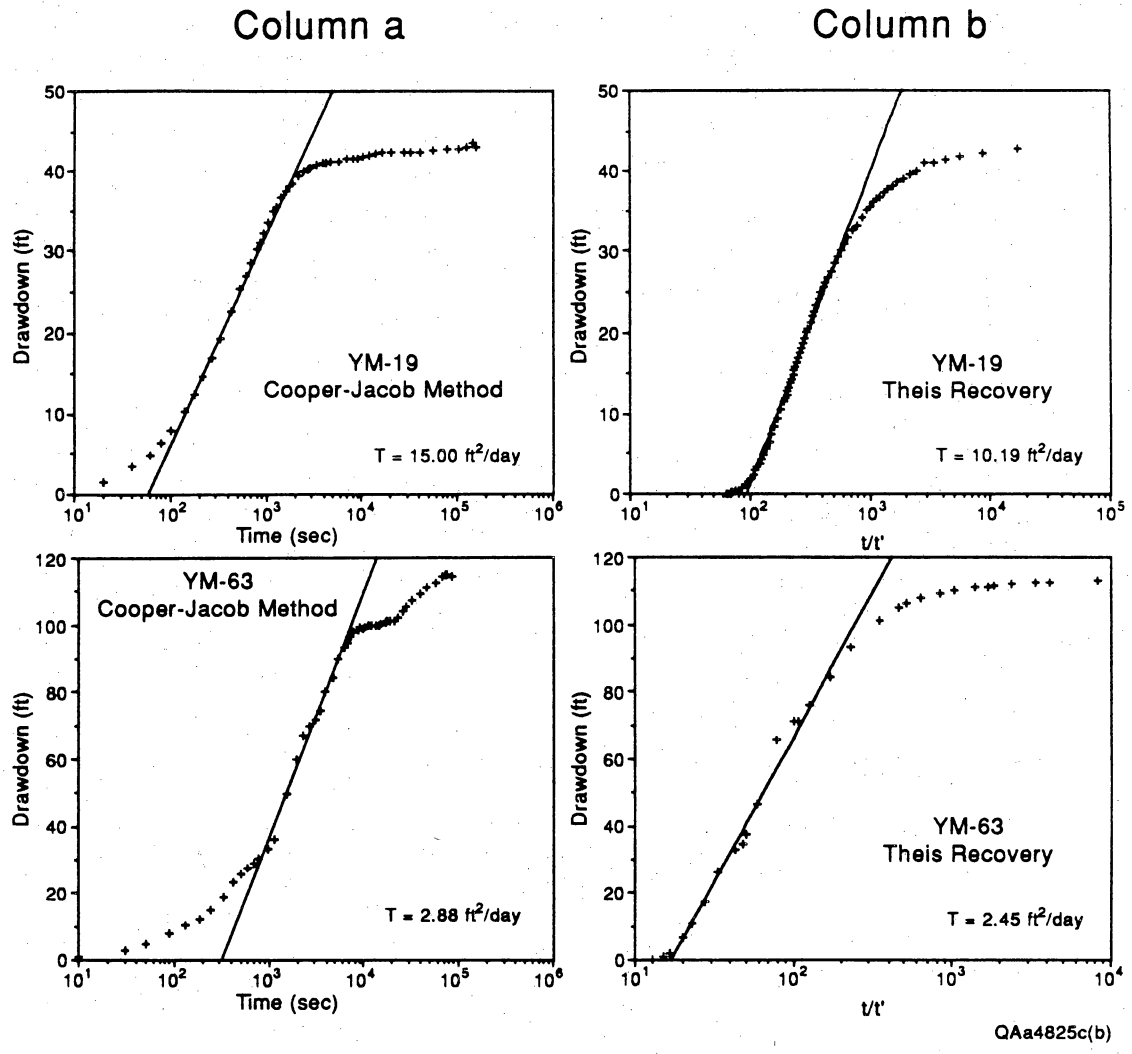

Figure 10 (continued). Semilog match of straight line segments of drawdown and recovery data for wells in northwest Eagle Flat. Semilog analysis of time-drawdown data provided by the Cooper-Jacob (1946) method (column a). Semilog analysis of recovery data provided by the Theis (1935) recovery method (column b). For Cooper-Jacob (1946) interpretations, wellbore storage effects during early time drawdowns probably cause the nonlinear curve segment to drift to the left of the linear segment. The sharp inflection away from the linear segment during late time drawdowns is due to vertical leakage from the semipervious confining layers. The straight line segment matched during intermediate times represents the withdrawal of water from storage from the confined aquifer, no part of which was contributed from the semipervious confining layers (i.e., during intermediate times, all the water pumped comes from storage in the confined aquifer). After intermediate times, leakage from the semipervious units forms a significant part of the water pumped.

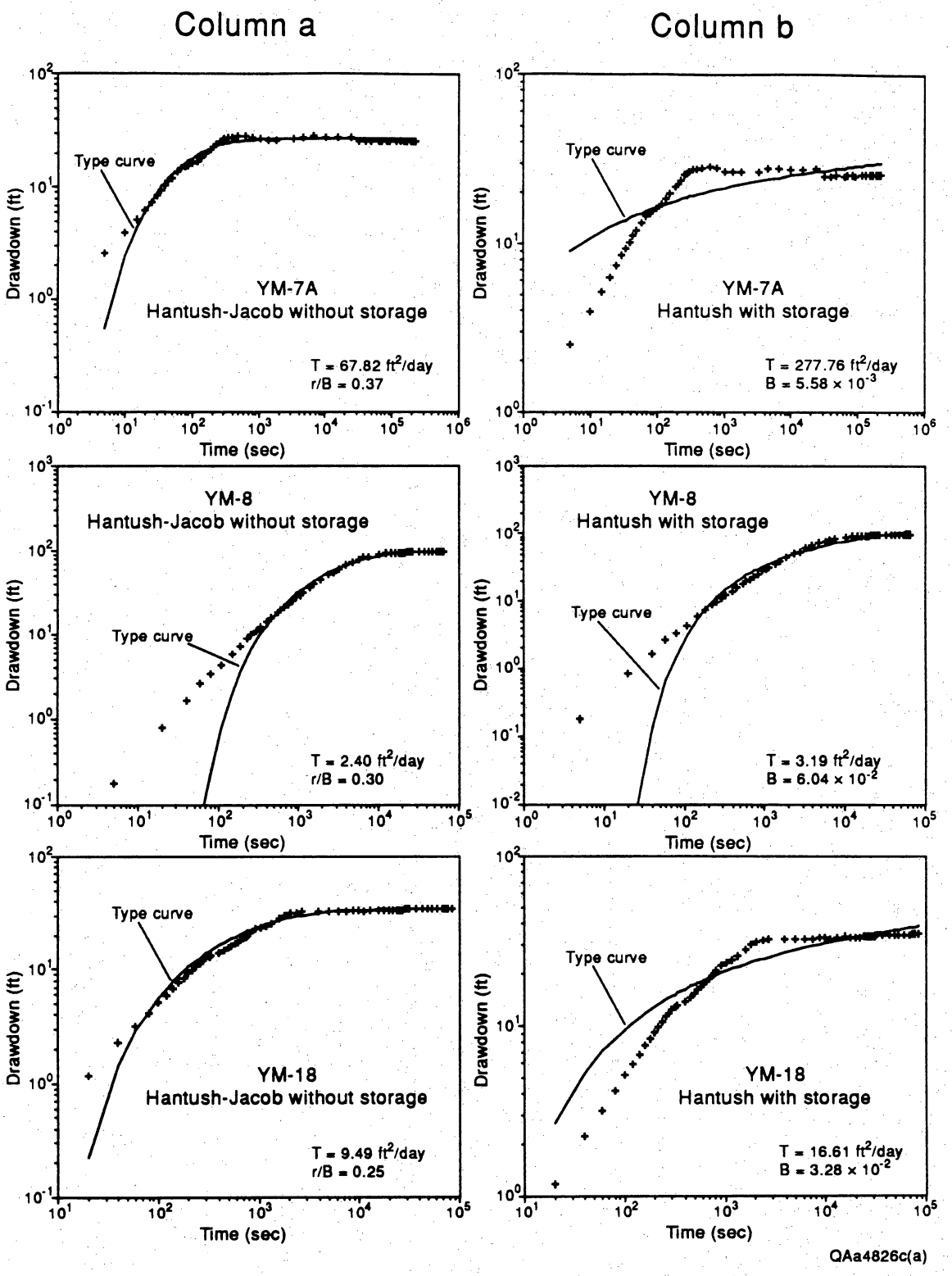

Figure 11. Comparison of curve matches for wells in northwest Eagle Flat, using analytical solutions for leaky confined aquifers. Curve matches for leaky aquifers without storage in aquitards (Hantush-Jacob, 1955) typically provided the best curve fit (column a). Curve matches for leaky aquifers with storage in aquitards (Hantush, 1960) generally provided a poor curve fit (column b). During early-time drawdowns (e.g., 10 to 500 seconds) curve matches are poor, probably as a result of wellbore storage. Very good fits were provided for intermediate and late-time drawdowns using the Hantush-Jacob (1955) method (column a). Poor curve fits generally were provided by the Hantush (1960) method for early, intermediate, and late-time drawdowns.

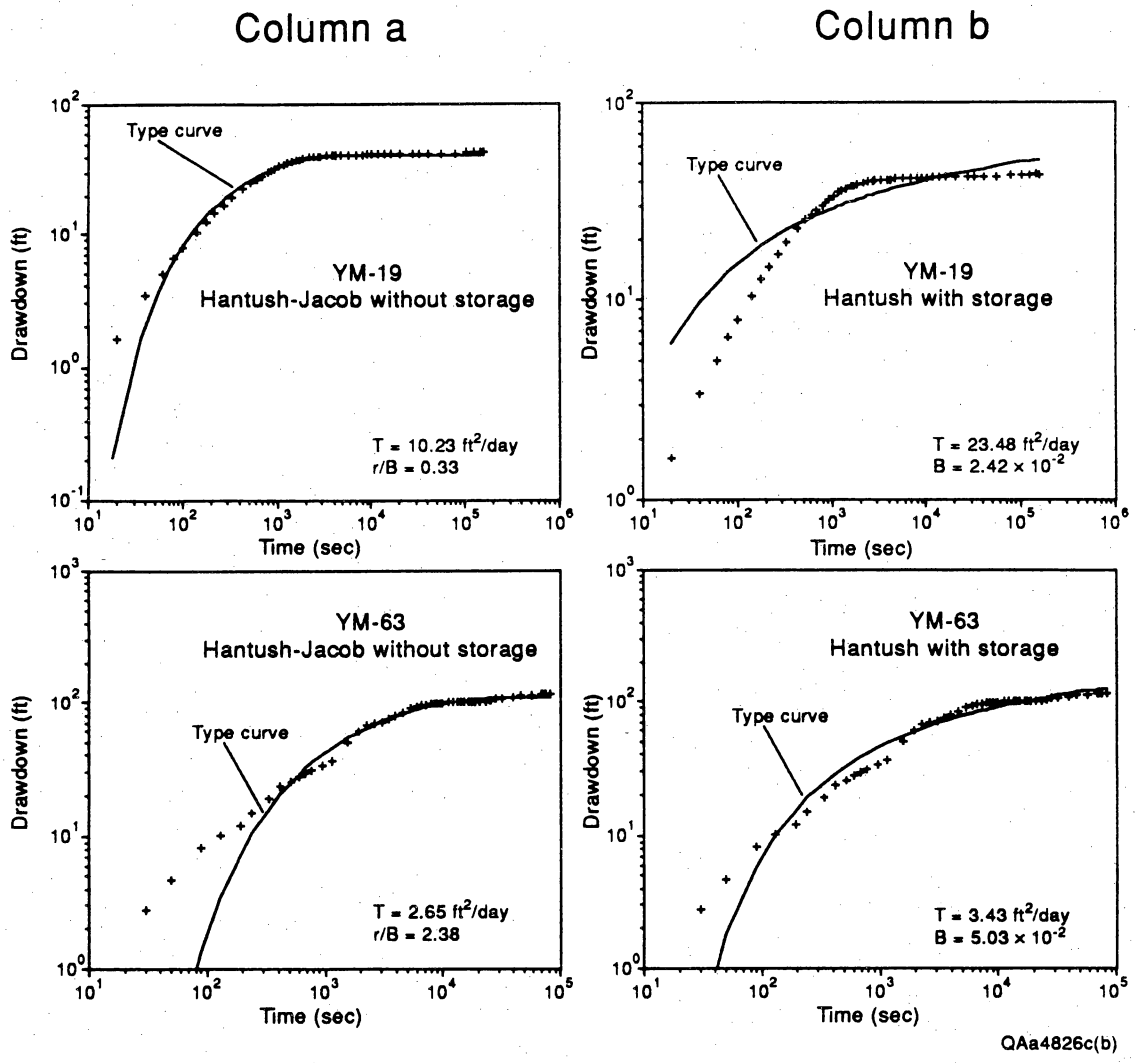

Figure 11 (continued). Comparison of curve matches for wells in northwest Eagle Flat, using analytical solutions for leaky confined aquifers. Curve matches for leaky aquifers without storage in aquitards (Hantush-Jacob, 1955) typically provided the best curve fit (column a). Curve matches for leaky aquifers with storage in aquitards (Hantush, 1960) generally provided a poor curve fit (column b). During early-time drawdowns (e.g., 10 to 500 seconds) curve matches are poor, probably as a result of wellbore storage. Very good fits were provided for intermediate and late-time drawdowns using the Hantush-Jacob (1955) method (column a). Poor curve fits generally were provided by the Hantush (1960) method for early, intermediate, and late-time drawdowns.

Table 3. Estimates of transmissivity and hydraulic conductivity provided by specific capacity data and Walton's (1962) method. Two storage coefficients are used in the formulation, one for an unconfined aquifer and one for a confined aquifer. Calibrated transmissivities obtained by multiplying raw transmissivity estimates by 1/3. Hydraulic conductivity computed by dividing the transmissivity by the saturated aquifer section occupied by the well. Such an approximation overestimates hydraulic conductivity if a well is partially penetrating.

TRANSMISSIVITY ESTIMATES FROM SPECIFIC CAPACITY DATA (FT-SQ./DAY)				
Well #	Raw estimates (S = 0.0005)	Raw estimates (Sy = 0.14)	Calibrated estimates (S = 0.0005)	Calibrated estimates (Sy = 0.14)
YM-7A	384.36	199.20	128.12	66.40
YM-8	10.96	5.61	3.65	1.87
YM-18	44.12	26.07	14.71	8.69
YM-19	61.50	36.10	20.50	12.03
YM-63	10.70	5.76	3.57	1.92
48-64-BTH	401.07	256.68	133.69	85.56
48-45-603	2673.80	1537.43	891.27	512.48
48-53-101	1.20	0.46	0.40	0.15
48-53-801	7620.32	5347.59	2540.11	1782.53
48-53-802	1671.12	989.30	557.04	329.77
48-53-902	2807.49	1898.40	935.83	632.80
48-54-201	61497.33	43048.13	20499.11	14349.38
48-54-401	167.25	106.95	55.75	35.65
48-56-802	244.65	140.37	81.55	46.79
48-62-TEX	7085.56	4278.07	2361.85	1426.03

HYDRAULIC CONDUCTIVITY ESTIMATES FROM SPECIFIC CAPACITY DATA (FT/DAY)				
Well #	Raw estimates (S = 0.0005)	Raw estimates (Sy = 0.14)	Calibrated estimates (S = 0.0005)	Calibrated estimates (Sy = 0.14)
YM-7A	1.89	0.98	0.63	0.33
YM-8	0.034	0.017	0.011	0.0058
YM-18	0.56	0.33	0.19	0.11
YM-19	0.65	0.38	0.22	0.13
YM-63	0.058	0.031	0.019	0.01
48-64-BTH	7.71	4.94	2.57	1.65
48-45-603	17.94	10.32	5.98	3.44
48-53-101	0.0028	0.0011	0.00094	0.00035
48-53-801	357.76	251.06	119.25	83.69
48-53-802	55.70	32.98	18.57	10.99
48-53-902	58.49	39.55	19.50	13.18
48-54-201	1618.35	1132.85	539.45	377.62
48-54-401	1.22	0.78	0.41	0.26
48-56-802	2.05	1.18	0.68	0.39
48-62-TEX	12.77	7.71	4.26	2.57

by the calibration factor (1/3). Columns 4 and 5 (table 3) present calibrated results.

Results indicate heterogeneity in the bedrock units in the regional study area (e.g., hydraulic conductivity estimates vary from 0.00094 ft/day to 539.45 ft/day [0.00029 m/day to 164.42 m/day] using calibrated hydraulic conductivity estimates and a storage coefficient of 0.0005). This heterogeneity probably arises as a result of different rock types in the stratigraphic column, and localized areas of more intensive fracturing resulting from Laramide or younger tectonism. Beneath Faskin Ranch, transmissivity values are very low (see tables 2 and 3; wells YM-8, YM-63, YM-18, YM-19). The small range of transmissivity (2.4 to 10.2 ft^2/day [0.2 to 0.95 m^2/day]; Hantush-Jacob [1955] method for example), indicates fairly homogeneous water-bearing units beneath the ranch.

Saturation Indices, Hydrochemical Facies, and Temperatures

WATEQF analyses (fig. 12) indicate that ground water is typically at equilibrium with respect to calcite, and dolomite, although there is a much wider range of values for the latter. Despite the high sulfate content of many samples, none of the areas appears to be consistently within the range of values indicating equilibrium with respect to gypsum. Many samples are either at or very near saturation with respect to fluorite. In all cases, waters are undersaturated with respect to halite.

Ground water in the northern half of southeast Eagle Flat is Ca-Mg-HCO_3 except near the village of Allamoore, where it is SO_4-dominant (48-64-602 and 47-57-401) (fig. 13). Total dissolved solids range from 600 to 1500 mg/L, and temperatures are 19 to 25°C (table 4). The depth to water is between 50 to 200 ft (15 to 61 m) across much of the area. Southward, the proximal area of the Eagle Mountains fan is dominated by Ca-HCO_3 ground water, with total dissolved solids around 500 mg/L, and temperatures of 14 to 22°C (table 4). Water depths are typically less than 50 ft (15 m), and temperatures at these locations fluctuate by several degrees centigrade from month to month.

Down gradient from the Eagle Mountains fan in the Scott's Crossing area, Na-HCO_3 ground water is found at depths as great as 600 ft (183 m) in thick deposits of basin fill. Total dissolved solids are less than 400 mg/L. Temperatures at Scott's Crossing are among the highest in southeast Eagle Flat. White and others (1980) reported a temperature of 42°C, and a geothermal

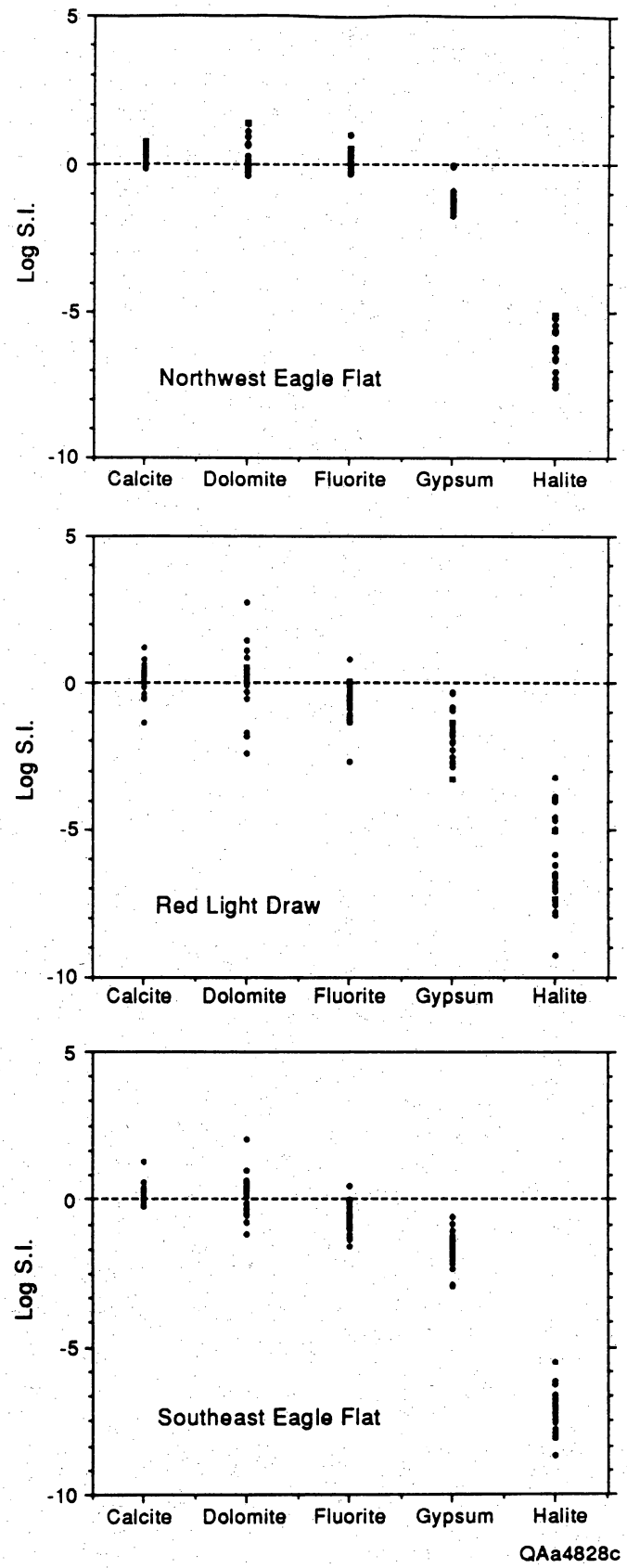

Figure 12. Range of saturation indices of calcite, dolomite, fluorite, gypsum, and halite for northwest Eagle Flat, Red Light Draw, and southeast Eagle Flat.

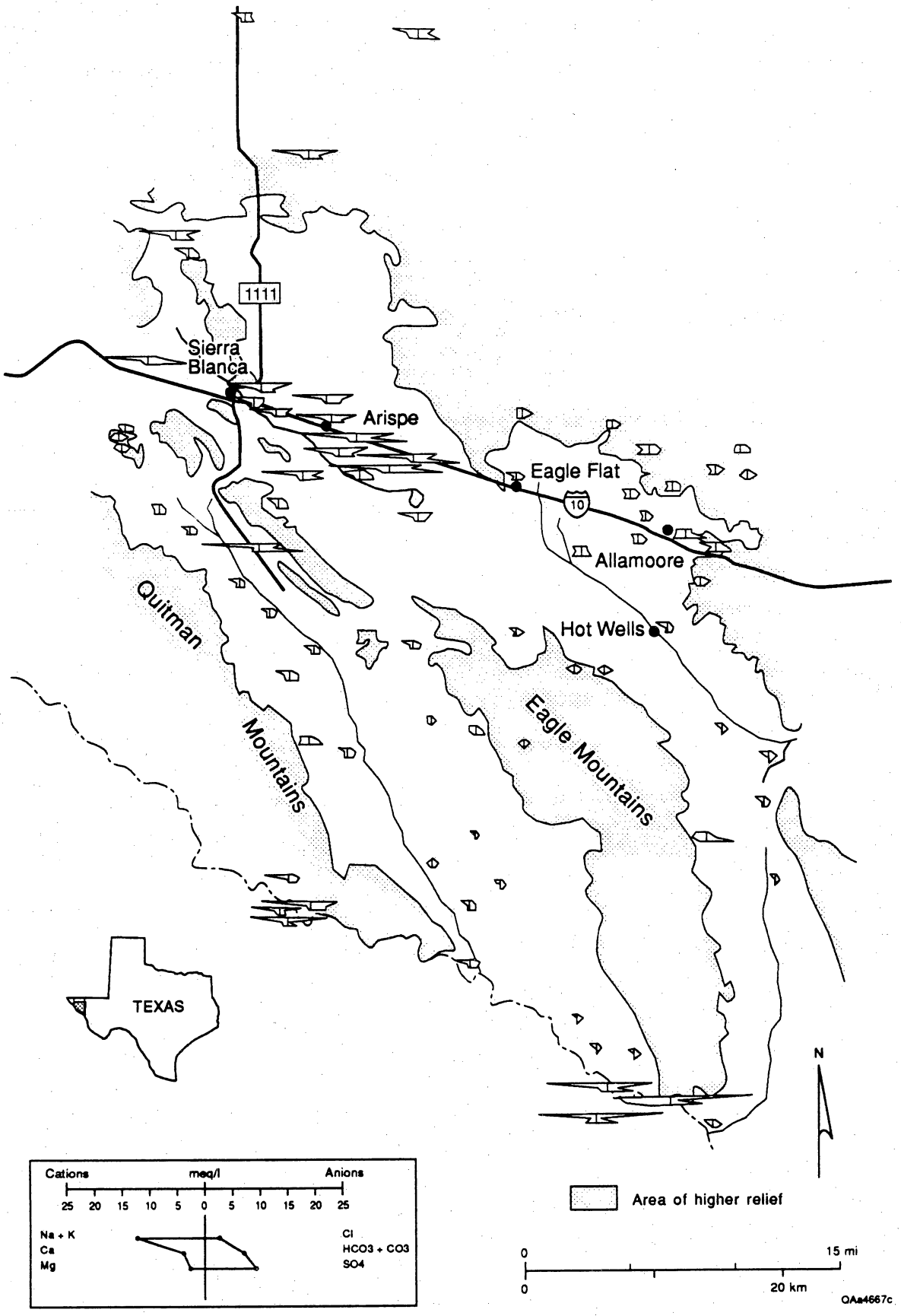

Figure 13. Hydrochemical composition of ground water in Eagle Flat and surrounding area. The hydrochemical composition is represented by Stiff diagrams.

Table 4. Hydrochemical analyses of ground-water samples from southeast Eagle Flat, northwest Eagle Flat, and Red Light Draw. Cations and anions reported in mg/L; $\delta^{18}O$ and $\delta^{2}H$ reported in $^{o}/oo$ values (SMOW); ^{3}H reported in tritium units (TU); $\delta^{13}C$ in $^{o}/oo$ values (PDB); and ^{14}C reported as percent modern carbon (PMC).

Sample ID Number	Date Collected	pH	Temp. Deg. C	SiO2	Na	K	Mg	Sr	Ca	Cl	F	Br	NO3	SO4	HCO3	O18	2H	3H	C13	C14
Southeast Eagle Flat																				
47-49-GTM	1/12/92	7.4	20.2		80	1.5	56.7		104	76	0.8		29.4	242	325	-6.7	-44	6.5	-9.4	103.3
47-49-GHM	1/12/92	7.1	21.5		33	1.5	15.6		85	12	0.4		10.8	43	342	-6.6	-42	6.3	-11.8	109.9
47-49-GHW	1/13/92	7.4	19.8		101	1.5	47.4		54	40	0.7		24.8	127	525	-7.0	-40	6.0	-10.1	108.5
47-57-401	10/29/91	7.5	18.8		284	5.6	65.3		48	107	5.8		14.9	449	526	-6.9	-44	2.2		
47-57-KHN	11/3/91	7.1	21.1		77	2.1	33.1		80	43	1.1		9.0	110	369					
47-57-KHN	1/8/92	7.2	21.8												370	-7.0	-41	7.7	-12.6	100.8
48-55-902	5/28/92	7.3	20.9	59.3	57	2.1	33.8	0.6	58	20	0.9	0.3	18.7	59	361	-5.2	-30			
48-56-803	1/10/92	7.3	19.2		63	1.5	30.0		55	39	0.4		27.0	79	284	-7.6	-49	3.7	-6.6	62.8
48-56-DES	1/10/92	6.9	18.7		178	1.5	81.2		89	178	0.9		28.4	262	456	-7.5	-40	4.5	-8.4	79.5
48-56-DES	8/11/92	7.1	20.2	34.2	182	1.9	85.4	1.42	92	166	2.2	1.4	28.3	293	502					
48-64-302	10/31/91	7.4	19.1		106	3.4	57.4		55	68	1.3		30.9	217	335	-6.8	-49	3.1	-6.9	47.1
48-64-301	10/29/91	7.4	20.1		121	2.1	56.3		65	83	2.2		39.6	189	366	-6.7	-46	5.2	-9.7	94.4
48-64-602	10/28/91	7.3	21.8		161	4.6	108.0		140	145	1.3		38.7	717	228					
48-64-602	12/18/91	7.2	21.6												230	-6.6	-42	1.5	-7.0	23.5
48-64-604	10/28/91	7.4	20.5		115	2.2	37.4		46	54	1.8		17.0	175	305					
48-64-604	12/15/91	7.1	20.2													-6.9	-49	3.0	-6.3	45.1
48-64-604	8/14/92	7.6	22.2	25.0	127	3.3	41.7	0.6	50	57	2.1	0.5	14.8	201	356	-7.1	-46	2.7		
48-64-LOV	10/29/91	7.4	21.4		74	2.2	36.7		49	45	0.9		14.5	99	311					
48-64-LOV	12/15/91	7.3	21.4												311	-7.2	-49	0.4	-8.2	52.5
50-08-101	11/1/91	7.0	18.7		30	2.3	7.7		95	21	1.5		5.8	74	326	-8.3	-56	6.8		
50-08-102	12/12/92	7.1	16.8	35.7	131	4.5	47.5	2.0	172	41	2.9	0.3	0.1	491	464	-8.3	-55			
50-08-202	11/2/91	7.1	18.7		20	1.4	9.3		113	16	1.0		78.7	107	285	-7.8	-52	7.0		
51-01-501	6/25/92	8.3	29.7	38.7	132	1.5	1.2	0.2	8	8	3.4	0.3	4.8	43	384	-9.7	-52	0.0	-7.0	5.4
51-01-501	1/9/92	8.1	14.0		132	1.5	1.1		8	8	3.9		4.3	43	280	-9.3	-59	0.0	-6.9	6.8
51-01-501	5/31/92	8.0	24.5	37.4	134	1.5	1.2	0.2	8	9	3.6	0.3	4.0	44	336	-9.3	-56			
51-01-503	10/31/91	8.3	23.3	18.0	98	2.4	3.2	0.2	8	5	2.4		3.0	34	307					
51-01-503	12/18/91	7.8	23.2													-9.5	-56	0.0	-4.7	2.2
51-01-801	6/28/92	8.7	26.9	16.9	82	1.7	1.9	0.3	8	17	1.5	0.3	5.5	35	215	-9.8	-63	0.0	-5.6	5.6
51-10-103	2/8/93	7.6	28.2	25.0	101	6.7	10.3	0.4	29	21	2.8	0.2	7.7	80	253					

Table 4

Sample ID Number	Date Collected	pH	Temp. Deg. C	SiO2	Na	K	Mg	Sr	Ca	Cl	F	Br	NO3	SO4	HCO3	O18	2H	3H	C13	C14
Northwest Eagle Flat																				
48-45-603	8/10/92	7.4	27.4	16.0	577	20.9	41.1	2.41	91	546	4.1	1.1	3.9	485	477	-8.7	-59	0.0	-5.0	6.1
48-45-901	5/24/92	7.3	27.5	26.9	226	3.0	27.1	1.17	64	87	3.2	0.6	16.4	316	373	-8.3	-51	1.4	-6.4	23.0
48-53-501	1/13/92	7.2	23.2		751	2.0	34.1	4.79	86	149	3.0	0.7	0.1	1170	703	-8.0	-52	0.4	-6.1	12.7
48-53-501	5/26/92	7.0	25.1	16.7	779	2.1	36.1		92	154	2.2	1.5	0.1	1250	670	-8.3	-52	0.3	-6.2	7.2
48-53-802	6/26/92	7.2	23.3	20.8	64	1.5	12.9	0.82	112	35	1.4	0.3	7.7	146	329	-7.9	-47	2.0	-9.4	47.3
48-53-803	5/28/92	7.2	20.6	25.7	52	1.7	13.9	1.01	141	22	1.3	0.3	1.9	158	361	-8.1	-45	1.7	-9.4	42.4
48-54-404	10/30/91	7.2	32.0		402	22.6	13.4		44	357	5.1		15.1	289	385					
48-54-404	6/1/92	7.2	32.0	22.9	433	25.0	14.2	1.50	51	361	4.9	0.9	13.1	332	356	-8.1	-54	0.7	-4.9	8.5
48-54-502	8/13/92	7.5	26.8	13.3	582	27.0	25.5	2.68	77	600	5.0	5.0	5.0	410	450	-8.8	-54	0.0	-4.3	4.7
48-62-TEX	3/3/93	7.8	24.0	14.1	163	2.9	27.4	1.87	64	70	2.2	0.6	5.7	277	313	-8.0	-55	1.0	-7.3	11.4
48-62-TEX	5/27/93	7.6	25.3	15.4	165	2.2	26.4	2.05	67	68	2.2	0.7	6.1	265	333	-8.4	-53		-6.7	9.8
48-62-TEX	7/28/93	8.2	27.1	28.8	185	8.7	5.9	0.59	11	25	5.5	0.2	0.2	128	339	-8.9	-57	0.9	-10.5	80.5
48-63-302	10/31/91	7.6	23.1		148	2.9	40.9		43	62	2.4		8.7	197	387					
48-63-302	12/17/91	7.3	23.6													-7.3	-46	0.4	-7.9	27.6
48-63-302	5/30/92	7.5	25.5	24.4	153	3.1	45.5	0.95	44	68	2.1	0.6	6.5	221	374	-7.7	-34	0.4	-7.5	29.5
YM-7A	6/23/92	7.2	29.5	20.2	305	20.3	26.6	1.23	70	316	3.2	0.8	0.8	161	439	-8.3	-47	0.0	-6.0	5.8
YM-7A	11/20/92	7.0	31.8	21.6	308	19.8	26.4	1.22	69	314	2.6	0.7	0.8	181	462	-7.8	-54	0.0	-6.4	8.1
YM-7A	3/5/93	7.1	33.4	20.3	303	20.4	25.0	1.15	71	320	2.3	0.5	1.4	202	380	-7.9	-55	0.0	-6.2	6.0
YM-7A	5/25/93	7.2	33.4	21.2	298	21.1	24.5	1.26	71	319	2.7	0.5	2.0	171	406	-9.1	-57	0.0	-6.5	6.0
48-63-902	11/2/91	7.6	16.1		96	2.2	24.4		31	22	3.8		10.2	63	348					
48-63-902	1/8/92	7.5	21.4													-7.8	-52	0.0	-6.6	21.2
48-63-902	7/16/92	7.6	22.0	39.4	93	2.6	23.8	1.36	29	19	3.1	0.1	8.9	63	340	-7.8	-45	0.2	-6.6	22.8
48-64-BTH	8/30/93	7.2	29.0	26.4	109	3.1	56.3	1.53	56	76	1.4	0.6	15.1	284	220	-7.4	-50	0.0	-7.7	10.1
50-07-301	8/30/93	7.0	20.0	36.4	35	1.5	5.7	0.36	86	25	0.5	0.4	7.0	47				4.1		
YM-18	3/1/93	7.5	28.2	12.4	934	17.5	26.7	2.11	75	464	4.9	2.3	24.8	1170	370	-8.3	-56	0.0	-5.7	3.8
YM-18	5/25/93	7.4	29.1	13.3	954	17.4	33.8	2.58	93	445	5.3	2.7	25.3	1380	447	-8.3	-53	0.0	-5.8	4.5
YM-18	7/29/93	7.2	29.0	13.1	962	16.5	29.5	2.07	79	457	6.3	2.3	24.8	1233	477	-8.0	-50	0.0	-5.9	1.7
YM-19	2/3/93	7.1	28.4	14.7	645	33.1	32.6	2.11	96	547	3.9	2.0	5.4	683	357	-9.2	-61		-5.9	3.7
YM-19	5/27/93	7.3	29.3	15.2	625	33.3	32.2	2.07	100	483	4.9	1.3	5.3	671	385	-9.2	-61	0.0		
YM-19	7/30/93	7.3	29.5	15.9	652	30.8	29.2	1.99	91	509	5.4	2.3	5.5	659	396	-10.0	-64	0.0	-7.4	1.3
YM-63	8/20/93	7.1	30.4	14.1	1200	28.6	59.3	4.36	180	779	6.5	3.9	46.3	1716	306	-8.3	-50	0.0	-7.2	1.3
YM-8	11/21/92	7.2	25.7	12.6	285	3.8	28.8	1.67	65	96	3.0	0.9	0.8	431	582	-8.3	-56	1.0	-5.2	3.9
YM-8	5/26/93	7.2	26.8	13.0	280	3.6	31.3	1.99	78	95	2.7	0.7	1.0	445	433	-8.6	-55	0.0	-5.3	4.6

Table 4

Sample ID Number	Date Collected	pH	Temp. Deg. C	SiO2	Na	K	Mg	Sr	Ca	Cl	F	Br	NO3	SO4	HCO3	O18	2H	3H	C13	C14
Red Light Draw																				
48-61-201	7/7/92	7.2	25.4	21.4	117	2.4	33.9	3.5	57	32	1.8	0.4	0.8	218	316	-8.3	-52	0.4	-5.0	5.9
48-62-BOR	7/7/92	7.4	22.5	14.8	1008	3.3	62.3	4.7	89	525	8.2	3.6	53.4	1390	539	-6.1	-39	0.0	-4.2	26.1
48-62-701	8/18/70	7.5	18.0	5.0	119		23.0		26	33	2.3		1.5	171						
48-62-805	7/18/92	7.6	25.8	19.4	141	2.8	19.0	1.5	35	45	2.2	0.4	6.7	156	275	-8.5	-55			
50-06-203	7/2/92	8.6	27.8	15.5	206	4.4	37.1	3.3	54	65	3.0	0.3	0.8	355	386	-8.1	-53	0.0		
50-06-301	5/29/92	7.6	27.3	22.9	131	2.2	18.2	1.7	37	39	1.9	0.3	4.7	164	336	-8.3	-50	0.0	-5.6	8.0
50-06-501	7/2/92	7.5	26.7	39.8	140	3.5	30.2	3.0	56	71	2.0	0.8	11.6	191	283	-8.4	-54	0.0		
50-06-501	5/14/93	7.3	25.9	44.5	134	3.2	27.3	3.1	58	73	2.1	0.5	10.2	203	323	-8.7	-55	0.0		
50-06-801	8/28/93	7.8	22.0	7.0	130	2.5	76.6	11.8	102	18	1.6	0.1	5.0	461	412	-6.8	-41	1.3		
50-07-401	6/27/92	7.7	29.0	35.7	48	1.7	6.6	0.6	47	14	0.6	0.1	6.7	50	217	-8.0	-47	0.0	-6.9	8.0
50-07-MCM	8/9/92	7.5	24.6	16.0	124	3.1	26.8	1.2	45	41	1.7	0.4	6.2	155	355					
50-07-MCM	7/18/92	7.4	23.4	15.1	147	3.2	28.1	1.2	47	49	1.9	0.5	5.8	179	392	-8.1	-43	0.0	-7.9	15.2
50-07-601	8/18/93	7.0	25.6	14.1	100	1.2	8.2	0.8	83	29	2.1	0.3	0.6	224	211	-7.9	-44	1.3	-10.7	54.3
50-07-FRC	7/3/92	6.8	19.3	33.2	27	2.5	7.0	0.3	76	19	1.0	0.3	6.7	51	236	-8.5	-45	6.9		
50-14-503	7/6/92	6.7	41.3	41.9	2420	143.0	33.0	3.7	140	2870	2.7	2.1	7.7	1230	970	-6.8	-49	0.0	-2.7	2.1
50-14-RBL	1/28/93	7.7	31.3	38.5	346	8.2	1.7	0.5	15	95	2.6	0.3	0.1	281	555	-8.6	-57			
50-15-101	5/15/93	7.7	22.0	46.0	12	1.2	14.5	1.5	55	2	1.6	0.1	18.5	14	220	-7.8	-49	6.2		
50-15-201	6/29/92	8.2	26.8	22.7	99	1.5	2.0	0.5	9	30	2.7		10.3	47	196	-8.5	-41	0.0	-5.4	3.7
50-15-WBG	6/30/92	8.4	24.6	24.6	126	4.1	15.9	1.9	48	86	1.0	0.6	11.6	167	201	-8.5	-58	0.0		
50-15-801	5/12/93	7.7	23.0	62.9	240	3.8	12.9	1.5	37	101	3.3	0.4	14.5	202	343	-8.1	-52	2.6		
50-16-703	5/13/93	8.4	26.6	32.3	62	2.3	3.5	0.5	11	17	2.8	0.2	9.0	25	223	-8.5	-54	0.0	-8.5	4.3
50-24-202	7/4/92	7.4	25.4	40.4	992	6.3	41.0	3.4	120	1040	0.8	1.5	0.8	842	322	-10.4	-76	0.0		
50-24-301	7/4/92	8.5	33.2	20.3	80	3.7	4.2	0.8	12	14	1.2	0.1	6.4	40	263	-7.7	-42	0.0	-7.1	3.4
50-24-503	1/9/93	7.0	23.0	29.9	811	13.4	150.0	22.0	585	1810	0.5	1.9	0.8	1040	196	-9.3	-64			
50-24-503	5/12/93	7.0	23.5	31.7	770	12.7	138.0	24.1	589	1894	0.4	1.7	0.8	1010	209	-9.2	-67	4.2		
50-24-SHT	10/22/92	8.8	25.4	55.2	88	2.3	1.4	0.1	4	17	2.3	0.5	6.3	31	170	-8.5	-54			

gradient of 75°C/km at Hot Wells (48-64-901). Gates and White (1976) also reported a temperature of 38°C and a geothermal gradient of 32°C/km in a 2100-ft (641 m) water test well (50-01-504) 5.5 mi (8.8 km) southeast of Hot Wells. Temperatures between 24 and 30°C were recorded at three other Scott's Crossing locations (51-01-501, 51-01-503, and 51-01-801) during this investigation.

Northwest Eagle Flat ground water (fig. 13, table 4) is distinguished from the water resources of southeast Eagle Flat by a marked increase in total dissolved solids, and warm temperatures throughout the basin. Ground water is characteristically Na-Cl to Na-SO_4-Cl, with salinities between 1,000 mg/L and 4,000 mg/L. The highest salinities are associated with the SO_4-dominated waters of 48-54-901, YM-18, and YM-63 (figs. 13 and 14).

Water wells in northwest Eagle Flat are among the deepest in the study area, many drilled to depths of 1,000 ft to 1,300 ft (305 m to 396 m). Average temperature is 30°C, decreasing to near 25°C in the vicinity of Devil Ridge, where some of the most dilute water in the area is extracted by wells drilled to depths of 900 ft and 1,500 ft (YM-8 and 48-62-TEX). Hoffer (1978) reported a temperature of 38°C from a 950-ft (290-m) well (48-54-402) at Sierra Blanca. Abandoned since Hoffer's (1978) study, the well is no longer usable, and the temperature could not be verified. Temperatures of 34°C were recorded in an 880-ft (268-m) deep monitor well (YM-7A) at Grayton Lake, 10 mi (16 km) east of Sierra Blanca. Ground water from areas west of Sierra Blanca is also highly variable in composition, ranging from dilute Ca-HCO_3 and Na-HCO_3 water in three wells (48-53-801, 48-53-801, and 48-53-804) in an abandoned municipal well field 5 mi (8 km) southwest of Sierra Blanca, to higher-TDS Na-SO_4-Cl and Na-Cl water in deep wells (48-53-501, 48-45-602, and 48-45-603) near the Sierra Blanca Peaks.

Many wells in Red Light Draw yield Na-HCO_3 ground water, except in areas near the Rio Grande, where substantially more saline Na-Cl ground water predominates. Total dissolved solids in Red Light Draw range from 300 mg/L to more than 10,000 mg/L, with the highest concentrations occurring in the Rio Grande alluvium, an area once heavily irrigated by cotton farmers (Mann Bramblett, personal communication, 1993). At Indian Hot Springs, Na-Cl water with more than 7,000 mg/L of dissolved solids discharges along the Caballo fault, into river alluvium (Henry, 1979).

Although ground water in most areas of Red Light Draw is of good quality, there is a noticeable increase in total dissolved solids toward the Quitman Mountains (figs. 13 and 14). Wells in the Eagle Mountains and in the

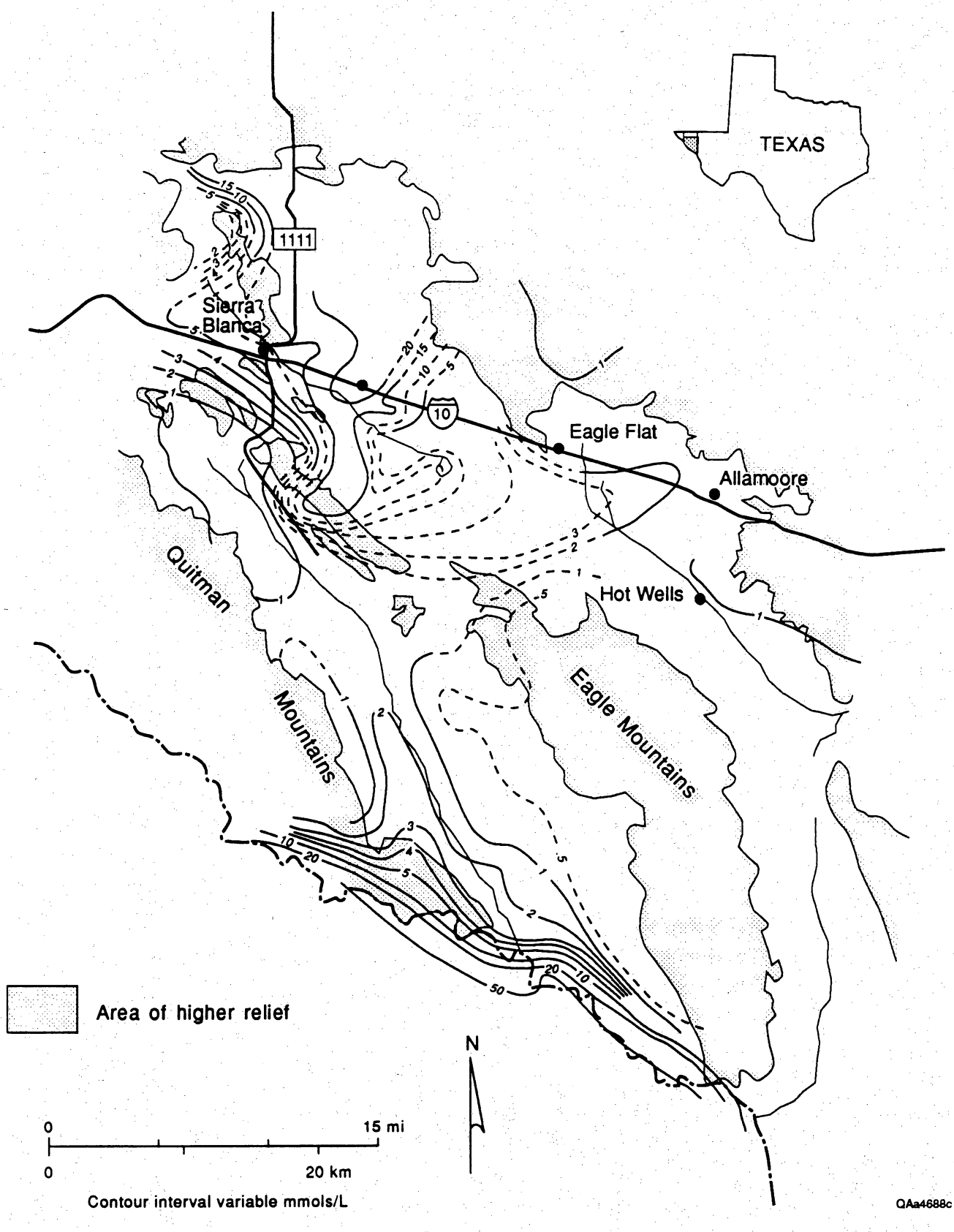

Figure 14. Chloride concentration (mmol/L) of ground water in Eagle Flat and surrounding area.

fans built outward from the Eagle Mountains and the Indio Mountains produce water that is Ca-HCO_3 to Na-HCO_3 in composition, with total dissolved solids typically between 300 and 500 mg/L. The wells are of variable depths, ranging from less than 50 ft (15 m) in the mountains to more than 500 ft (152 m) in the fan deposits. Gates and White (1976) drilled a 1,200-ft (366-m) water test well (50-07-501) as part of their exploration program for potable ground-water resources in the Trans-Pecos region. A water sample collected from fan material at a depth of 1,100 ft (335 m) showed no appreciable increase in total dissolved solids (326 mg/L) over other wells in the eastern half of the basin (Gates and White, 1976). Samples from shallower depths were contaminated by drilling fluid (Gates and White, 1976).

Wells in the western half of Red Light Draw yield water that is Na-HCO_3-SO_4 to Na-SO_4-HCO_3 in composition, with TDS and SO_4 increasing toward the south. Dissolved solids increase from 600 to 800 mg/L in the upper part of Red Light Draw, to 1,200 mg/L (50-07-801) in the lower part of the draw. With the exception of a few wells and springs near the Rio Grande, ground-water temperatures are generally 3 to 4°C lower than temperatures in northwest Eagle Flat. Average water temperature is 26°C; low temperatures are around 22°C; and high temperatures range from 33°C in southeast Red Light Draw (50-24-301) to more than 40°C at Indian Hot Springs (50-14-501).

Chloride concentration varies significantly in southern Hudspeth County (fig. 14). The lowest levels are in areas with HCO_3-dominant ground water. This includes all of southeast Eagle Flat, the abandoned well field west of Sierra Blanca, and most of Red Light Draw. In northwest Eagle Flat, chloride rises to more than 700 mg/L (20 mmol/L) at the proposed low-level radioactive waste disposal site, decreasing to less than 70 mg/L (2 mmol/L) at the northwest end of Devil Ridge (48-62-TEX). With the exception of 48-62-BOR (depth unknown), drilled to supply water to a 16,000-ft (4877-m) exploration well, most wells in Red Light Draw produce water with less than 50 mg/L (1.4 mmol/L) of chloride. Well 48-62-BOR lies on the southwest side of Devil Ridge, 2 mi (3.4 km) south of 48-62-TEX, a well with one of the lowest chloride levels in northwest Eagle Flat.

Chloride rises sharply within 2 mi (3.4 km) north of the Rio Grande, but the increase is first seen nearly 10 mi north of the river, in 50-06-LOV, where the concentration is 72 mg/L (2.03 mmol/L) (fig. 14). From there southward, Cl rises to more than 1,000 mg/L in wells along the terrace overlooking the Rio Grande floodplain (table 4; White and others, 1980). The increased chlorinity in southern

Red Light Draw is accompanied by a sharp rise in the Cl/Br molar ratio (fig. 15). Figure 16 shows the marked differences in Cl/Br ratios with increasing TDS. Wells within the high-TDS zone form a distinct linear trend that extends upward from the cluster of low-TDS, low-Cl/Br points of lower Red Light Draw. This trend has significant implications for tracing the source of salinity in southern Red Light Draw (see "Origin of Solutes").

The ratio of sodium to chloride decreases with increasing salinity, approaching a value near 1.00 within the high-TDS zone of Red Light Draw (fig. 17A). The differences among the three basins are further underscored by the plot of Na versus Cl (fig. 17B). Only among the higher-TDS waters of Red Light Draw is there nearly a 1:1 relationship between Na and Cl. In northwest Eagle Flat, Na exceeds Cl by an average of 2:1; and the ratio is 3:1 or higher among the dilute ground waters of southeast Eagle Flat and Red Light Draw. Consistent with this observation is the increase in excess Na, estimated as (Na - Cl), with SO_4 (fig. 18).

Other binary plots not only point toward the variable hydrochemical signature of southern Hudspeth County ground water but also suggest the influence of dissolution, weathering, and ion-exchange processes. The (Ca + Mg)/HCO_3 molar ratio (fig. 19) varies from 0.10 to more than 1.00 within each area. Similarly, subtracting SO_4 from total Ca and Mg yields an estimate of the concentration of Ca and Mg not associated with sulfates. The plot of Ca + Mg - SO_4 versus excess Na (or Na - Cl) forms a downward-sloping trend described by the least-squares equation (fig. 20), (Ca + Mg - SO_4) = -0.414(Na - Cl) + 2.912, for which the coefficient of variation (r^2) is 0.95.

Carbon-14 and Tritium

The ^{14}C values of southern Hudspeth County ground water range from 109 PMC to less than 2 PMC (figs. 21 and 22). In southeast Eagle Flat, ^{3}H and ^{14}C values are locally among the highest in the study area, with median levels of 3.11 TU and 49.80 PMC (table 5). The highest TU and PMC values occur in the Bean and Millican Hills, the Carrizo Mountains, and the Eagle Mountains—areas where the potentiometric surface is high (fig. 5) and where bedrock is either

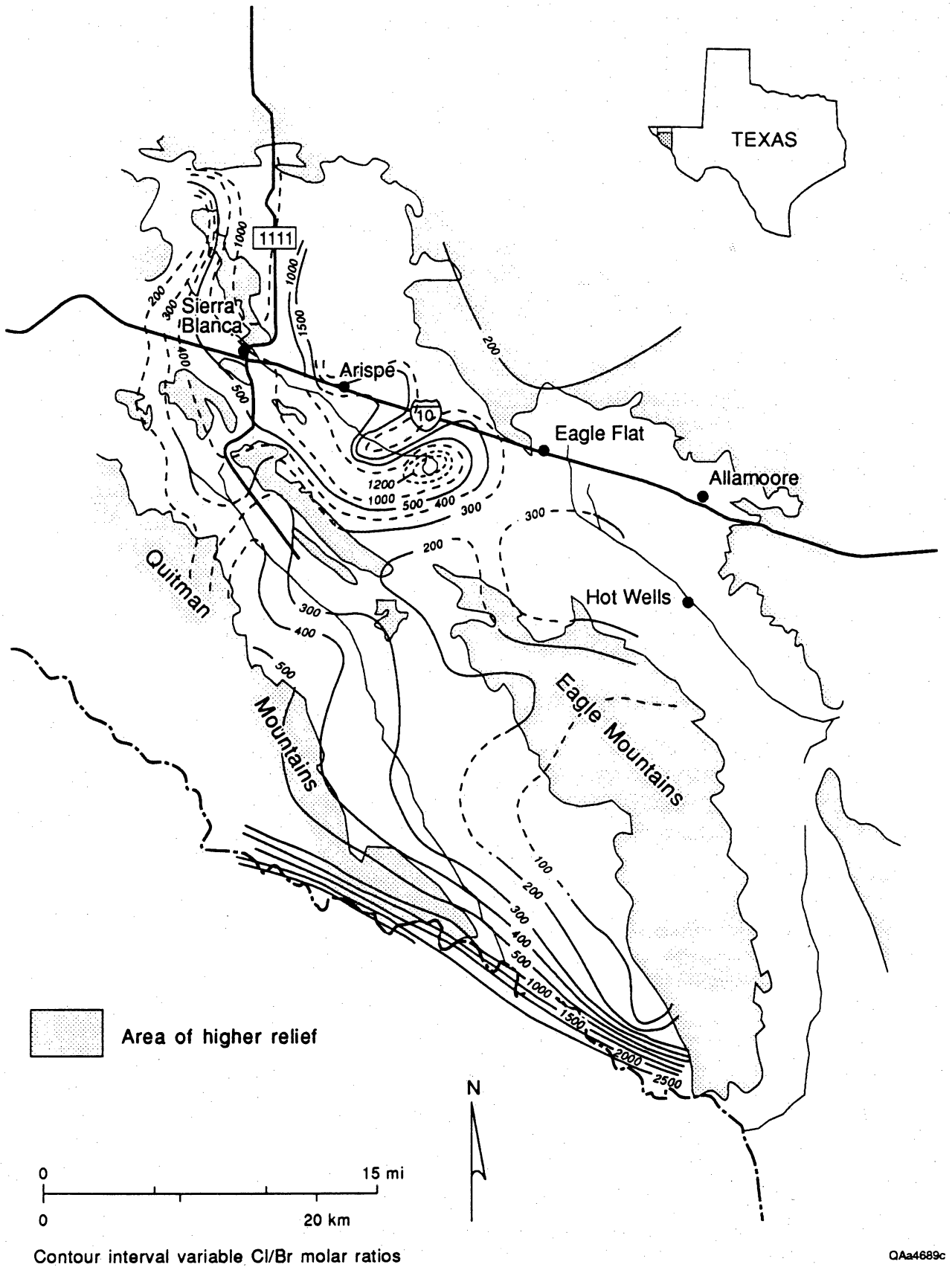

Figure 15. Map of Cl/Br mole ratios.

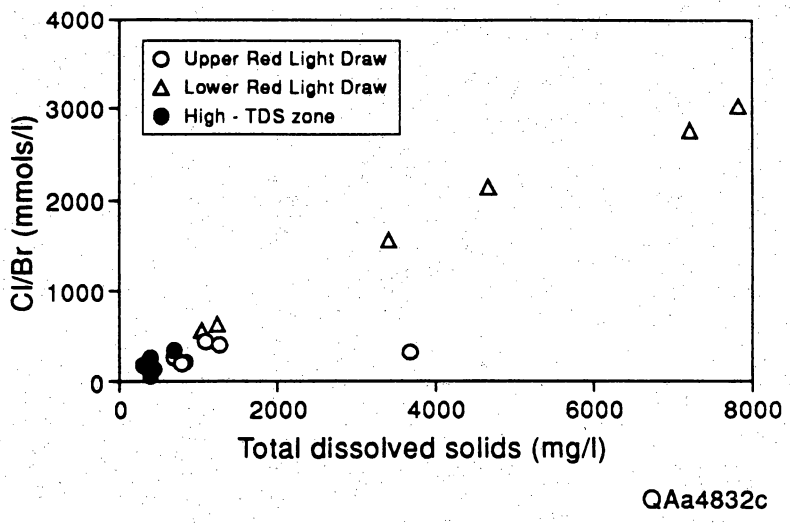

Figure 16. Plot of Cl/Br mole ratios versus TDS for Red Light Draw. The points within the high-TDS zone form an upward-sloping trend originating from within the lower TDS points of lower Red Light Draw. This is interpreted as an indicator of mixing between high-TDS, high-Cl/Br water with the more dilute ground water of lower Red Light Draw.

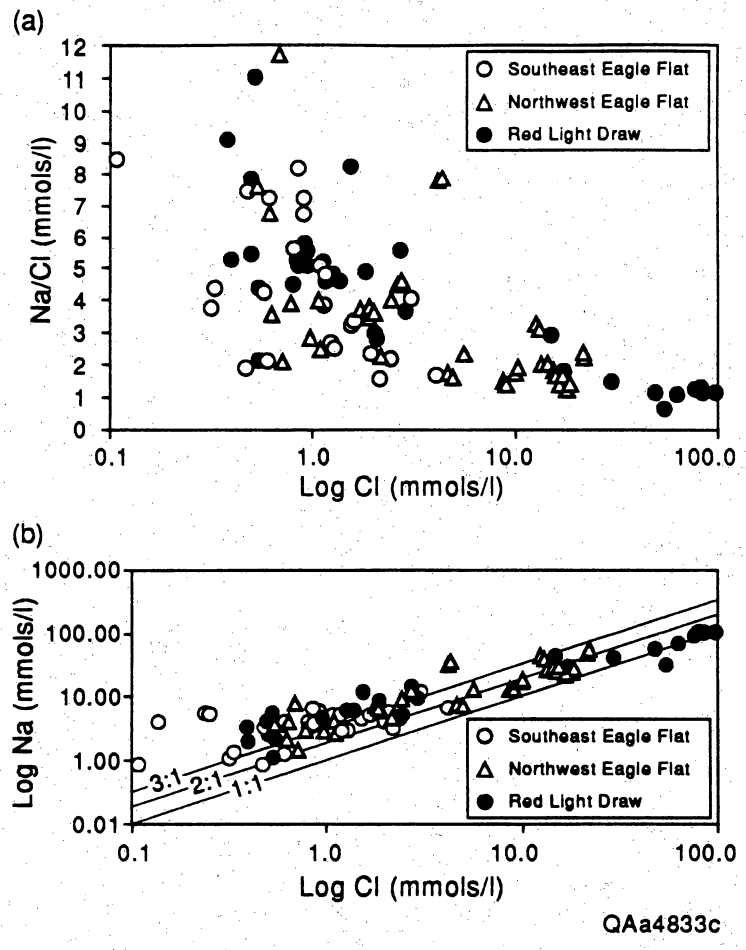

Figure 17. (A) Binary plot of Na/Cl mole ratios versus Cl (mmol/L). The downward sloping trend approaches a value of 1.00 at the highest Cl levels in Red Light Draw. The trend toward decreasing Na/Cl ratios suggests the influence of NaCl on the hydrochemical composition of ground water in the study area. (B) Binary plot of Na versus Cl (mmol/L) for southeast Eagle Flat, northwest Eagle Flat, and Red Light Draw. Dissolution of NaCl produces equimolar concentrations of sodium and chloride. A 1:1 mole ratio would result in a line with a slope of 1:1, as indicated for Red Light Draw. Situations involving excess Na lead to higher Na/Cl ratios, and to lines with slopes greater than 1:1 (southeast Eagle Flat and northwest Eagle Flat). The excess sodium may be contributed by mineral weathering or by exchange of divalent cations for Na on mineral surfaces.

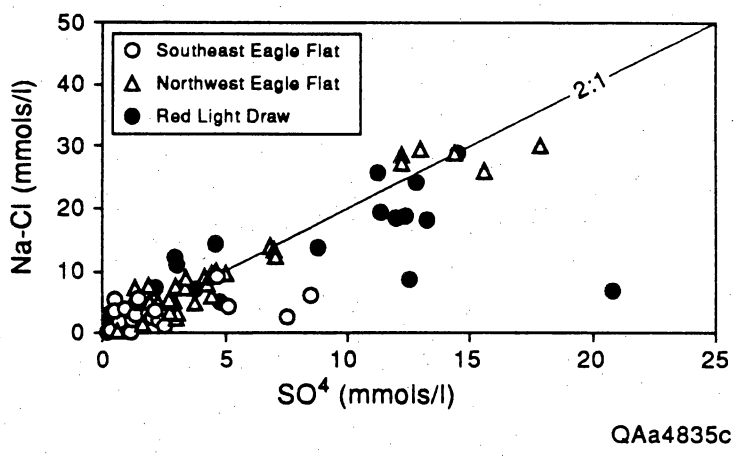

Figure 18. Binary plot of (Na-Cl) versus SO_4 for all areas. The quantity (Na-Cl) represents excess sodium, or that amount not attributable to dissolution of NaCl. The points form an upward sloping trend with an approximate slope of 2:1. This is interpreted as an indicator of the gain of Na through exchange reaction with calcium derived from the dissolution of gypsum. The slope of 2:1 is what would be expected in a divalent/monovalent cation exchange process.

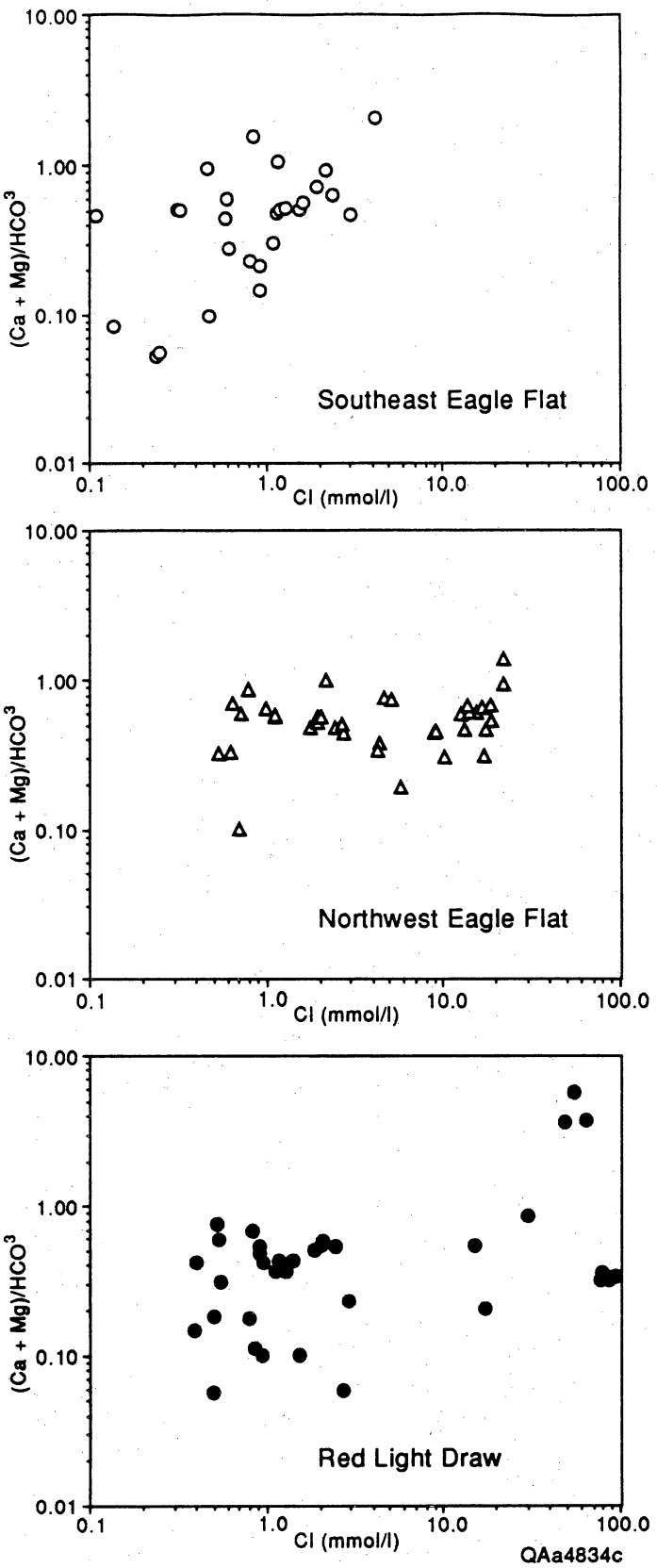

Figure 19. Binary plots of (Ca+Mg)/HCO^3 versus Cl (mmol/L) for (A) southeast Eagle Flat, (B) northwest Eagle Flat, and (C) Red Light Draw. If Ca and Mg were contributed only by calcite dissolution or by weathering of pyroxene and amphiboles, the (Ca + Mg)/HCO^3 ratio would equal 0.50. Lower ratios may indicate loss of Ca and Mg through exchange reactions for Na. Ratios greater than 0.50 indicate accessory sources of Ca and Mg, possibly from dissolution of evaporites.

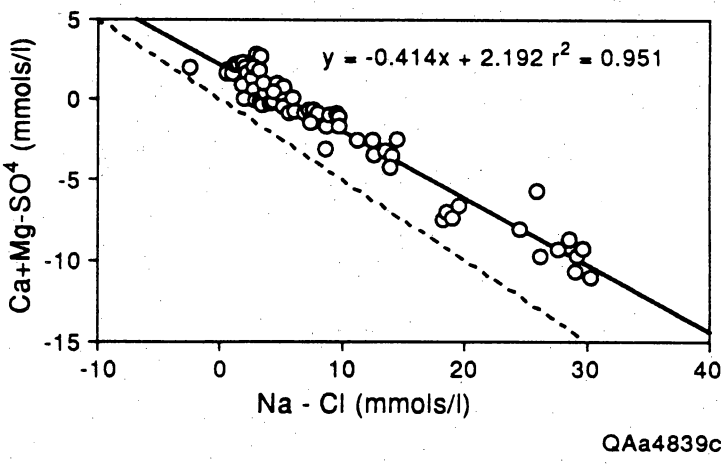

Figure 20. Binary plot of (Ca + Mg - SO_4) versus (Na - Cl). The quantity (Ca + Mg - SO_4) represents the molar concentration of Ca and Mg not associated with sulfates. The points for a downward trend interpreted to be the result of the loss of Ca and Mg in exchange reactions for Na. The quantity (Na-Cl) represents excess Na, as described in the text and in figure 14.

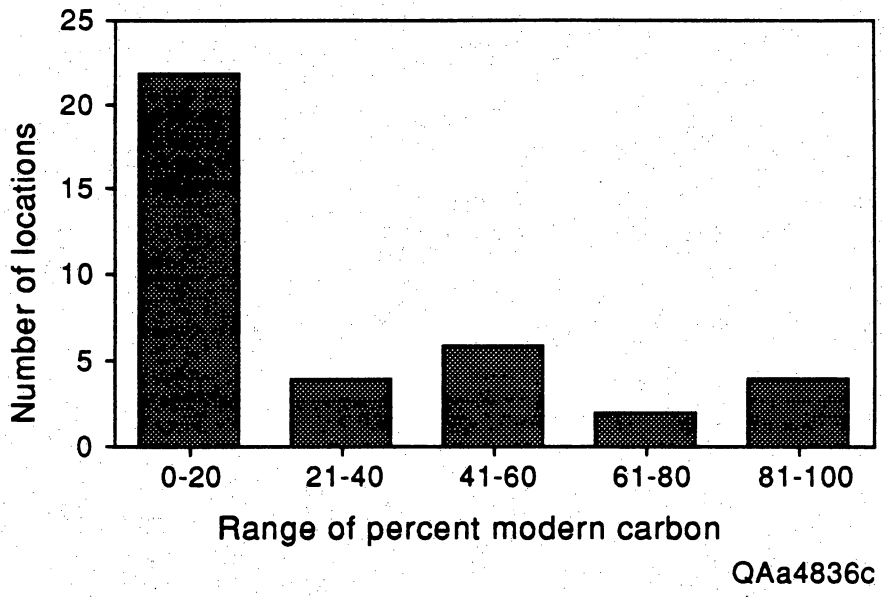

Figure 21. Histogram of percent modern carbon (PMC) values in southern Hudspeth County ground water.

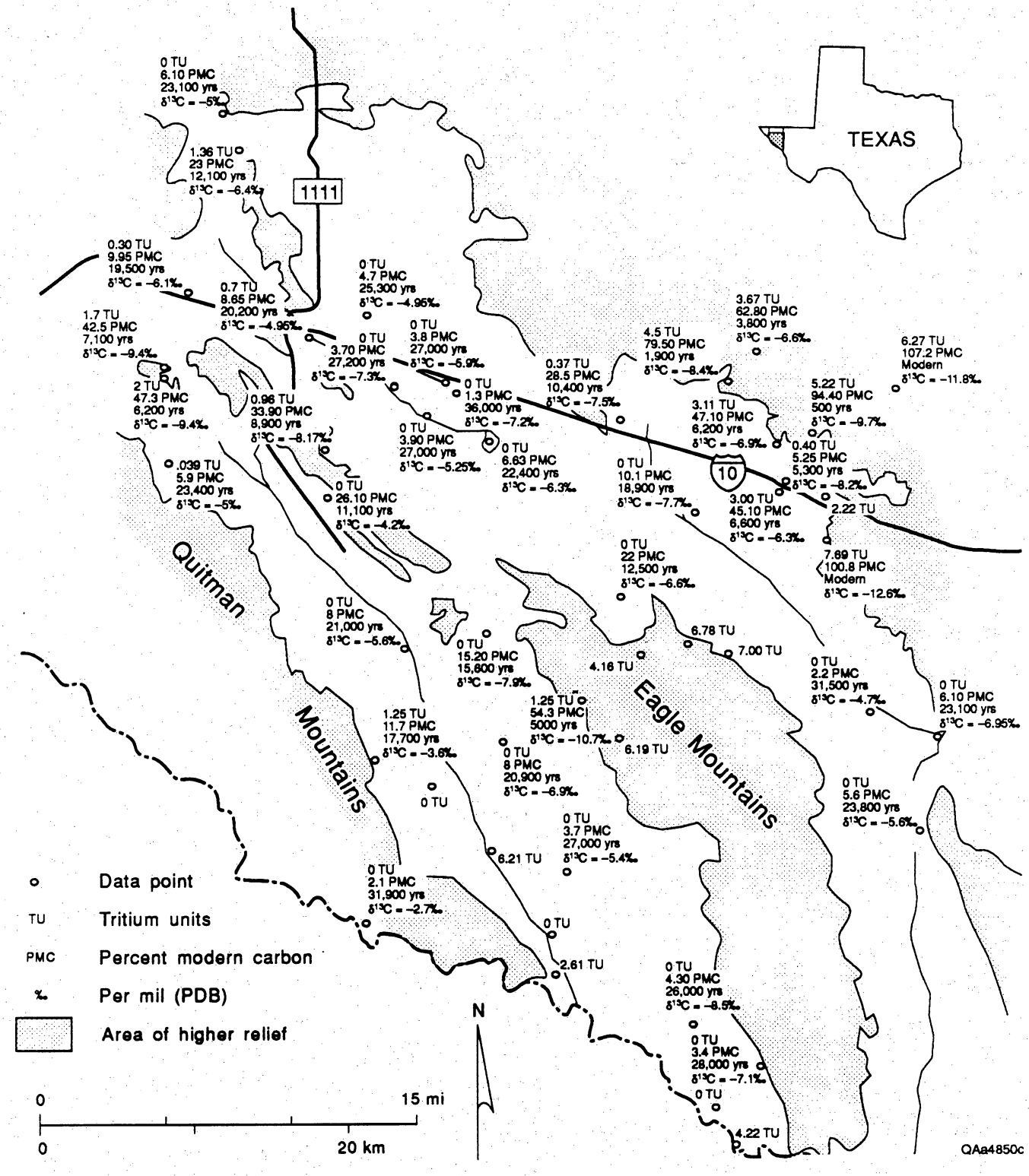

Figure 22. Map of ^{3}H, ^{14}C and $\delta^{13}C$ in southern Hudspeth County ground water. Carbon-14 is shown as percent modern carbon (PMC), along with uncorrected ages. Tritium is reported as tritium units. $\delta^{13}C$ is measured with respect to PDB standard.

Table 5. Range of tritium units (TU) and percent modern carbon (PMC) in southern Hudspeth County ground water.

RANGE OF TRITIUM UNITS

AREA	WELLS	MEAN	MEDIAN	HIGH	LOW
S.E. Eagle Flat	17	3.74	3.11	7.69	0.00
N.W. Eagle Flat	17	0.68	0.50	4.16	0.00
Red Light Draw	18	1.27	0.00	6.91	0.00

RANGE OF PERCENT MODERN CARBON VALUES

AREA	WELLS	MEAN	MEDIAN	HIGH	LOW
S.E. Eagle Flat	12	58.25	49.80	109.90	2.20
N.W. Eagle Flat	16	15.78	9.95	80.50	1.30
Red Light Draw	11	12.99	8.00	54.30	2.10

exposed or covered by thin basin fill. Intermediate values of both isotopes are found in the Allamore area, where water depths average 175 ft (53 m), and where wells draw water from basin fill. The lowest ^{3}H and ^{14}C levels are associated with samples from three Scott's Crossing area wells (51-01-501, 51-01-503, and 51-01-801) that extract water from depths as much as 600 ft (183 m) in basin fill.

Carbon-14 measurements decrease from levels near or greater than 100 PMC in bedrock exposures in the Bean and Millican Hills to 40 to 50 PMC at Allamoore and less than 5 PMC near Scott's Crossing. The overall pattern is consistent with flowpaths inferred from the potentiometric map, as it suggests that ground-water age increases toward the east-southeast. Shallow wells producing from gravels in the proximal area of the Eagle Mountains fan in southeast Eagle Flat were not sampled for carbon isotopes, but tritium values were between 6 and 7 TU.

Tritium units and percent modern carbon are positively correlated in northwest Eagle Flat (fig. 23), and some of the highest values are associated with wells of shallow to intermediate depth (200 to 300 ft, 61 to 91 m) in the abandoned well field. Two wells from this field (48-53-802 and 48-53-803) yielded samples with ^{14}C values of 47.30 and 42.40 PMC, respectively, and tritium concentrations of 1.99 and 1.73 TU. Seven miles (11.3 km) north of Sierra Blanca, an 1,100-ft well (48-45-901) on the north side of Triple Hill yielded a sample of Na-SO_4-HCO_3 ground water (1,040 mg/L) with 23 PMC and 1.36 TU. Well 48-45-901 is adjacent to another deep well (48-45-603) with substantially higher dissolved solids (2,200 mg/L), no measurable tritium, and only 6.10 PMC.

The lowest ^{14}C and ^{3}H values in northwest Eagle Flat occur near the proposed repository site. Several wells were drilled in this area during the period September 1991–August 1993 as part of the characterization and monitoring program. The wells range in depth from 880 to 1,100 ft (268 to 335 m), and produce water from the Cox Sandstone and the Finlay Limestone. Pumping tests indicate that the aquifer is leaky confined, with transmissivities of less than 11 ft^2/day (1.02 m^2/day) at the proposed waste disposal site (YM-8, YM-18, YM-19, and YM-63) to 70 ft^2/day (6.50 m^2/day) at Grayton Lake (YM-7A).

All of the monitor wells were sampled several times between June 1992 and August 1993 as part of the quarterly monitoring program. With the exception of 48-62-TEX, average ^{14}C is less than 6.63 PMC. Only YM-7A, YM-8, and YM-19 were in operation by November 1992. YM-19 and 48-62-TEX were added by February 1993, and YM-63 was completed in August 1993. YM-8 was

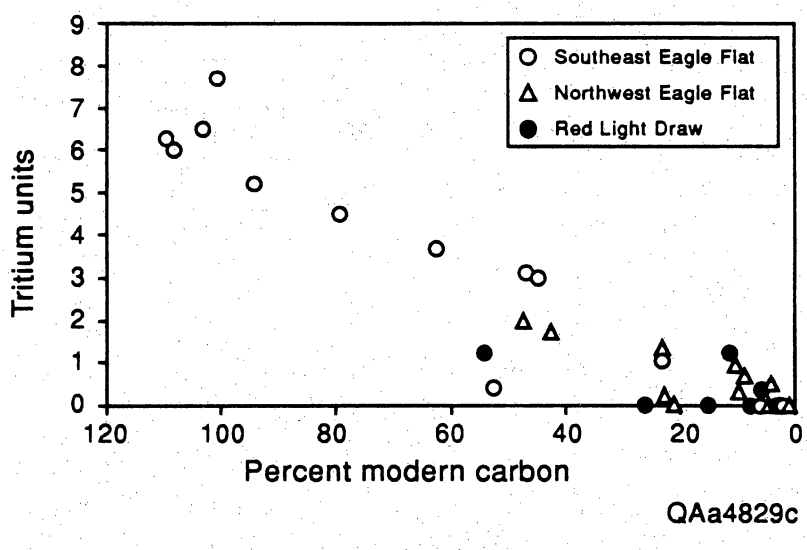

Figure 23. Plot of ^{3}H versus ^{14}C in study area. The downward sloping trend for southeast Eagle Flat and northwest Eagle Flat indicates mixing between recent recharge water and older ground water. Points from Red Light Draw exhibit no apparent trend.

not sampled in February and August of 1993 because of mechanical problems, and YM-7A was not accessible due to standing water at Grayton Lake in August 1993. Except for 48-62-TEX, no significant variation in ^{14}C is observed through August 1993.

There is no readily discernible pattern of decreasing ^{14}C along flowpaths in northwest Eagle Flat, as several key locations lie along the same potentiometric contour. YM-7A, YM-8, YM-19, YM-63, and 48-54-502, for example, are close to the 3,600-ft (1,097-m) isopleth along the east side of the basin (fig. 5). Average ^{14}C measurements and uncorrected ages are 6.63 PMC (22,400) at YM-7A; 3.9 PMC (26,800 years) at YM-8; 3.7 PMC (27,300 years) at YM-19; 3.8 PMC (27,000 years) at YM-18; 1.3 PMC (36,000 years) at YM-63; and 4.7 PMC (25,300 years) at 48-54-502. These figures suggest significantly long residence time for ground water in the aquifer underlying northwest Eagle Flat.

Between May and August 1993, ^{14}C increased from 9.8 to 80.5 PMC at 48-62-TEX. The increase was accompanied by a change in $\delta^{13}C$ from -6.7 °/oo to -10.5 °/oo, and a decrease in total dissolved solids from 923 to 713 mg/L. Tritium was 0.94 TU, essentially unchanged from the 0.96 TU reported for an earlier sample. The $\delta^{2}H$ and $\delta^{18}O$ values were also consistent with earlier values.

In Red Light Draw, median ^{14}C based on 11 samples is 8 PMC, and the median ^{3}H activity from 18 locations is 0 TU (table 5). The highest ^{14}C values are associated with wells in the Eagle Mountains and along the northwestern part of Devil Ridge (50-07-601, 54.3 PMC; and 48-62-BOR, 26.1 PMC). Along flow lines from the Eagle Mountains, ^{14}C and ^{3}H decrease rapidly toward the axis of the basin (fig. 5). There is only one ^{14}C measurement within the high-TDS zone along the Rio Grande. A sample from 50-14-503 (Chief Spring) yielded 2.1 PMC, and no tritium. Two other locations in the high-TDS zone (50-15-801 and 50-24-503) had 2.61 and 4.22 TU, respectively.

Stable Isotopes

Figure 24 consists of plots of $\delta^{2}H$ versus $\delta^{18}O$ for southeast Eagle Flat, northwest Eagle Flat, and Red Light Draw, with the points from each area grouped according to whether their ^{14}C signatures are greater than 20 PMC or less than or equal to 20 PMC. Samples for which carbon-14 analyses were not performed are indicated by an open triangle. The Global Meteoric Water Line (GMWL) (Craig, 1961a, 1961b) is included as a reference line on each plot.

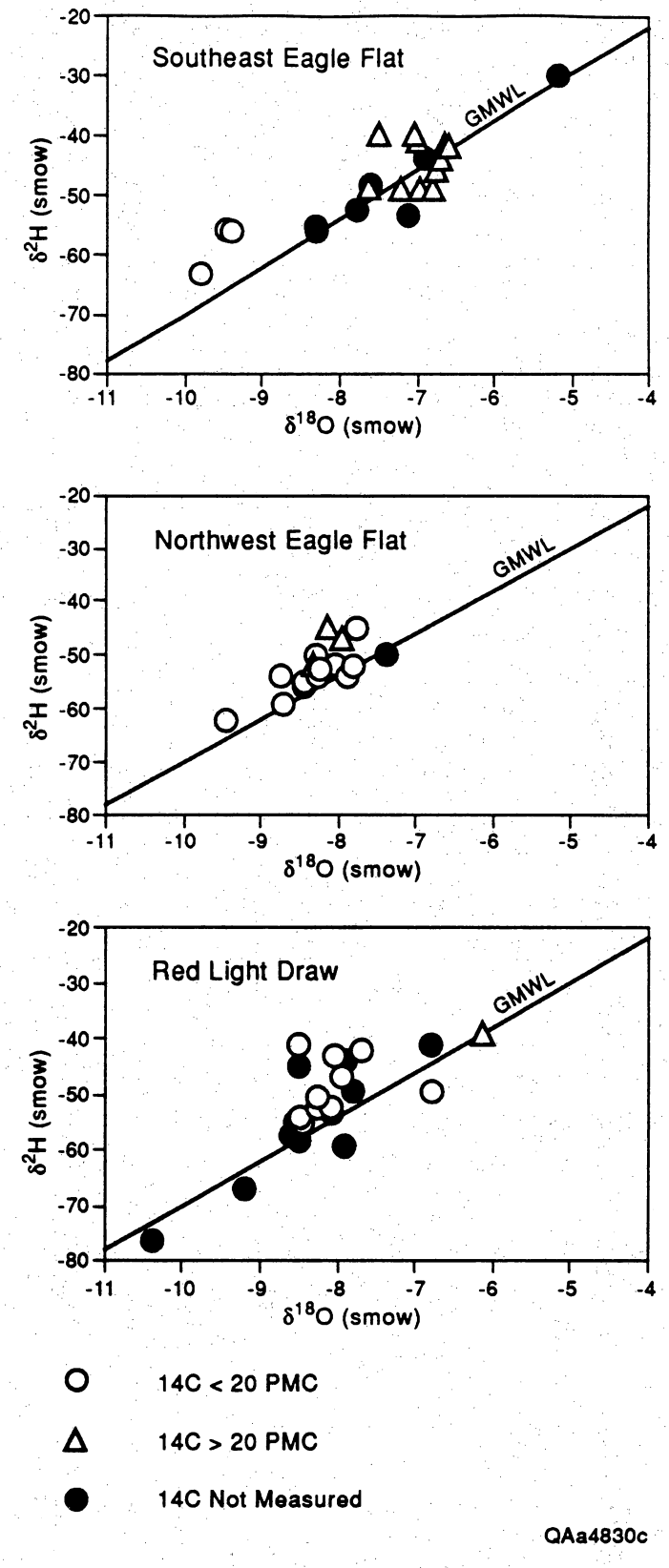

Figure 24. Binary plots of δ^2H versus $\delta^{18}O$ for southeast Eagle Flat, northwest Eagle Flat, and Red Light Draw. The points are grouped according to their respective ^{14}C values (PMC). Water with less than 20 PMC is shown to be more depleted in both δ^2H and $\delta^{18}O$ than points with more than 20 PMC.

The proximity of the points to the GMWL indicates not only that the waters are of meteoric origin, but also that δ^2H and $\delta^{18}O$ values have not been altered significantly by rock-water interaction (Banner and Hanson, 1990). Furthermore, there also exists an apparent ordering of points, based on their accompanying ^{14}C values, such that those points for which ^{14}C is less than or equal to 20 PMC are generally more depleted in ^2H and ^{18}O than are those for which ^{14}C is greater than 20 PMC.

Southeast Eagle Flat ground water (fig. 25) can be divided into three groups based on differences in δ-values, and unstable-isotope (^{14}C and ^3H) signatures. Clustered around δ^2H and $\delta^{18}O$ medians of -45.7 °/oo and -6.98 °/oo, respectively, the first group predominates in areas where Precambrian bedrock is either exposed or covered by thin basin fill. Water depths in this area are 20 to 230 ft (6 to 70 m). Tritium values from samples collected over the period October 1991–December 1992 are 1.5 to 8.0 TU. Most ^{14}C measurements are between 40 and 107 PMC.

The second group is associated with three Scott's Crossing-area wells (50-01-501, 50-01-503, and 50-01-801) that extract water from basin fill at depths as great as 600 ft (183 m). Median δ^2H and $\delta^{18}O$ values are the lowest in southeast Eagle Flat, -56 °/oo and -9.7 °/oo, respectively; median ^{14}C is 5 PMC, and ^3H is zero. A third group in southeast Eagle Flat is found in the Eagle Mountains at elevations ranging from 4,800 ft (1,463 m) to 5,100 ft (1,554 m). Stable isotope values are intermediate to those of the above groups. The δ-values are probably indicative of depletion from the combined effects of elevation and precipitation over the Eagle Mountains.

Northwest Eagle Flat ground water δ^2H and $\delta^{18}O$ values of (fig. 25) are clustered around medians of -52 °/oo and -8.24 °/oo, respectively. The $\delta^{18}O$ contours indicate increasing depletion toward the proposed repository site in the south-central part of the basin. Figure 25 also reveals a $\delta^{18}O$ trend coincident with the axis of Red Light Draw, with the most depleted δ-values at the center of the contour pattern. Another trend is developed within the high-TDS zone along the Rio Grande, in the area between southeast Red Light Draw and Indian Hot Springs. In southeast Red Light Draw, δ-values are the lowest in the study area (-9.5 to -10.4 °/oo $\delta^{18}O$ and -64 to - 76 °/oo δ^2H). At Indian Hot Springs, however, the values are much less depleted (-6.9 to -7.8 °/oo $\delta^{18}O$ and -49 to -59 °/oo δ^2H).

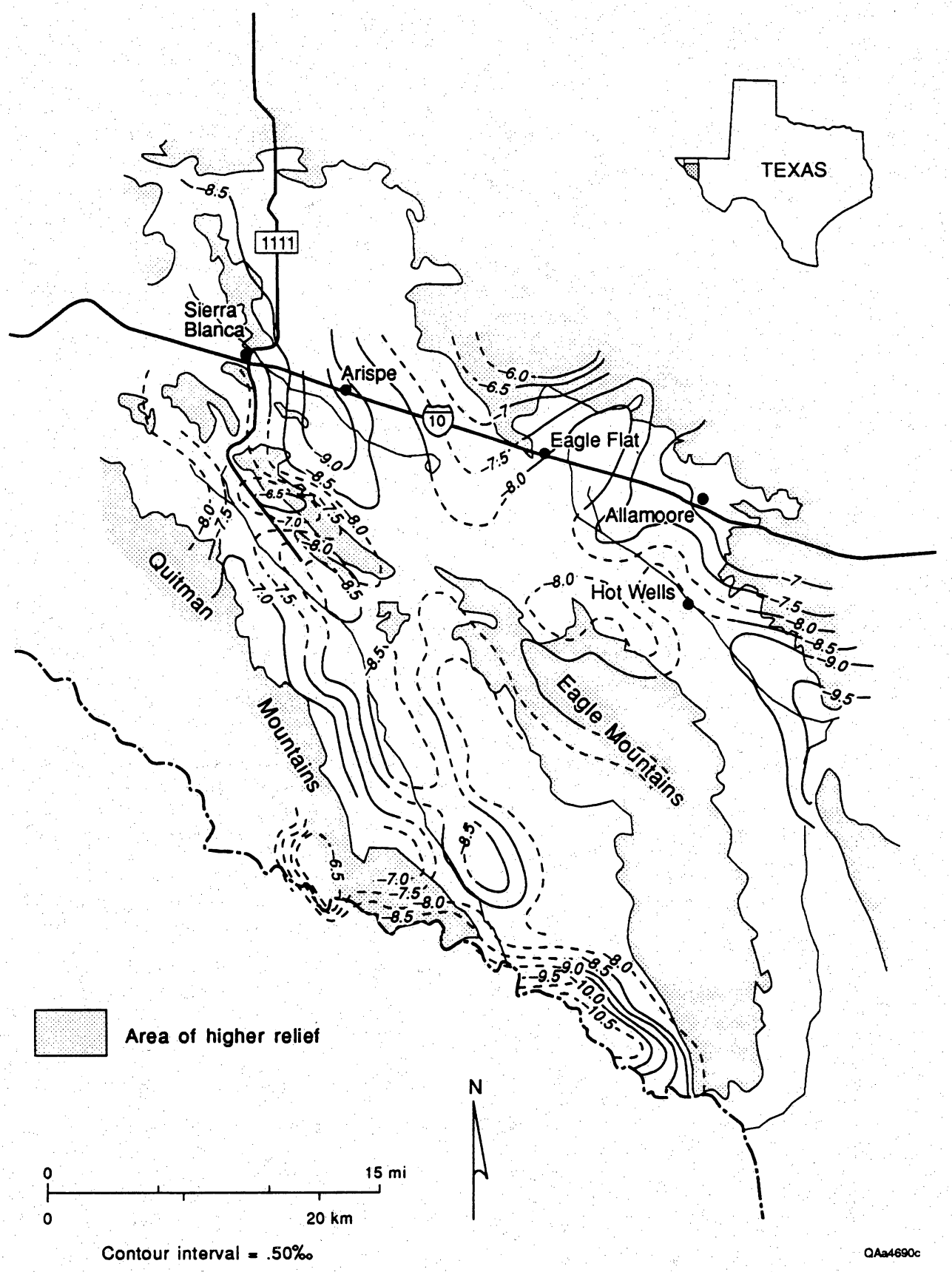

Figure 25. Map of $\delta^{18}O$ values in southern Hudspeth County ground water.

The δ^2H vs $\delta^{18}O$ plot for Red Light Draw (fig. 24) includes 18 points, 10 of which have associated carbon-14 measurements. Only 2 of the 10 samples have radiocarbon greater than 20 PMC. Despite the unmistakable meteoric signature of Red Light Draw ground water, the binary plot suggests that there are at least two distinct bodies of water in this system. Figure 26 shows the δ^2H-$\delta^{18}O$ trend for three thermal springs and three wells in the high-TDS zone (50-14-RBL, 50-14-501, 50-14-503, 50-15-801, 50-24-202, and 50-24-503). Stump Spring and Chief Spring (50-14-501 and 50-14-503) are two of five springs discharging a total at least 400 L/min of Na-Cl-SO_4 water (TDS > 7000 mg/L) into river alluvium at Indian Hot Springs. The discharge occurs near the point where the trace of the Caballo fault, which bounds the southwest flank of the Quitman Mountains, disappears beneath floodplain sediments of the Rio Grande (Henry, 1979). The temperatures of the five springs (Soda, Chief, Stump, Squaw, and Beauty) range from 27 to 52°C (Henry, 1979), and Dorfman and Kehle (1974) reported temperatures greater than 60°C from a shallow well nearby. Red Bull Spring (50-14-RBL), located 2.5 mi (4.0 km) northwest of Indian Hot Springs, discharges 50 L/min of moderately saline (TDS = 1040 mg/L) Na-HCO_3-SO_4 water, with temperatures of 34° to 37°C, through fractured calcareous claystone (Henry, 1979). The spring is situated at the point where the Red Bull fault terminates against the Caballo fault (Henry, 1979). The three wells (50-15-801, 50-24-202, and 50-24-503), which provide water for livestock, are located along the edge of the southernmost terrace overlooking the Rio Grande floodplain in Red Light Draw. The wells are shallow (45 to 65 ft, 13.7 to 19.8 m), with water depths between 35 to 48 ft (10.7 to 14.6 m). Temperatures are 23° to 25°C.

Values of δ^2H and $\delta^{18}O$ from the above wells form a clearly defined linear trend that runs nearly parallel to the GMWL. The four with the highest salinities lie below the GMWL. The equation describing the line of best fit is:

$$\delta^2H = 7.65(\delta^{18}O) + 4.99,$$

and the coefficient of determination (r^2) is 0.88. Samples from other wells in Red Light Draw (fig. 27) form a more widespread cluster of points above the GMWL. The least-squares equation for this group is:

$$\delta^2H = 5.91(\delta^{18}O) - 0.82,$$

and r^2 is 0.43.

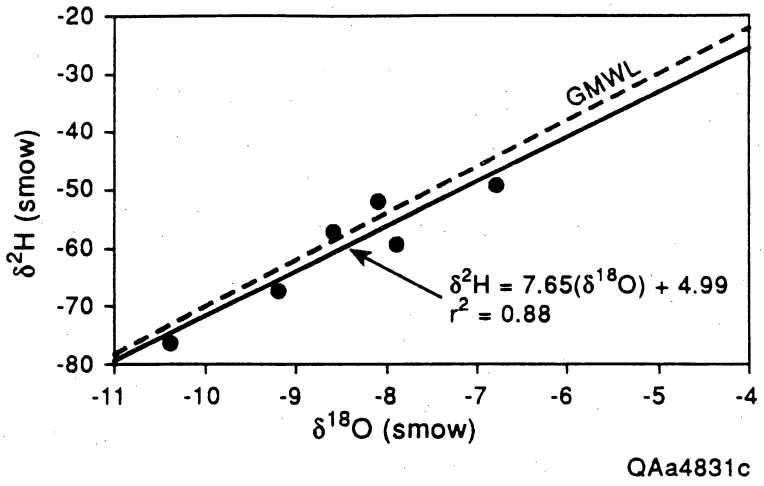

Figure 26. Plot of δ^2H versus $\delta^{18}O$ for locations within the high-TDS zone in lower Red Light Draw.

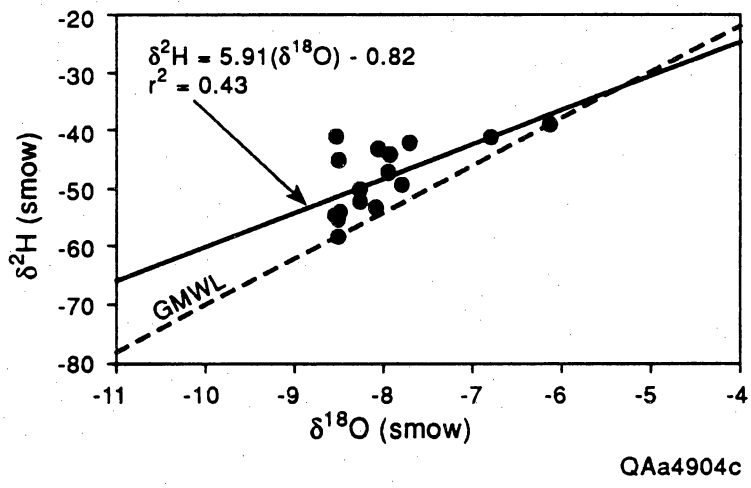

Figure 27. Plot of δ^2H versus $\delta^{18}O$ for low-TDS samples in Red Light Draw.

DISCUSSION

Origin of Solutes

The variable hydrochemical signature of southern Hudspeth County ground water (table 4, figs. 12 and 13) is attributable to the relative solubilities of aquifer materials, cation exchange, and mixing. Calcium and magnesium concentrations, for example, are controlled not only by the weathering of Ca- and Mg-bearing minerals, such as calcite, pyroxene, or amphiboles, but also by the dissolution of sulfates and by exchange for the monovalent cation Na.

If Ca and Mg originate entirely from dissolution of carbonates and from the weathering of pyroxene or amphiboles, the molar ratio of Ca and Mg to HCO_3 would be 0.50 (Sami, 1992). The governing equations for the weathering of the above minerals are:

Calcite:

$$CaCO_3 + H_2O + CO_2 = Ca + 2HCO_3$$

Pyroxene:

$$CaMg(Si_2O_6) + 4CO_2 + 6H_2O = Ca + Mg + 4HCO_3 + 2SI(OH)_4$$

Amphiboles:

$$Ca_2Mg_5Si_8O_{22}(OH)_2 + 14CO_2 + 22H_2O = 2Ca + 5Mg + 14HCO_3 + 8Si(OH)_4.$$

Each of the above reactions yields two moles of HCO_3 for every mole of Ca, or Ca and Mg. Ratios less than 0.50 may be attributed to the loss of Ca and Mg through cation exchange, and ratios greater than 0.50 may indicate additional sources of Ca and Mg, possibly associated with the dissolution of sulfates. Figure 19 shows the covariation between the (Ca + Mg)/HCO_3 ratio and Cl in each of the three basins. The wide scatter around a molar (Ca + Mg)/HCO_3 ratio of 0.50 indicates that Ca and Mg are not only lost by cation exchange, but also gained by weathering of sources other than calcite, pyroxene, or amphiboles (Sami, 1992).

Furthermore, if all Cl originates as NaCl, then (Na - Cl) represents a maximum value of Na from cation exchange (Sami, 1992). The plot of (Na - Cl) versus SO_4 (fig. 18) offers support for the hypothesis that dissolution of sulfates

is a factor accounting for regional hydrochemical patterns. In figure 18, points from all three basins form an upward trend with a slope of approximately 2.00. If Ca derived from the dissolution of gypsum replaces Na through exchange, then the molar ratio of Na to SO_4 should be 2:1, as traced by the line in figure 18.

Figure 20, a plot of (Ca + Mg - SO4) versus (Na - Cl), best illustrates the interrelationship between Ca, Mg, and Na, as it allows for direct evaluation of the significance of exchange and mineral weathering on concentrations of the three cations (Sami, 1992). The linearity indicates a highly correlated relationship between the increase of Na and the loss of the divalent cations Ca and Mg. Specifically, Na increases at slightly more than twice the loss rate of Ca and Mg, as would be expected from cation exchange. The dashed line traces the amount of Ca and Mg lost solely as a result of cation exchange, and the position of the points above the dashed line indicates that Ca and Mg are also derived by processes other than dissolution of sulfates (Sami, 1992).

The trend of decreasing Na/Cl ratios (fig. 17A-B) with increasing chlorinity suggest the influence of NaCl on the chemistry of southern Hudspeth County ground waters, especially from the lowermost reaches of Red Light Draw. Dissolution of NaCl yields equimolar concentrations of Na and Cl, so that the Na/Cl ratio should equal 1.00. Ratios much greater than 1.00, especially at lower salinities, signify additional sources of Na, such as weathering of albite, or exchange of divalent cations (Ca and Mg) for Na.

Cl/Br ratios have significant implications for tracing sources of salinity in Red Light Draw, as illustrated by a plot of Cl/Br ratios versus TDS (fig. 16). In this figure, the six wells and springs in the high-TDS zone along the Rio Grande fall along a line that extends upward from the cluster of low-TDS samples of lower Red Light Draw. This is an indicator of mixing of ground waters of different hydrochemical compositions (Mazor, 1991; Mazor and others, 1993). The chemistry in this zone is dominated by the higher-TDS waters. Red Bull Spring (50-14-RBL) and well 50-15-801, with salinities and Cl/Br ratios that are intermediate to the dilute waters of Red Light Draw, are the first locations where the effects of the ground-water mixing can be seen.

The source of the high-TDS water is problematic, as no other example of ground water of similar composition is found in Red Light Draw. Chloride-bromide systematics, however, offers some insight into a possible origin. As members of the halide group of elements, chloride and bromide are conservative anions, and few processes other than precipitation or dissolution of salts, and

ground-water mixing will significantly affect their concentrations in natural waters, although Hem (1985) notes that clay-membrane effects may selectively concentrate bromide.

In a review of the trace-element geochemistry of evaporites, Holser (1979) observed that the molar ratio of Cl to Br is sensitive to the origin of water as marine (~ 300), as a second-cycle solution of marine salt (~ 1000), or as a brine residue from the precipitation of halite (< 250). Cl/Br molar ratios in the high-TDS zone lie above the characteristic molar ratio of second-cycle evaporites, possibly indicating the presence of saline water linked to the dissolution of marine salt. Another, although less likely, possibility is the flushing of salts crystallized from recycled irrigation water in floodplain sediments along the Rio Grande (Kreitler and others, 1986). That the Na/Cl molar ratios are approximately 1.00 for all wells within the high-TDS zone (fig. 17A-B) offers additional support for the hypothesis that salt dissolution accounts for the anomalous Cl/Br ratios.

Henry (1979) observed that Indian Hot Springs and Red Bull Spring lie near the edge of the Jurassic evaporite basin described by DeFord and Haenggi (1970). He concluded that meteoric water mixes with salt-dissolution brine before moving upward along the Caballo fault to discharge points near the Rio Grande. If waters from deeper aquifers in Mexico upwell and eventually discharge to the Rio Grande alluvium, there is reason to expect a similar phenomenon to occur from the north, since flow systems on both sides of the Rio Grande will tend to be imperfect mirror images of each other. One regional flow system may dominate the overall pattern of flow, depending on its relative dimensions, hydraulic gradients, and permeabilities. Aquifers to the south presumably dominate patterns of flow, as high Cl/Br molar ratios are found more than a mile north of the Rio Grande. Unfortunately, the geochemical signatures of waters from northwest Eagle Flat do not allow us to trace saline waters directly where they upwell near the Rio Grande. These waters, having evolved in areas where halite deposits are unknown, have only moderate Cl/Br ratios.

Paleoclimatic Labeling

In many areas of southern Hudspeth County ^{14}C signatures indicate that ground water was recharged thousands of years ago (fig. 22). Highly accurate age estimates based solely on carbon isotopes, however, are difficult to derive

because of the complex nature of carbon chemistry in ground-water systems. This problem may be traced to the effects of dilution and isotope exchange, which have been shown to alter significantly the carbon signature of ground water (Mook, 1980), leading to falsely old age estimates.

Many researchers have proposed the use of correction factors to adjust raw ^{14}C ages for the effects of dilution and isotope exchange. Fontes and Garnier (1979) reviewed the factors used in most ground-water age-dating studies, and Muller and Mayo (1986) evaluated the sensitivity of models to variations in input parameters, such as $\delta^{13}C$ of limestone and soil gas. It is clear that a correction factor should not be used without regard to the specific set of conditions which the model was designed to address (Muller and Mayo, 1986). Proper application of ^{14}C correction factors presupposes a thorough understanding of the many geochemical factors likely to have an impact on ^{14}C signatures, and the use of an inappropriate correction factor may yield age estimates that are thousands of years older or younger than the true age of an unmixed sample.

No effort is made in this report to derive adjusted ^{14}C ages, because of the many factors known to influence the chemistry of dissolved inorganic carbon. Dutton (1993) cites similar reasons for relying on ^{14}C activities instead of adjusted ages in his study of ground water in confined and unconfined aquifers underlying the High Plains: "estimating the amount of dissolved calcite or dolomite and other subsurface sources of dissolved carbon, assuming the $\delta^{13}C$ of paleorecharge waters, and documenting the history of ^{14}C and ^{3}H in precipitation." Absolute values of ^{14}C are accepted as conveying significant information only about relative differences in ground-water ages and flow directions (Dutton, 1993). Unadjusted ages are assumed to represent maximum limits.

Despite the many problems involving the ^{14}C dating method in hydrological investigations, it is still possible to derive reasonable age estimates indirectly, by comparing $\delta^{18}O$ in ground water with $\delta^{18}O$ of modern rainfall, as the effects of climate and atmospheric temperature on the fractionation of deuterium and oxygen-18 are well-documented (Dansgaard, 1964; Siegenthaler and Oeschger, 1980; Schoch-Fischer and others, 1983). The assumptions underlying this approach are that (1) low ^{14}C values indicate late Pleistocene ages, and (2) the combination of significantly depleted δ-values and low ^{14}C activities may reflect the cooler and wetter climatic conditions of late Pleistocene glacial stages (Gonfiantini and others, 1974; Dutton and Simpkins, 1989). Other

factors that may account for greater depletion of ^{18}O are elevation (Siegenthaler and Oeschger, 1980; Payne and Yurtsever, 1974; Musgrove, 1993) and distance from the source of moisture (Sonntag and others, 1979), but these are not related in any systematic manner to ^{14}C values.

Lambert and Harvey (1987) observed that the isotopic signatures of ground water in the confined aquifers of southeastern New Mexico are more depleted in ^{18}O and ^{2}H than is observed for modern rainfall in the Carlsbad area. Lambert (1967) estimated ground-water ages of 12,000 to 16,000 years, using the correction method of Evans and others (1979), and Lambert and Harvey (1987) concluded that the confined waters were recharged under a more humid climatic regime.

Weighted-averages of $\delta^{18}O$ in precipitation from eight sample stations in West Texas (Alpine, Amarillo, Lubbock, and Midland) and southeast New Mexico (Carlsbad, Clovis, Elk, and Roswell) are shown in figure 28. The weighted averages, based on more than 500 samples representing wide ranges of temperature and elevation (Hoy and Gross, 1982, Lambert and Harvey, 1987; Nativ, 1988; Lawrence, personal communication, 1993) establish a baseline against which the $\delta^{18}O$ of southern Hudspeth County ground water may be compared. Southern Hudspeth County lies between stations in Roswell (southeastern New Mexico), and Alpine, and lies west-southwest of Midland. The stable isotope composition of rainfall in the study area, therefore, may be expected to be more similar to that from surrounding stations than to rainfall from more distant locations, such as Amarillo and Clovis.

Figure 29A is a plot of $\delta^{18}O$ versus ^{14}C activity (PMC) for southern Hudspeth County ground waters. The PMC axis is reversed, so that apparent ^{14}C age increases from left to right. The degree of depletion in ^{18}O is shown to increase with decreasing PMC (increasing age). This downward shift of $\delta^{18}O$ is consistent with Lambert and Harvey's (1987) observations regarding the stable-isotope values of southeastern New Mexico ground waters. The probability that this is related to paleoclimatic factors is underscored by research on the Pleistocene climatic history of the desert Southwest, as summarized by Langford (1993):

> During the early Pleistocene, the climate of the southwestern United States was cooler and more moist than that of the present (Hall, 1985). The Late Wisconsinan glacial period from 25,000 to 14,000 yr B.P. was a time of moist and cooler climate throughout

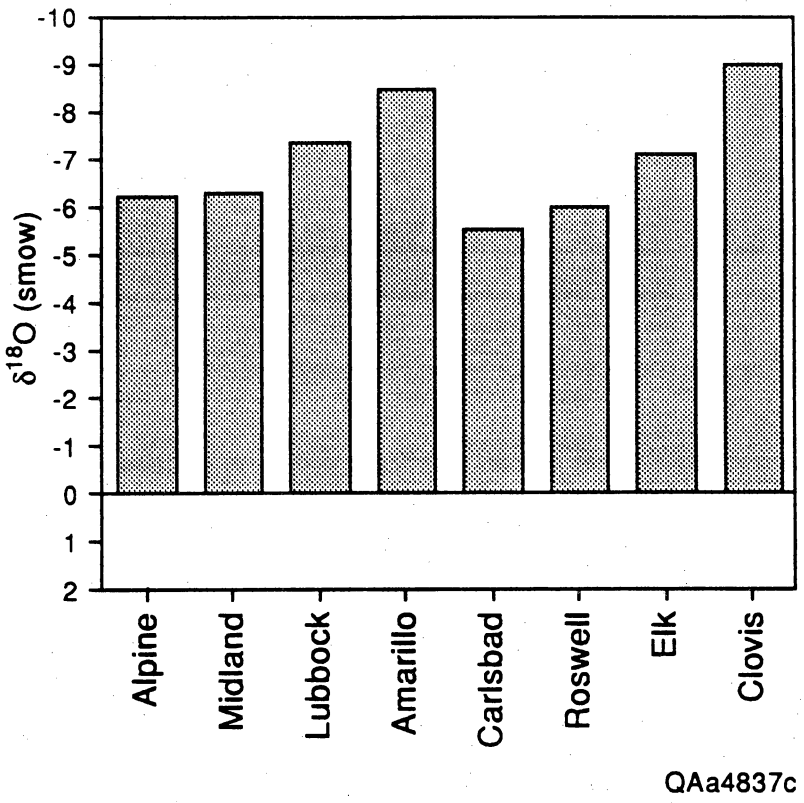

Figure 28. Weighted-average $\delta^{18}O$ values for precipitation from stations in West Texas and southeastern New Mexico.

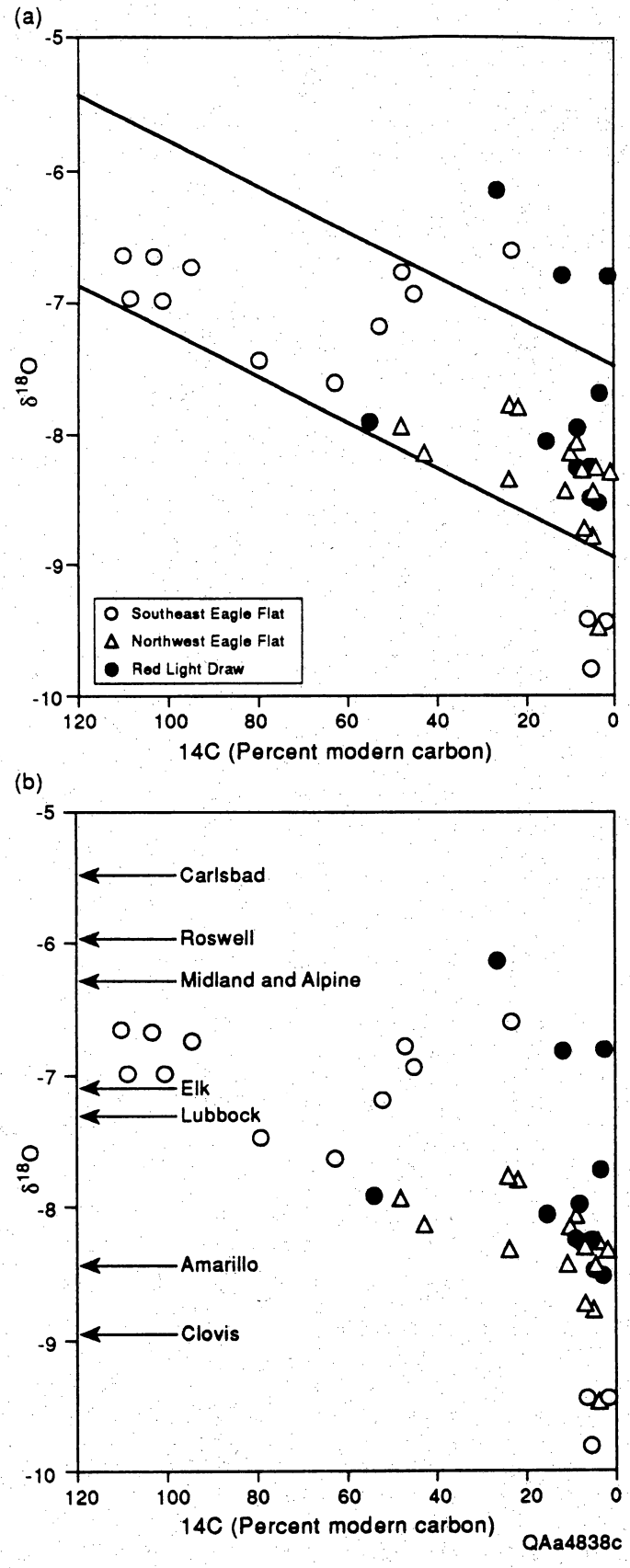

Figure 29. (A) Binary plot of $\delta^{18}O$ versus PMC in southern Hudspeth County ground water. Downward-sloping lines mark decreasing trend of $\delta^{18}O$ values. (B) Binary plot of $\delta^{18}O$ versus PMC in southern Hudspeth County ground water. Weighted-average $\delta^{18}O$ values for precipitation from stations in West Texas and southeastern New Mexico are marked along the vertical axis. With few exceptions, ground-water δ-values with less than 20 PMC are apparently lower than δ-values from six of the eight locations.

the southwestern United States (Wells and others, 1982; Hall, 1985). At the end of the Wisconsinan, 14,000 to 10,000 yr B.P., the climate became warmer and drier, although still cooler, and more moist than that of the present, and there was a gradual transition from glacial to post-glacial vegetation (Wells and others, 1982; Hall, 1985). Dry woodlands of juniper lasted in the deserts of the southwest until 8,000 to 10,000 yr ago (Alexrod and Bailey, 1976; Van Devender and Spaulding, 1979; Wells and others, 1982). Juniper woodlands persisted in the Hueco Basin, immediately to the west of Eagle Flat, until 8,000 to 4,000 yr ago, when they were replaced by grasses (Horowitz and others, 1981). Because the Eagle Flat and Red Light Draw Basins lie at generally higher elevations than the floor of the Hueco Basin, and therefore would have had higher rainfall, woodlands should have persisted as long as in the Hueco Basin. To the north, wetter climatic regimes with woodlands persisted even longer, to about 5,000 yr B.P. in the San Augustin Plains of New Mexico (Markgraf and others, 1984), and to about 5,800 yr B.P. in Chaco Canyon (Hall, 1977).

The weighted-average $\delta^{18}O$ at Alpine (-6.28 °/oo), Midland (-6.31 °/oo), Carlsbad (-5.50 °/oo), Roswell (-6.00 °/oo), Elk (-7.10 °/oo), and Lubbock (-7.32 °/oo) are apparently heavier than $\delta^{18}O$ measurements of all southeast Eagle Flat, northwest Eagle Flat, and all but two Red Light Draw samples with less than 20 PMC (29B). Ground water with demonstrably modern $\delta^{2}H$ and $\delta^{18}O$ signatures is found primarily in southeast Eagle Flat. These points are clustered near the weighted averages of Midland, Alpine, Elk, and Lubbock. The stable isotope values of the oldest waters appear to be more similar to the weighted averages of Amarillo (-8.48 °/oo) and Clovis (-8.97 °/oo). The downward drift of $\delta^{18}O$ with lower ^{14}C values indicates a time-dependent component that may be related to the climatic history outlined by Langford (1993).

Support for this hypothesis is offered by the $\delta^{18}O$ contour map (fig. 25). The occurrence of isotopically light δ-values in the middle of northwest Eagle Flat, and along the axis of Red Light Draw suggests dependence of stable isotope signatures on flowpaths and climatic conditions at the time of recharge. The decrease of hydraulic head from the topographically high boundaries of the study area toward the center of the basins enables one not only to trace ground-water flowpaths but also to identify areas where the oldest waters would be expected to occur (i.e, along the axes of the basins and draws). Patterns of ^{14}C and ^{3}H suggest that the major recharge areas are in bedrock exposures in mountains and the uppermost areas of the mountain fans. Excluding the

relatively depleted $\delta^{18}O$ values of modern ground water from the higher elevations of the Eagle Mountains (explained as a function of rainout over a topographically high area), the progression toward lower $\delta^{18}O$ with distance from the mountains toward the proposed repository site and the axis of Red Light Draw suggests that the isotopic signature of meteoric water falling over recharge areas might have been more negative in the past.

Recharge Areas

Recently recharged waters are identified on the basis of major ionic signatures, and unstable isotope values. These waters are Ca-HCO_3 to mixed-HCO_3 in character (fig. 13), with ^3H greater than 1 TU, and ^{14}C ranging from 50 to 100 PMC (fig. 22). Mixtures of old water and recently recharged water are indicated by the occurrence of ^3H values greater than 1 TU with moderate to low ^{14}C values.

The most significant recharge area is in southeast Eagle Flat, between the Bean Hills and Allamoore to the east, the Streeruwitz Hills to the west, and the Diablo Plateau to the north. The Eagle Mountains constitute the second major recharge area; but within short distances of the mountain front, low ^{14}C values and ^3H levels that are indistinguishable from background suggest very slow rates of ground-water drainage.

The distribution of unstable isotope values in northwest Eagle Flat indicates that recharge is centered in the area around the northern Quitman Mountains, the Sierra Blanca Peaks, and possibly Devil Ridge. Sufficient pathways for recharge may be provided by fractures that allow rapid percolation of meteoric water. The situation appears very different in the flats, as there is no substantial geochemical evidence that the aquifer is recharged through the basin floor.

The conceptual model that emerges from Red Light Draw is similar to that of northwest Eagle Flat. Outside of recharge zones in the Quitman Mountains and the Eagle Mountains, tritium is typically below detection limits (fig. 22), and carbon-14 is less than 8 PMC (table 4). Recharge occurs along the southwest and northeast boundaries, in the Quitman Mountains, and the Eagle Mountains, as indicated by tritium measurements ranging from 1.25–6.91 TU, but unstable isotope values decrease substantially within short distances basinward.

Alluvial fans do not constitute significant recharge areas for Red Light Draw. The ^{14}C activities are consistently less than 8 PMC, and ^{3}H activities are effectively zero, which suggests very slow-moving water or perhaps dead-end flow cells. Langford (1993) documented the existence of well-developed Stage 4 calcic soil horizons in all fan areas of Red Light Draw. These impermeable soils may contribute to runoff by acting as barriers to the percolation of meteoric water (Gile and others, 1981).

Site-Specific Hydrogeology

Depth to ground-water varies between 667 to 751 ft (203.5 to 229 m) below land surface in Faskin Ranch wells. Ground water flows southwest, underneath the proposed sit on Faskin Ranch, and later merges with the southeasterly sloping hydraulic gradient (fig. 30). Ground water entering Faskin Ranch from the northeast probably originated in the Diablo Plateau and Streeruwitz Hills to the northeast several millenia ago.

Curve matches with Hantush-Jacob (1955) type curves suggested a leaky confined aquifer beneath Faskin Ranch. Despite the match, the precise mechanism(s) of leakage could not be determined because many aquifer models emulate a leaky confined aquifer without storage in aquitards. For example, a diagrammatic representation of three different types of leaky confined aquifer systems is shown in figure 31. In systems one and two, each aquifer is composed of a semipervious upper layer confining a main artesian aquifer. The distinction between models 1 and 2 is that an unconfined aquifer does not exist above the upper confining unit in model 2. In system three, a series of high-permeability and low-permeability strata form the main artesian aquifer, which emulates a leaky aquifer due to its partitioning into multiple confining and permeable water-bearing units. All of these leaky aquifer models can emulate a Hantush-Jacob (1955) type curve without storage in aquitards depending upon the hydraulic and elastic properties of the semipervious confining units and permeable strata. The Hantush-Jacob (1955) and Hantush (1960) analytical solutions were derived under a simplified set of boundary conditions that have varying interpretations in field data.

For example, model 2 can emulate a leaky aquifer without storage in aquitards if the confining unit has storage *and* fracture permeability. In this

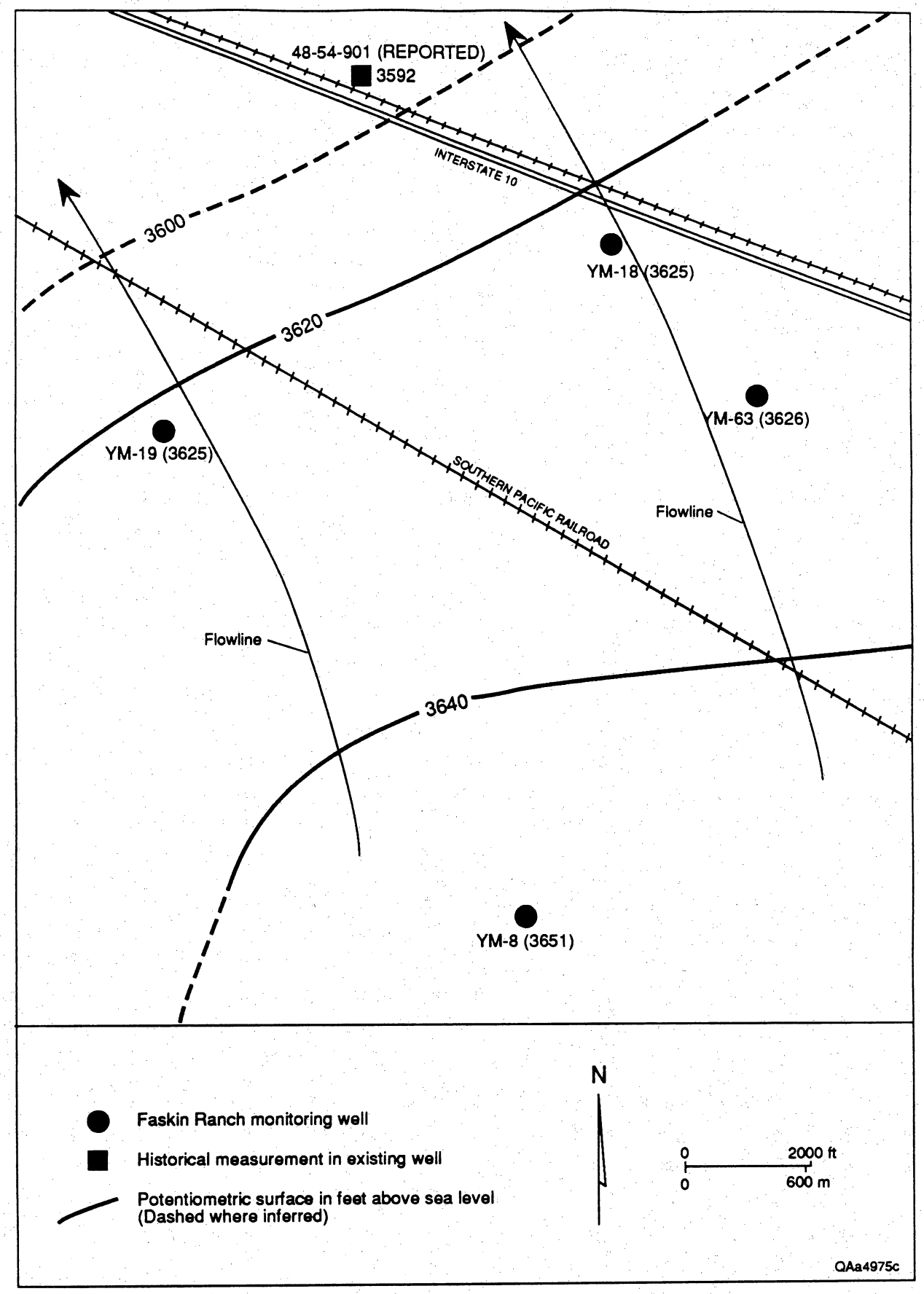

Figure 30. Map showing locations of monitoring wells and the potentiometric surface at Faskin Ranch.

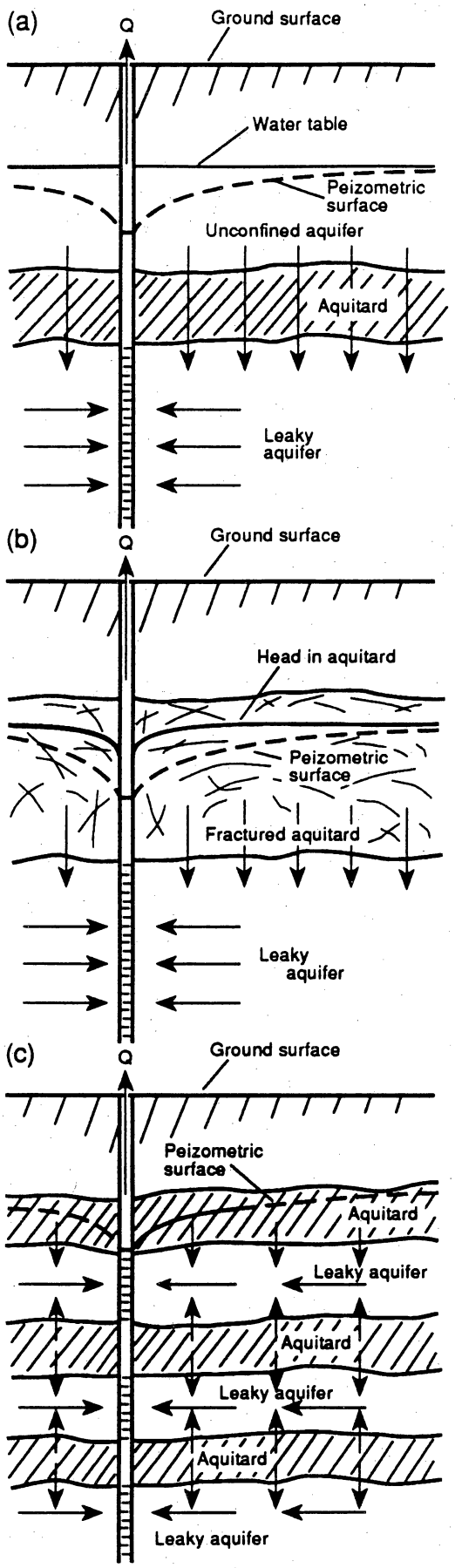

Figure 31. Various aquifer models (1, 2, and 3) that generate time-drawdown curves that emulate Hantush-Jacob (1955) type curves in leaky aquifers. Model 1 (a) has an unconfined aquifer above the semipervious unit; this model idealizes the Hantush-Jacob (1955) analytical model. Model 2 (b) has a semipervious unit with relatively high hydraulic conductivity and storage; in fact, this unit may almost be considered part of the aquifer. Model 3 (c) has a series of high and low permeability interbeds that emulate a leaky confined aquifer during a pump test. One cannot distinguish between these conceptual models with time-drawdown data only. Additional knowledge of the hydrogeology was needed to distinguish between these models in northwest Eagle Flat.

QAa4827c

instance, ground-water can leak in substantial quantities through the confining unit matrix into confining unit fractures and replenish the leaky confined aquifer by vertical leakage as readily as could a water table above the confining unit. The slightly fractured confining unit acts as a confining layer because its overall permeability is less than the permeability of the aquifer, for example, by a factor of 10.

Models 1 and 3 can emulate a leaky aquifer without storage in aquitards depending on the physical properties of the confining unit(s). In the case of model 1, the aquitard transmits water from saturated units above or below the semipervious layer, but contains negligible water in storage. In model 3, the less permeable interbeds contain moderate amounts of available water in storage and are permeable enough to vertically convey water to adjacent, more permeable interbeds. In all of these models, leakage may come from underneath as well as above the aquifer if wells are partially penetrating.

Additional knowledge of the hydrogeology of the aquifer at Faskin Ranch was needed in order to discriminate between these conceptual models. To determine why the Hantush-Jacob (1955) method for leakage without storage in aquitards generally provided the best curve match, the upper hydrostratigraphic unit at YM-63 was hydraulically tested as the test hole was progressively deepened during drilling. At drilling depths of 735, 760, and 785 ft (224, 232, and 239 m), the estimated depth to either the confining unit(s) (if the aquifer emulates models 2 and 3) or water table aquifer (if the aquifer emulates model 1), the borehole was evacuated of water three times, and water-level recovery rates in the borehole were monitored after final evacuation (fig. 32). Theis (1935) recovery analysis was used to provide a preliminary estimate of the transmissivity of the strata at these depths.

In addition to the monitoring of recovery rates, drilling mud was spiked with a rhodamine dye tracer, and water samples were collected for analyses of bromide, chloride, and rhodamine dye. These data were collected during testing for comparison with drilling mud samples before the well was completed and for comparison with water samples from the completed well.

Figure 33 compares recovery water for two penetration depths in the strata above 785 ft (239 m), the finished well, and a drilling mud sample. These data indicate that concentrations of conservative anions in recovery water are much higher than in drilling mud, and are similar to ionic concentrations in the finished well. Moderately low concentrations of rhodamine dye also indicate that

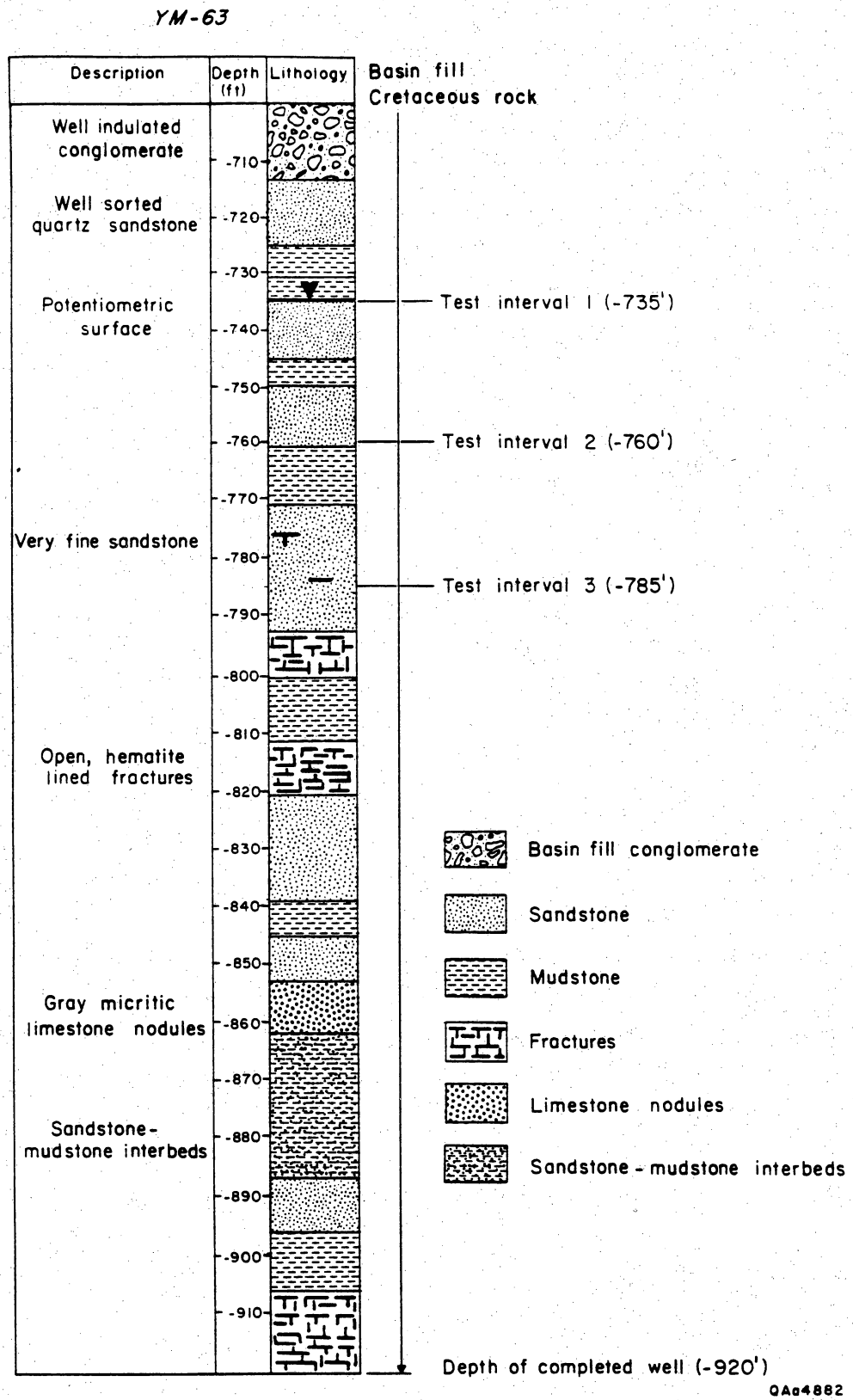

Figure 32. Schematic diagram that illustrates lithologies and depth intervals tested during coring operations at YM-63. At depths of 735, 760, and 785 ft below land surface, water samples were collected after the borehole was blown dry. Well recovery rates were analyzed and compared with recovery rates in the completed well (well depth = 920 ft). Water samples were collected during each recovery phase, and compared with drilling mud and formation water from samples later collected at the completed well. Testing indicated confining strata at these test intervals. Testing of the confining layer at these core depths helped to distinguish between conceptual aquifer models 1 through 3 (see fig. 31).

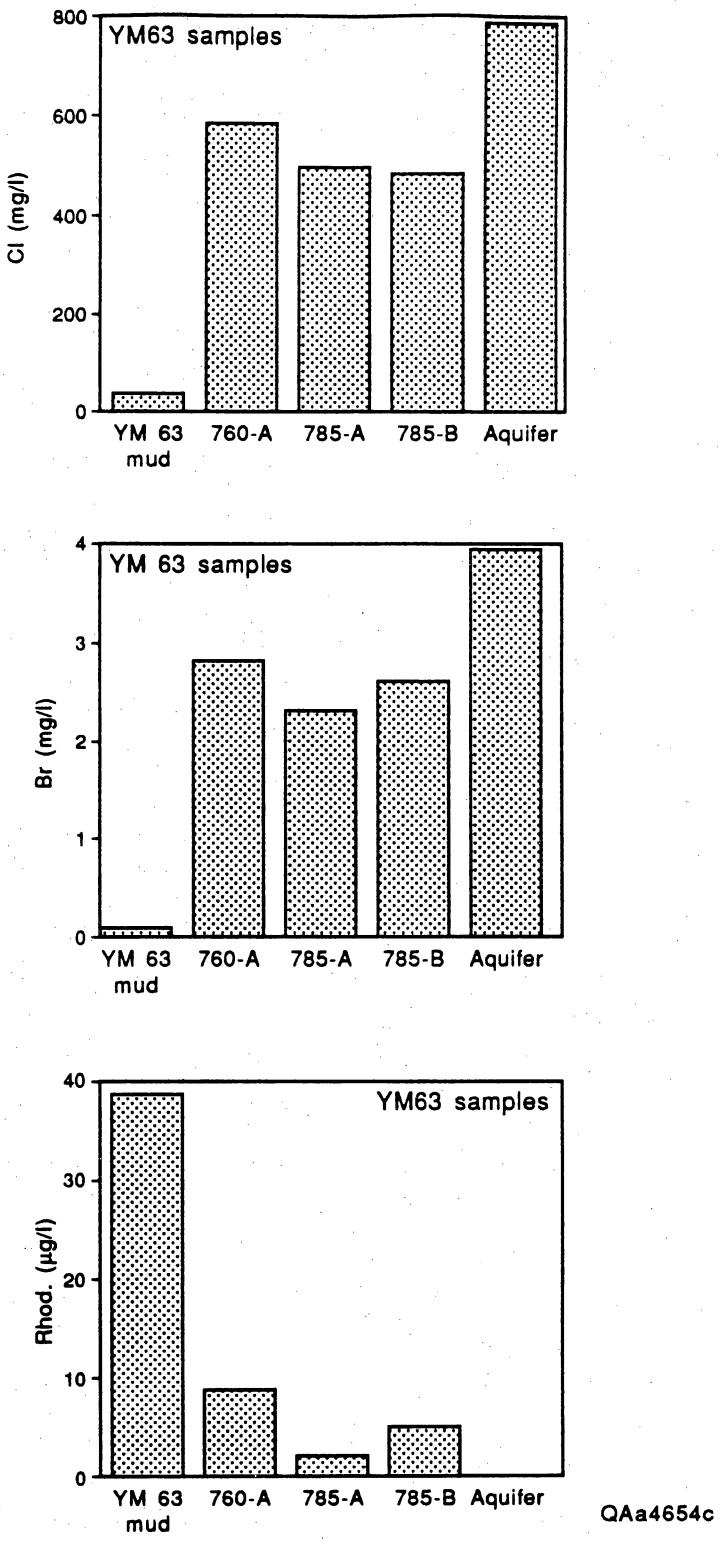

Figure 33. Comparison of conservative anions and rhodamine dye in drilling mud, recovery waters from well test intervals, and water collected from the completed well at YM-63. Two test samples collected at 785 ft (785-a and 785-b) and one test sample collected at 760 ft (760-a). Results of analysis of a drilling mud sample (YM-63 mud) and a sample from the completed well are shown. Comparisons between conservative anions and rhodamine dye indicate that almost 3/4 of recovery water is formation water at 760 and 785 ft. These results, along with recovery rates indicate considerable storage and yield from the semiconfining unit, or semiconfining interbeds at YM-63. These results imply conditions similar to conceptual models 2 or 3 (fig. 31) at YM-63.

almost 3/4 of the recovery water is formation water for penetration depths of 760 and 785 ft (232 and 239 m; fig. 33). No recovery water was collected at 735 ft (224 m) because the borehole was dry at that depth. Identical static water-level elevations at the 785 ft (239 m) test interval and in the completed water well (both 734 ft [224 m] below land surface) indicate hydraulic equilibrium between saturated strata above 785 ft (239 m) and in the aquifer.

Theis recovery analysis at the 785 ft (239 m) test interval provided a transmissivity estimate of 0.13 ft^2/day (0.012 m^2/day). Theis recovery analysis in the completed well provided a transmissivity estimate of 2.45 ft^2/day (0.23 m^2/day). Such a transmissivity value in the upper strata suggests either fractured blocks and the release of water from storage in the matrix blocks (emulating model 2) or leakage from permeable interbeds above 785 ft (239 m; emulating model 3). A water table aquifer does not exist above 785 ft (239 m) because the relatively slow rate of recovery at the 785 ft (239 m) test interval is indicative of a confining layer, or layers above that test interval.

The core data (fig. 32) may indicate that model 3 depicts the aquifer in northwest Eagle Flat (at least at YM-63) because few fractures were found in the upper confining unit, and more and less permeable sandstone and mudstone interbeds were present above 785 ft (239 m). The data are not fully adequate to distinguish between model types 2 and 3, however, because wells may not fully penetrate the aquifer. One can only speculate on the hydraulic properties of the underlying strata that could leak small amounts of water vertically upward into strata adjacent to the pumping well. Even so, the data permit us to eliminate conceptual model 1 because a water table aquifer does not exist above 785 ft (239 m), where a confining unit was identified by Theis recovery analyses.

The leaky aquifers at Faskin Ranch had a small range of transmissivity (2.4 to 10.2 ft^2/day [0.2 to 0.95 m^2/day]) with the Hantush-Jacob [1955] method) but the transmissivity distribution between boreholes is unknown. Small variance of values at widely distributed test holes probably indicates fairly uniform transmissivities between boreholes. Assuming that the aquifer transmissivity is uniform, the average linear ground-water velocity beneath Faskin Ranch can be computed simply:

$$v = \frac{Ki}{n} = 1.61 \text{ ft/year } (0.49 \text{ m/year})$$

where

K is the hydraulic conductivity (0.11 ft/day) [0.034 m/day]

i is the hydraulic gradient (0.002)

n is the effective porosity (assumed to equal 5 percent).

The hydraulic conductivity selected for the calculation was the highest in situ estimate at Faskin Ranch (using Hantush-Jacob [1955], table 3).

Ground water in the vicinity of Faskin Ranch, which is primarily Na-Cl to Na-SO_4-Cl in composition, is moderately saline (1,100 to 4,400 mg/L), with the highest salinities associated with the SO_4-dominated waters of wells 48-54-901, YM-18, and YM-63. Salinity increases significantly from Devil Ridge (figs. 13 and 14), toward YM-18 and YM-63. The high-Cl water can be traced southward, across Devil Ridge and into the northeastern margin of Red Light Draw, where it is tapped by well 48-62-BOR. Average ^{14}C is less than 6.63 PMC at YM-7A, decreasing to less than 4 PMC at Faskin Ranch, the proposed disposal site. With few exceptions, tritium levels are among the lowest in the region (0.00 TU).

Regional Conceptual Flow Model

The regional ground-water flow system is more heterogeneous and complex than that at Faskin Ranch, with circuitous three-dimensional flow components, fracture and double-porosity flow, hydrochemically zoned water in alternating permeable and low-permeability rock and poorly consolidated strata, and areal transitions between unconfined, confined, and leaky confined aquifers.

A conceptual model of ground-water flow, presented in map view, is shown in figure 34. Lines identifying two-dimensional cross-sectional models are shown in figure 35, and the conceptual models are presented in figures 36–38. Local flow systems originate in recharge areas in mountains and along mountain fronts and replenish the aquifers in the low-lying draws and flats. Precipitation recharge is mostly absent in flats and draws, except where water is shallow (i.e., 3 to 40 ft [0.9 to 12 m]) in terrace and alluvial deposits adjacent to the Rio Grande.

The extremely flat hydraulic gradients in northwest Eagle Flat, southeast Eagle Flat, and the northwestern part of Red Light Draw make it difficult to precisely delineate ground-water flowpaths in some low-lying areas (fig. 34),

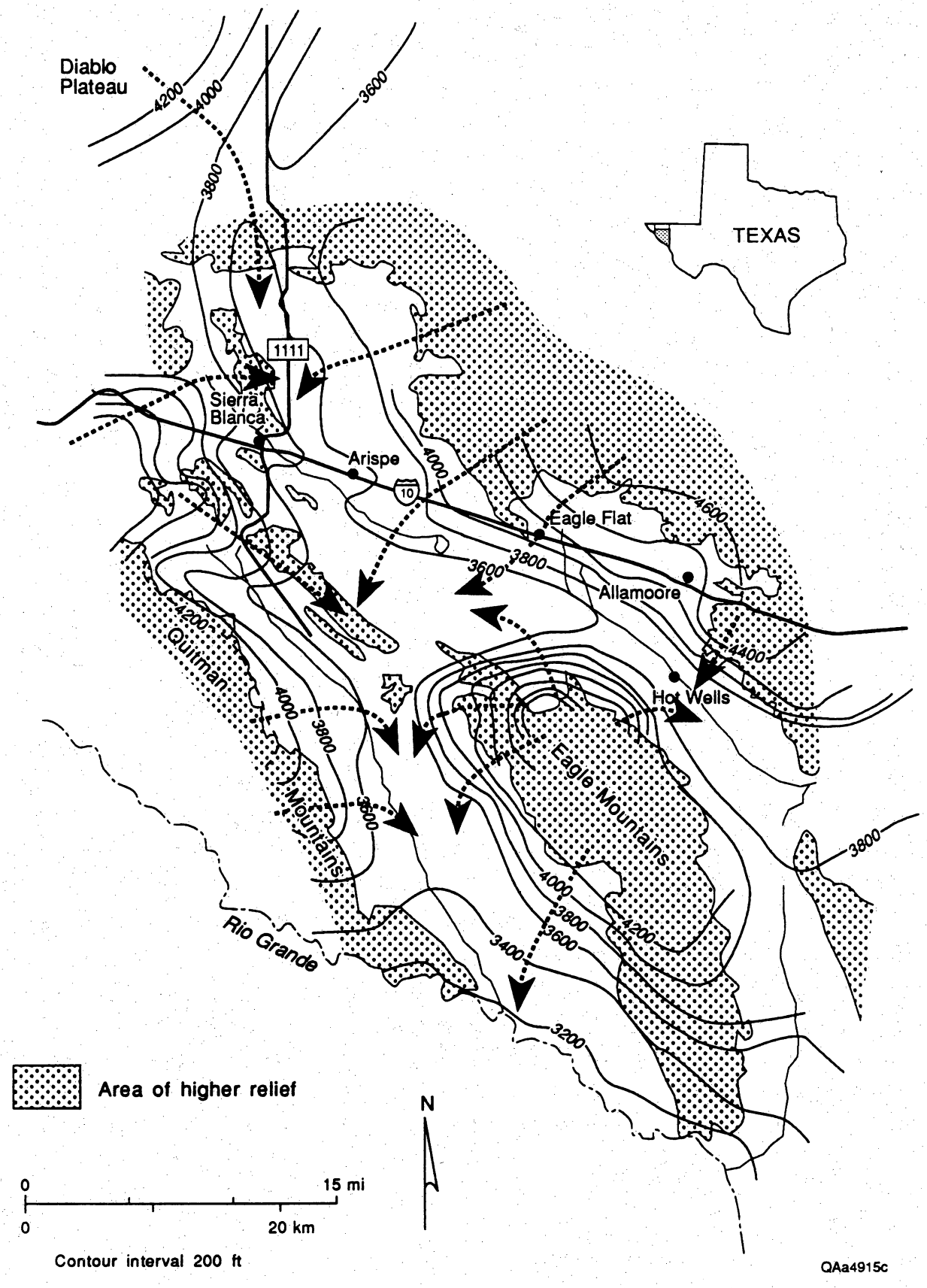

Figure 34. Planar conceptual model showing ground-water flow paths and potentiometric contours in map view.

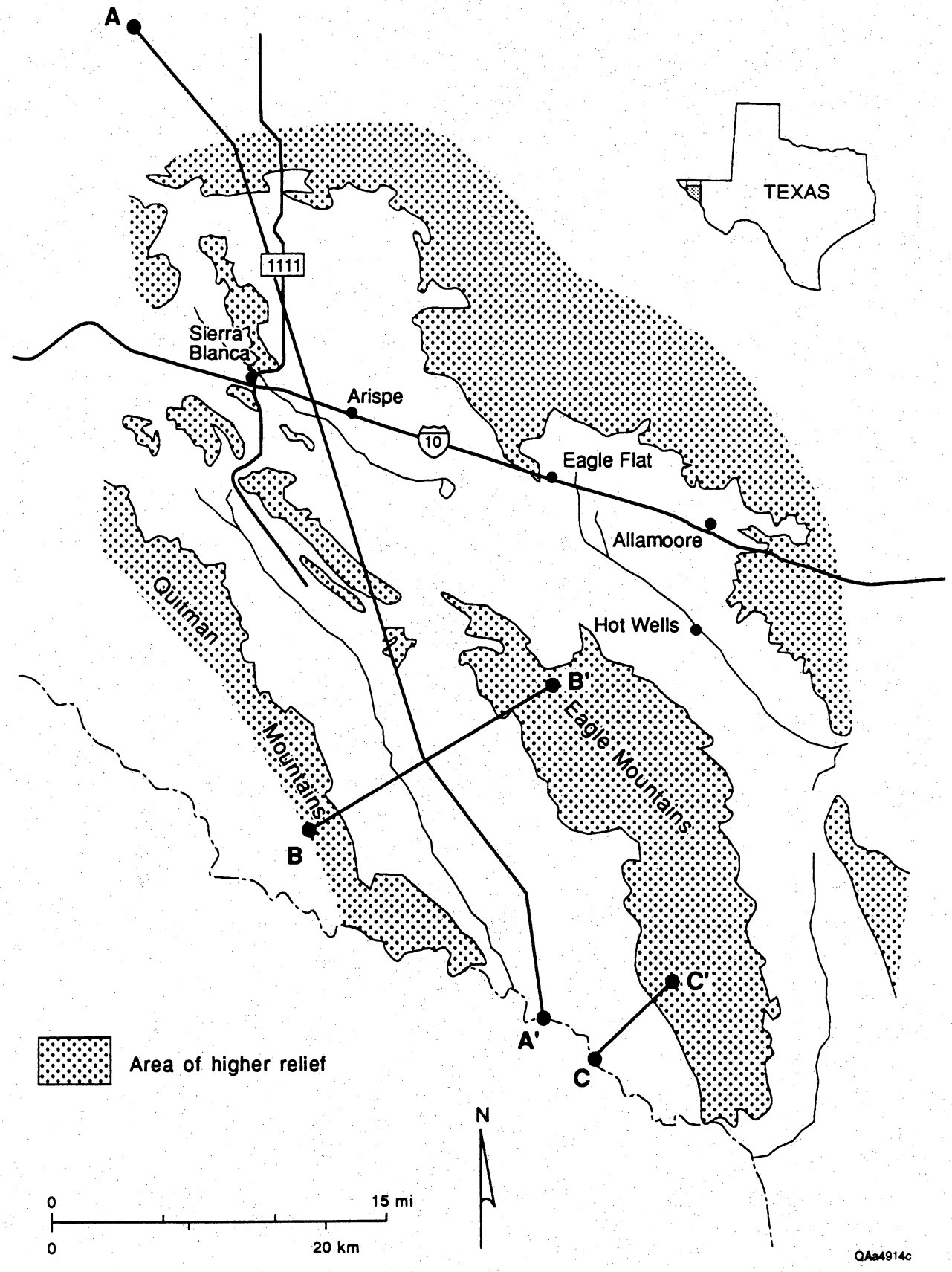

Figure 35. Location map showing orientation of conceptual hydrogeologic cross sections A-A′, B-B′, and C-C′.

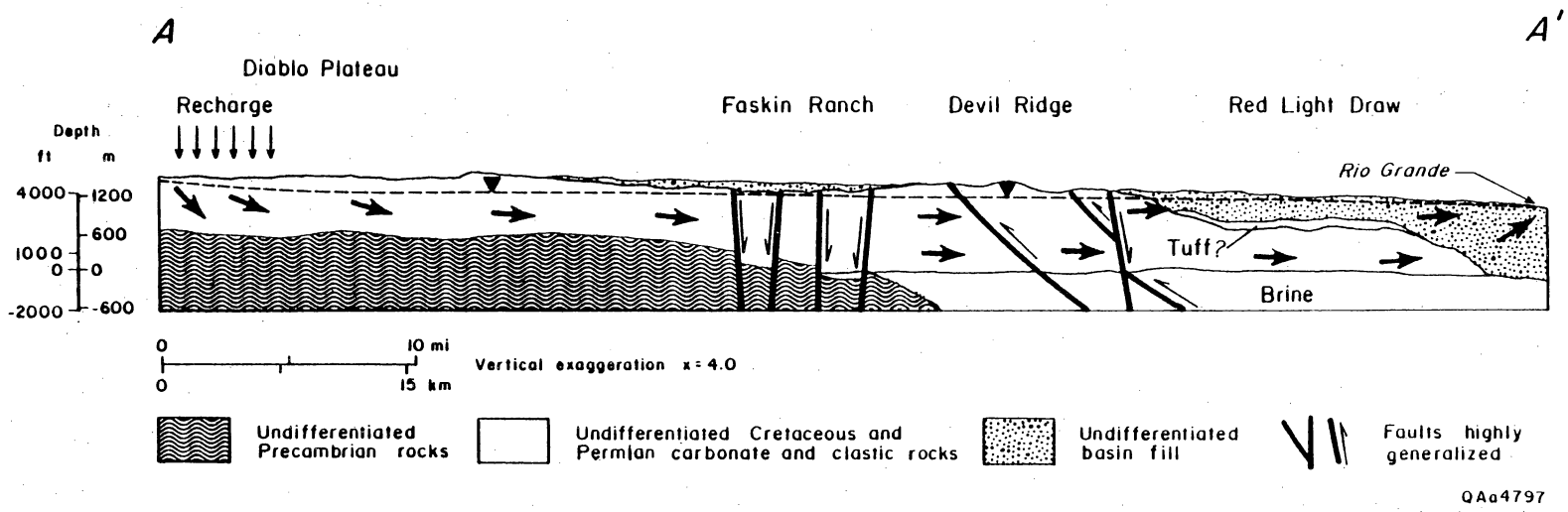

Figure 36. Conceptual hydrogeologic cross section A-A'.

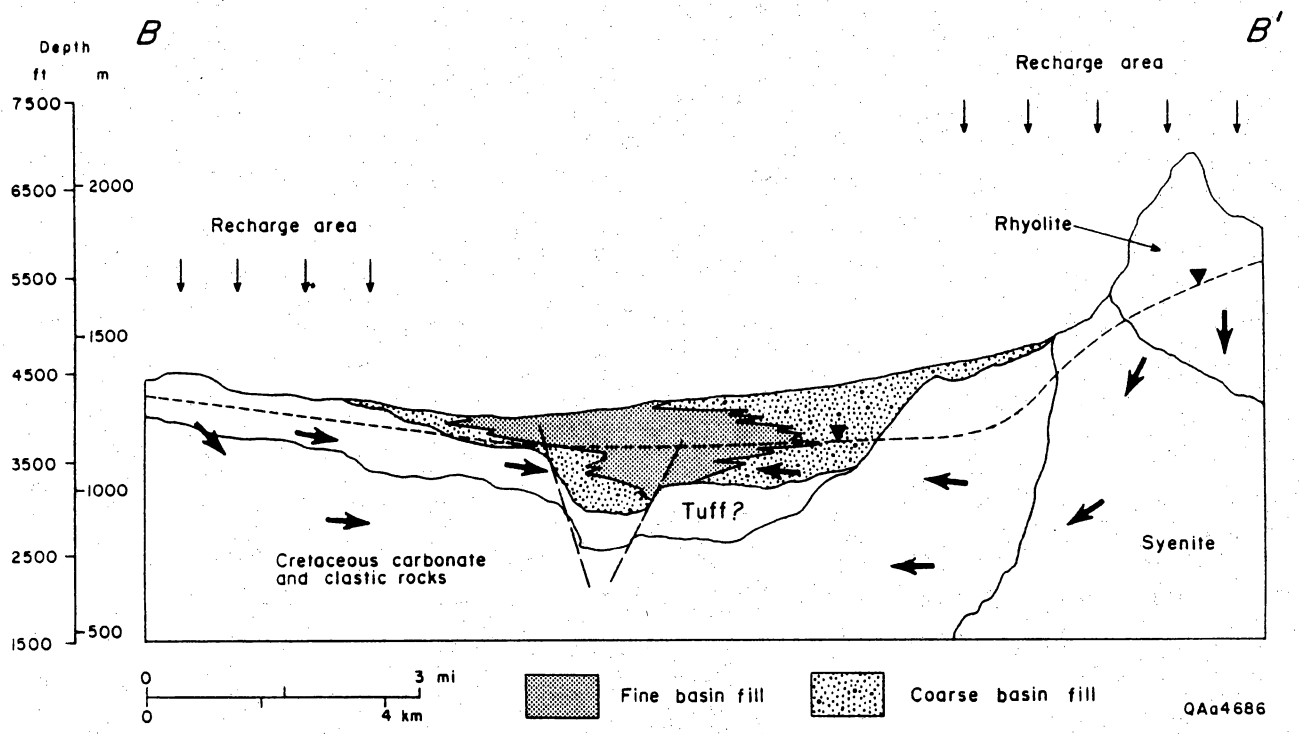

Figure 37. Conceptual hydrogeologic cross section B-B'.

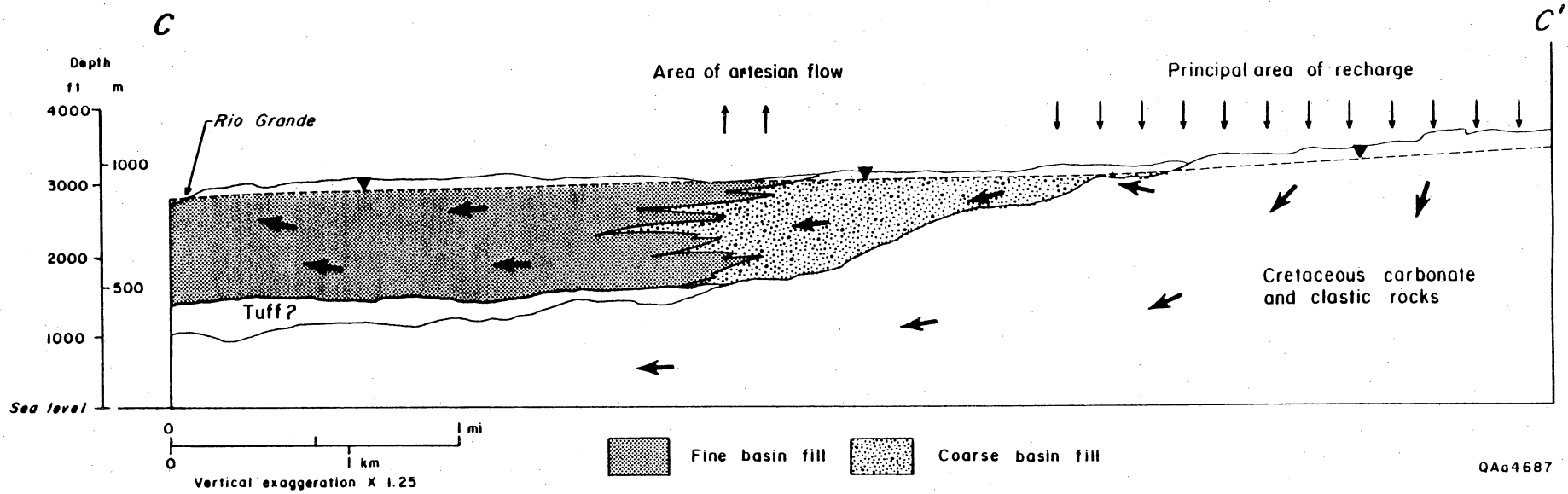

Figure 38. Conceptual hydrogeologic cross section C-C′.

although the regional trends of flow paths are evident. With a reasonable degree of certainty, regional ground-water flow paths are interpreted to be oriented along a trough in the potentiometric surface, from the Diablo Plateau, across northwest Eagle Flat and down Red Light Draw. Ground water probably discharges in very small amounts to low-lying areas along the Rio Grande. Because areas of high head in mountainous terrains bound the trough in the potentiometric surface, it is the only hydrologically plausible pathway for regional ground-water flow.

Hydrochemical similarities between ground waters in northwest Eagle Flat and ground water to the south of Devil Ridge at well 48-62-BOR possibly establish a hydraulic connection between the basins and suggests flow, probably in very small quantities, via circuitous routing along pathways controlled by stratigraphy and fractures around Devil Ridge. Even though hydraulic gradients and potentiometric surface elevations are similar in northwest and southeast Eagle Flat, the hydrochemical differences and slightly higher hydraulic heads to the east probably preclude flow from northwest Eagle Flat toward Scott's Crossing. In our interpretation, a ground-water divide separates the ground-water system in Eagle Flat into two completely separate hydrological systems.

The planar conceptual model (fig. 34) and geochemical data do not allow us to trace ground-water movement via the geochemical signature of waters from well 48-62-BOR in Red Light Draw to wells along the draw's southeast-trending axis. The lack of moderately saline waters along the trough may occur as a result of mixing of large quantities of much less saline water in the bolson aquifer of Red Light Draw or may occur as a result of submergence of waters beneath the bolson aquifer and movement along the northwest-striking bedrock formations subparallel to the axis of Red Light Draw (fig. 34). Under the latter scenario, these saline waters eventually discharge to low-lying areas adjacent to the Rio Grande by upwelling at the lower (southeast) end of the basin.

Hydraulic segregation of saline waters may be enhanced by the presence of a semiconfining unit of pyroclastic flows and tuffs that locally rest on the valley floor in Red Light Draw, separating Cretaceous carbonate and sandstone formations from moderately to poorly indurated bolson fill (fig. 36). The low permeability of the volcanic rocks might keep the waters separate. Segregation may also be an artifact of sample depths, as many wells in Red Light Draw do not penetrate deeply into the saturated bolson fill. These wells yield fresh waters that originally were derived from the Eagle and Quitman recharge areas, and

may be stratified atop the more saline waters that are not intercepted by small cones of depression associated with low production from livestock and domestic wells.

Unfortunately, our sampling plan cannot prove stratified waters because deep wells do not exist in Red Light Draw. There is only indirect geochemical evidence of submergence of saline waters beneath Red Light Draw (e.g., Cl/Br ratios), along with the acknowledged view that "there commonly is a deep ground-water flow system that causes an upwelling of mineralized water at the lower end of the basins" along the Rio Grande (Kernodle, 1992). Numerical flow modeling and pathline simulations are the only means available at present to test flow hypotheses.

Numerical Flow Modeling

The numerical flow model tests hypotheses regarding segregation of slightly saline waters in Cretaceous bedrock aquifers beneath freshwaters in Red Light Draw and eventual upwelling near the Rio Grande floodplain. The profile model, oriented northwest-southeast between the Diablo Plateau and the Rio Grande, corresponds to hydrogeologic cross section A–A′ (fig. 36). The model estimates ground-water flow velocities, horizontal and vertical pathlines, and residence times along the line of section.

The model mesh consists of 37 layers and 114 columns. Several model layers were constructed in order to simulate vertical flow components if and where they exist. Expected areas of vertical flow include recharge areas on the Diablo Plateau and discharge areas near the Rio Grande. The dimensions of the finite difference blocks are 125 by 2,500 ft (38 by 762 m), for a total of 4,218 nodes.

Boundary conditions were selected to correspond as closely as possible to actual hydrologic boundaries (fig. 39). A no-flow boundary was established at a depth of about 200 ft (61 m) below sea level at the brackish/brine water interface. The absolute depth to this transitional interface, though uncertain, is selected to correspond to the elevation of the brine/brackish water interface identified at other Trans-Pecos aquifers near the Rio Grande (Alvarez and Buckner, 1980).

The northern boundary of the model is no flow, which corresponds to a ground-water divide on the Diablo Plateau (Kreitler and others, 1990; Mullican and Senger, 1992). A prescribed flux (Neumann) boundary replenishes the aquifer to the south of the divide. The southern boundary of the model

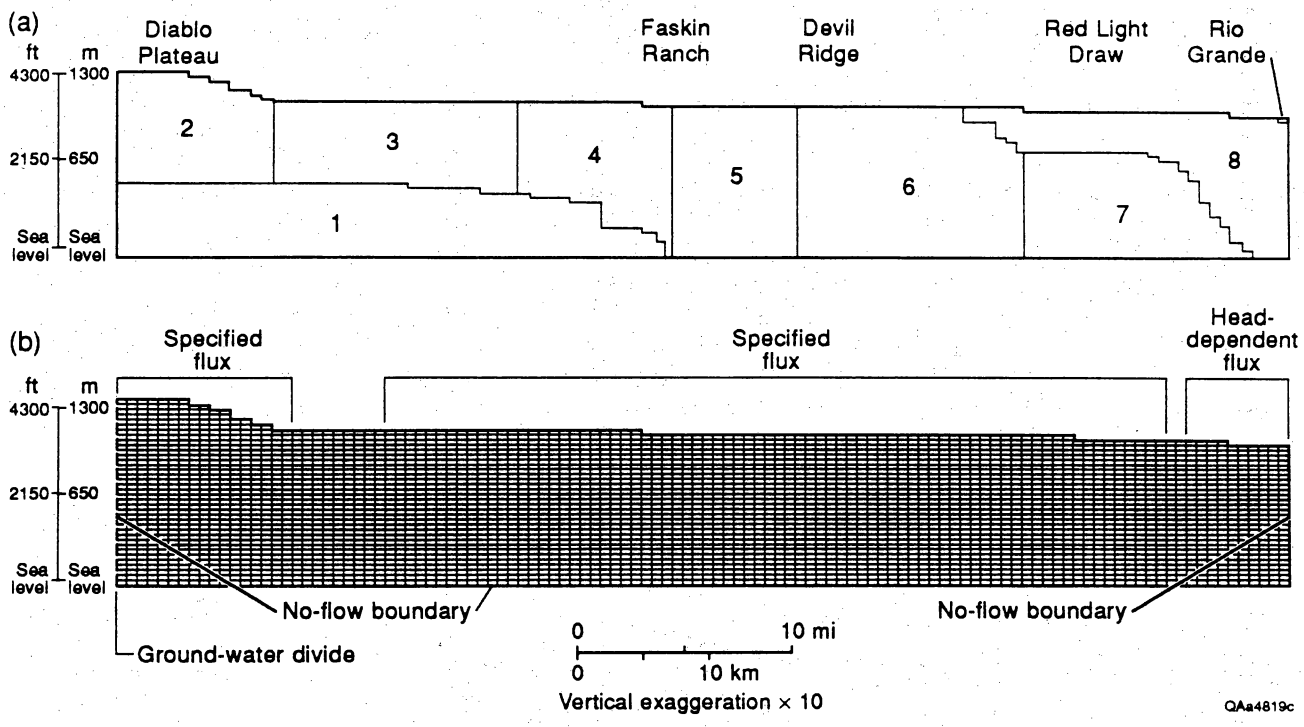

Figure 39. Diagram showing the discretization scheme, the aquifer zones, and the boundary conditions selected for the numerical profile model oriented between the Diablo Plateau and the Rio Grande.

corresponds to a head-dependent flux boundary at the Rio Grande, developed with the river package of MODFLOW. Head-dependent flux boundaries were also selected to correspond to low-lying areas close to the Rio Grande where discharge by evapotranspiration occurs.

The governing equations of the model are solved with the preconditioned conjugate gradient solver package of MODFLOW (Hill, 1990). The model includes a routine that allows cells to rewet during model iteration (McDonald and others, 1991). This routine is used because very large head changes during the first few model iterations resulted in the dewatering of an excessive number of cells. As the numerical model begins to converge to an acceptable solution, dry cells must rewet so that the cells are included in the final solution. Dry cells are not allowed to rewet in MODFLOW unless this routine is used.

Definition of Model Properties

Hydraulic conductivities assigned to the model grid (fig. 39) were selected to correspond to major rock units and sediment types on hydrogeologic cross section A–A′ (fig. 36). Where pump test and specific capacity data were available, rock types were separated into zones that correlated with spatial variations of transmissivity. These zones were refined after lithologic, structural, and geologic descriptions were summarized (e.g., Albritton and Smith, 1965; Jones and Reaser, 1970; Underwood, 1972). Where well test data were not available, hydraulic conductivity values of rocks were selected from published values (Davis, 1969; Brace, 1980; Wolff, 1982; Bedinger and others, 1986; Kernodle, 1992; Mullican and Senger, 1992) and from lithologic descriptions of the rocks and sediments (King and Flawn, 1953; Albritton and Smith, 1965; Jones and Reaser, 1970; Underwood, 1972; Gates and others, 1976; Gates and others, 1980).

On the basis of published values (Brace, 1980; Bedinger and others, 1986) and lithologic descriptions (King and Flawn, 1953), the Precambrian basement rocks of zone 1 were assigned a low permeability value of 0.006 ft/day (0.002 m/day). Permian and Cretaceous carbonate and siliciclastic rocks were assigned permeabilities by zone. These zones were selected on the basis of field estimated parameters, the structural characteristics of the rocks, and the potentiometric surface. Six zones (zones 2–7; fig. 39, and table 6) were selected for Permian and Cretaceous rocks.

Table 6. Initial hydraulic conductivities assigned to permeability zones in the model.

Permeability zone	Description	Initial hydraulic conductivity (ft/day)
1	Undifferentiated Precambrian Strata	0.006
2	Undifferentiated Cretaceous and Permian Strata (Diablo Plateau)	0.5
3	Undifferentiated Cretaceous and Permian Strata (Blanca Draw Area)	2
4	Undifferentiated Cretaceous and Permian Strata (Sierra Blanca Area)	0.17
5	Undifferentiated Cretaceous and Permian Strata (Faskin Ranch Area)	0.09
6	Undifferentiated Cretaceous and Permian Strata (Red Hills and Devil Ridge Thrust Belt)	3.2
7	Undifferentiated Cretaceous and Permian Strata (Beneath Red Light Draw)	0.9
8	Basin Fill (Red Light Draw)	0.25

Zone 2 is in the Diablo Plateau recharge province, where steep hydraulic gradients probably indicate locally low transmissivity (e.g., 10 to 50 ft^2/day [0.9 to 4.6 m^2/day]. An initial hydraulic conductivity value of 0.5 ft/day (0.15 m/day) was selected for this carbonate and siliciclastic zone. Zone 3 is enclosed by Blanca Draw, where steep hydraulic gradients characteristic of the margins of the Diablo Plateau become very flat (fig. 34). The flat hydraulic gradient may be associated with a considerable increase in permeability of the rocks. Specific capacity tests at wells 48-54-201 and 48-45-603 indicated relatively high transmissivity values (respectively, 20,499 ft^2/day and 891 ft^2/day [1,904 m^2/day and 83 m^2/day]) in this zone. High transmissivities may have resulted from fracturing and arching of these sedimentary rocks during emplacement of tertiary intrusives (e.g., the Sierra Blanca laccolith). An initial hydraulic conductivity value of 2 ft/day (0.6 m/day) was selected for zone 3.

Hydraulic conductivity values of 0.17 and 0.09 ft/day (0.05 and 0.03 m/day) were selected, respectively, for zones 4 and 5. The permeability of these zones were selected from a specific capacity test on a 1,100-ft (335-m) deep well in Sierra Blanca (well 48-54-401; calibrated transmissivity = 56 ft^2/day [5 m^2/day]; table 3) and from well tests on Faskin Ranch (table 2), where the lowest transmissivity values were obtained. Zone 6 corresponds to the Red Hills and Devil Ridge thrust belt, where rocks are more highly jointed and fractured and are presumably quite permeable. A specific capacity test on well 48-62-TEX and calibrated test results of 2362 ft^2/day (219 m^2/day) confirmed a moderately high transmissivity in the zone. A hydraulic conductivity of 3.2 ft/day (1.0 m/day) was specified for rocks in zone 6.

Well test data were not available for carbonate and siliciclastic rocks beneath Red Light Draw (zone 7). The geologic and structural history of the draw would suggest that these rocks have moderate permeabilities (Underwood, 1962; Jones and Reaser, 1970). An initial hydraulic conductivity value of 0.9 ft/day (0.3 m/day) was selected for this zone.

Basin fill that comprises zone 8 was assigned a hydraulic conductivity value of 0.25 ft/day (0.08 m/day). This bulk value may overestimate hydraulic conductivity because geophysical information and test hole data suggest that low permeability volcanic tuffs and volcaniclastic materials may comprise most of the lower basin fill (Gates and others, 1976; Gates and others, 1980). Higher in the stratigraphic column, the bolson fill is predominantly mud-rich sediments that have characteristically low permeabilities (see figs. 37 and 38). A somewhat high

hydraulic conductivity value (0.25 ft/day [0.08 m/day]) is chosen for zone 8 because the bolson fill along the axis of Red Light Draw contains sand-and-gravel interbeds in the mud-dominated stratigraphic column.

Vertical flow within and between individual units was simulated by specifying vertical conductance between model layers. Vertical conductance is the thickness-weighted harmonic mean of the values of vertical hydraulic conductivity of each layer. Vertical conductance is computed with the following equation:

$$VCONT = \frac{1}{\frac{B_{(K+1)}/2}{K_{V(K+1)}} + \frac{B_K/2}{K_{VK}}}$$

where

B_{K+1} = thickness of upper layer K+1

B_K = thickness of lower layer K

$K_{V(K+1)}$ = vertical hydraulic conductivity of upper layer K+1

K_{VK} = vertical hydraulic conductivity of lower layer K.

Vertical hydraulic conductivity distribution in the model was not influenced by overburden pressure. Bedinger and others (1986) suggest that hydraulic conductivity is as much as an order of magnitude higher in the upper 100 to 500 ft (30.5 to 152 m) of bedrock due to weathering and expansion of fracture apertures that succeeds erosional unloading of overburden pressures. At depths greater than 100 to 500 ft (30.5 to 152 m), the hydraulic conductivity of the rocks is only slightly influenced by additional overburden pressures. Overburden pressures, therefore, probably do not cause a systematic decrease in hydraulic conductivity at depths greater than 100 to 500 ft (30.5 to 152 m) beneath the bedrock surface (Bedinger and others, 1986).

In most areas, the profile model simulates flow in water bearing strata at depths greater than 500 ft (152 m) beneath the top of bedrock. No data exist on the hydraulic conductivity of water-bearing strata beneath the uppermost saturated units. Therefore, a systematic decrease (or increase) in hydraulic

conductivity with depth cannot be simulated in the model. Horizontal and vertical hydraulic conductivity values are assumed constant with depth in any particular zone.

Porosity values for particle-tracking simulations were assumed as follows: Precambrian rocks (0.02), Permian and Cretaceous carbonate and siliciclastic rocks (0.05), and bolson fill (0.18). These values were compiled from literature values (Wolff, 1982; Bedinger, 1986), and from lithologic descriptions of the rocks and sediments (King and Flawn, 1953; Jones and Reaser, 1970; Gates and others, 1980).

Steady-State Simulation

Inflows occur along the flanks of the profile where areas of high head bound the trough in the potentiometric surface (fig. 40A). These inflows influence hydraulic gradients and account for added water mass to the system. These additions of water mass are represented as prescribed fluxes at the upper model boundary (fig. 40B). The model was developed by matching the simulated hydraulic gradient with the measured hydraulic gradient between the Diablo Plateau and the Rio Grande. This was accomplished in four separate model scenarios (table 7) with varying prescribed flux inputs in areas where water mass is added along the trough flanks (zones 4, 5, 6, and 8).

In the first model scenario the agreement between the measured and simulated potentiometric surface is good (fig. 41). Where prescribed flux inputs were maintained at constant rates at zones 2 and 3, the hydraulic conductivity values were adjusted from initial values of 0.5 and 2 ft/day (0.2 and 0.6 m/day) to final values of 0.0091 and 0.97 ft/day (0.0028 and 0.30 m/day; table 8). Through repeated trials, the match between the measured and simulated heads was obtained with only very small fluxes at zones 4 to 8 (table 9). The recharge rate in the Diablo Plateau that established the fit is 0.123 in/yr (0.312 cm/yr; or 1.02 percent of mean annual precipitation).

Pathline modeling illustrates vertical flow between northwest Eagle Flat and Red Light Draw, downward beneath Devil Ridge in the thrust belt zone (zone 6). Waters move laterally underneath Red Light Draw and then discharge by vertical upwelling beneath the Rio Grande discharge boundary in the model (fig. 42). Each particle path is flagged by time-markers at 4,000-year intervals. These results estimate a total travel time of 60,178 years between the Diablo

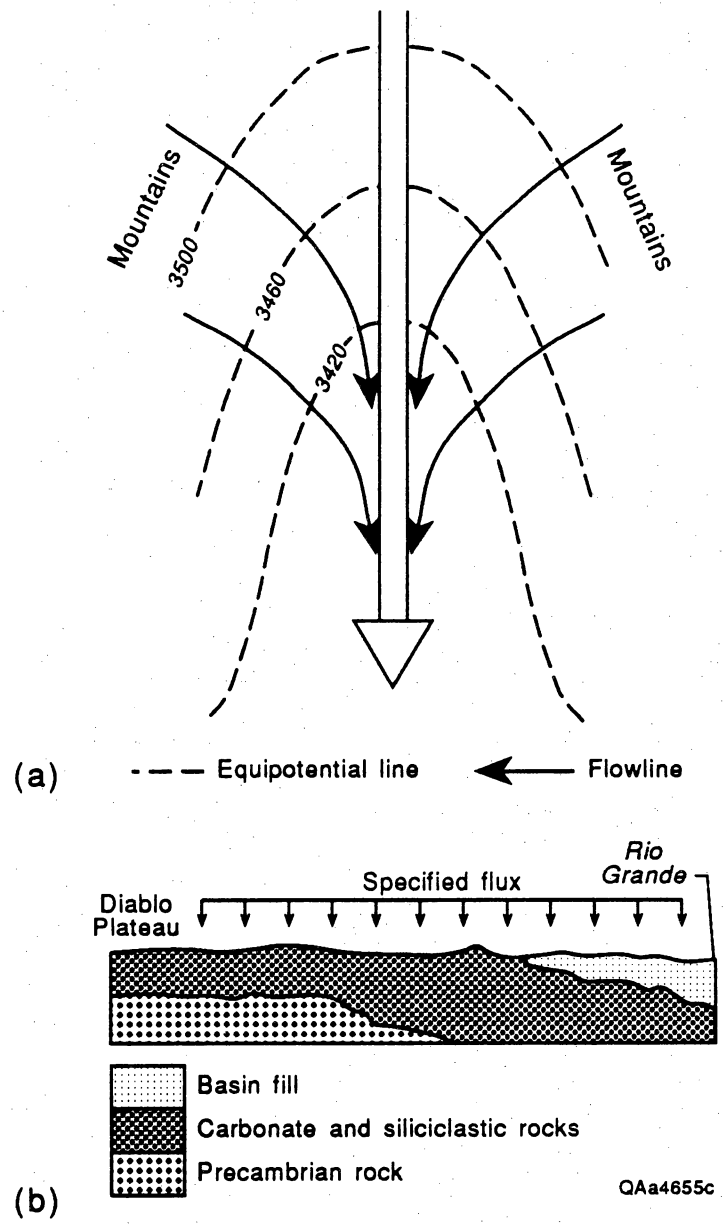

Figure 40. Conceptual diagram indicating how inflows of water from adjacent highlands (a) add water mass to regional flowpath A-A'. This is evident in figure 34. These inflows must be accounted for in the profile model and are treated as specified flux rates to the upper model grid (b). These rates are adjusted during model development to match the simulated hydraulic gradient along the regional flowpath with the measured hydraulic gradient.

Table 7. Summary of hydraulic conductivity and horizontal to vertical anisotropy ratios specified in four model scenarios.

HYDRAULIC CONDUCTIVITY AND ANISOTROPY VARIATION IN 4 MODEL SCENARIOS		
Model scenario	**Hydraulic conductivity**	**Horizontal to vertical anisotropy ratio**
1	Initial input values from table 8 modified slightly to match the simulated and measured hydraulic gradient.	1
2	Final values used in model scenario 1.	100
3	Final values used in model scenario 1, except for zone 7, which is decreased by one order of magnitude.	1
4	Final values used in model scenario 1 increased by one order of magnitude in every zone.	1

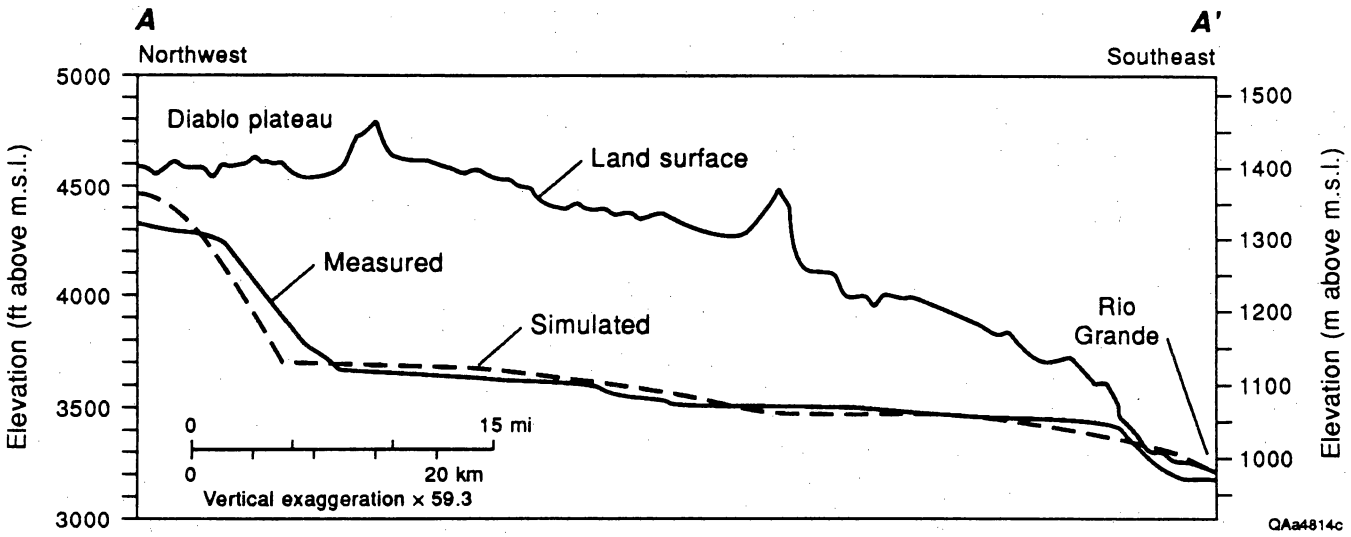

Figure 41. Comparison of measured and simulated potentiometric surface shown in cross section for model scenario 1. Simulated potentiometric surface obtained by using the simulated head value in the uppermost saturated cell in each column of the model.

Table 8. Comparison of initial and final model hydraulic conductivities in model scenario 1, and other model parameters specified in model scenarios 1 through 4.

INITIAL AND FINAL MODEL PARAMETERS IN 4 MODEL SCENARIOS					
Model scenario	Zone and rock or sediment unit	Initial hydraulic conductivity (ft/day)	Final hydraulic conductivity (ft/day)	Effective porosity	Horizontal to vertical anisotropy ratio
1	#1: Precambrian Rocks	0.006	0.006	0.02	1
1	#2: Carbonate & clastic	0.5	0.0091	0.05	1
1	#3: Carbonate & clastic	2	0.97	0.05	1
1	#4: Carbonate & clastic	0.17	0.17	0.05	1
1	#5: Carbonate & clastic	0.09	0.09	0.05	1
1	#6: Carbonate & clastic	3.2	3.2	0.05	1
1	#7: Carbonate & clastic	0.9	0.9	0.05	1
1	#8: Basin fill	0.25	0.25	0.18	1
2	#1: Precambrian Rocks	-	0.006	0.02	100
2	#2: Carbonate & clastic	-	0.0091	0.05	100
2	#3: Carbonate & clastic	-	0.97	0.05	100
2	#4: Carbonate & clastic	-	0.17	0.05	100
2	#5: Carbonate & clastic	-	0.09	0.05	100
2	#6: Carbonate & clastic	-	3.2	0.05	100
2	#7: Carbonate & clastic	-	0.9	0.05	100
2	#8: Basin fill	-	0.25	0.18	100
3	#1: Precambrian Rocks	-	0.006	0.02	1
3	#2: Carbonate & clastic	-	0.0091	0.05	1
3	#3: Carbonate & clastic	-	0.97	0.05	1
3	#4: Carbonate & clastic	-	0.17	0.05	1
3	#5: Carbonate & clastic	-	0.09	0.05	1
3	#6: Carbonate & clastic	-	3.2	0.05	1
3	#7: Carbonate & clastic	-	0.09	0.05	1
3	#8: Basin fill	-	0.25	0.18	1
4	#1: Precambrian Rocks	-	0.06	0.02	1
4	#2: Carbonate & clastic	-	0.091	0.05	1
4	#3: Carbonate & clastic	-	9.7	0.05	1
4	#4: Carbonate & clastic	-	1.7	0.05	1
4	#5: Carbonate & clastic	-	0.9	0.05	1
4	#6: Carbonate & clastic	-	32	0.05	1
4	#7: Carbonate & clastic	-	9	0.05	1
4	#8: Basin fill	-	2.5	0.18	1

Table 9. Model recharge rates specified in the Diablo Plateau (zone 2) and inflow rates specified in zones 4, 5, 6, and 8. Annual precipitation is assumed to equal 12 inches/year (30.5 cm/year).

FINAL RECHARGE AND INFLOW RATES FOR MODEL SCENARIOS 1 TO 4			
Model scenario	**Recharge area or inflow zone**	**Average recharge or inflow (in/year)**	**Percentage of annual precipitation (%)**
1	Diablo Plateau	0.123	1.02
1	Inflow to zones 4,5,6,8	0.131	1.10
2	Diablo Plateau	0.0876	0.73
2	Inflow to zones 4,5,6,8	0.0569	0.47
3	Diablo Plateau	0.0788	0.66
3	Inflow to zones 4,5,6,8	0.0394	0.33
4	Diablo Plateau	1.231	10.26
4	Inflow to zones 4,5,6,8	1.73	14.42

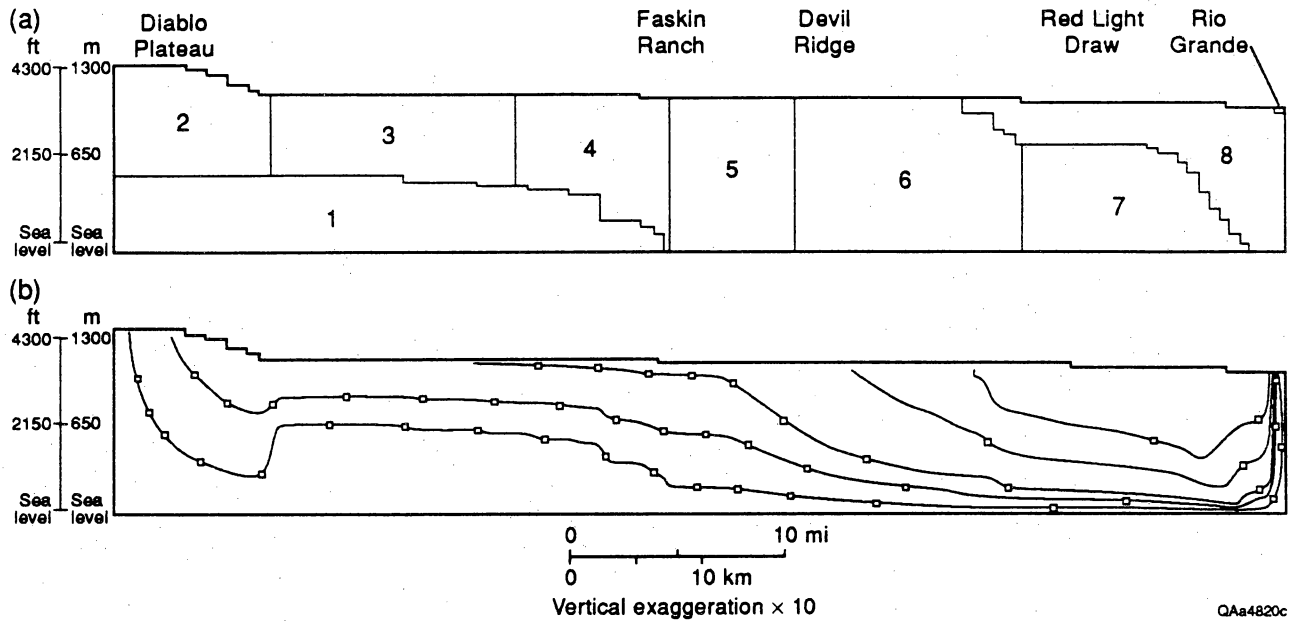

Figure 42. Particle-tracking simulations showing pathlines moving underneath the Red Light Draw bolson; model scenario 1; heterogeneous, isotropic units. Each pathline marker indicates a travel time of 4,000 years. Pathlines originating at the top of the model profile (zones 3 through 8) are representative of inflows from adjacent highlands (see fig. 41).

Plateau recharge area and the Rio Grande (table 10). Travel times along intermediate pathways are shown in the diagram. A travel time of 19,134 years, for example, is estimated between Faskin Ranch and the Rio Grande.

Horizontal to vertical anisotropies may vary between 10 and 1000 in basin fill (Hearne and Dewey, 1988; Frenzel and Kaehler, 1992; Kernodle, 1992). These ratios also may vary in rock aquifers depending upon the orientation and interconnectedness of fractures, and the strike and dip of the strata and bedding planes. The effect of horizontal to vertical anisotropy was tested in the second model scenario.

The vertical conductance is decreased by a factor of 100 at all model nodes to simulate a horizontal to vertical anisotropy ratio of 100 (table 8). A slightly lower recharge rate of 0.0876 in/yr (0.223 cm/yr; or 0.73 percent mean annual precipitation) in the Diablo Plateau provided a match between the measured and simulated gradient (table 9 and fig. 43). Vertical pathlines are slightly more subdued in this simulation despite longer residence times (fig. 44). Particles of water require additional time to "leak" through the less permeable interfaces between adjacent model layers. A total travel time of 97,789 years is shown for particles tracked from the Diablo Plateau to the Rio Grande (table 10). The simulated travel time between Faskin Ranch and the Rio Grande is 29,775 years.

In the third model scenario, the sensitivity of model pathlines to lower bedrock permeabilities beneath Red Light Draw was tested. The hydraulic conductivity of zone 7 was decreased to 0.09 ft/day (0.03 m/day) from an initial value of 0.9 ft/day (0.3 m/day; table 8). This hydraulic conductivity value is about 2.5 times less than the simulated hydraulic conductivity of Red Light Draw bolson (zone 8).

A recharge rate of 0.0788 in/yr (0.200 cm/yr; or 0.66 percent mean annual precipitation) in the Diablo Plateau provided a match between the measured and simulated gradient in model scenario 3 (table 9 and fig. 45). Vertical pathlines move beneath Red Light Draw, although the effect of higher relative permeability in zone 8 is evident on pathlines beneath the bolson fills (fig. 46). A total travel time of 101,820 years is shown for particles tracked from the Diablo Plateau to the Rio Grande (table 10). The simulated travel time between Faskin Ranch and the Rio Grande is 43,619 years in the third model scenario.

In order to demonstrate that hydraulic conductivities selected for model scenarios 1 to 3 are reasonable, a fourth model scenario was developed to test the extent to which ground-water velocities increase with uniformly higher

Table 10. Summary of ground-water travel times between the Diablo Plateau and the Rio Grande and between Faskin Ranch and the Rio Grande in four model scenarios.

MODEL ESTIMATED TRAVEL TIMES IN YEARS		
Model Scenario	**Diablo Plateau - Rio Grande**	**Faskin Ranch - Rio Grande**
1	60,178	19,134
2	97,789	29,775
3	101,820	43,619
4	8,054	2,995

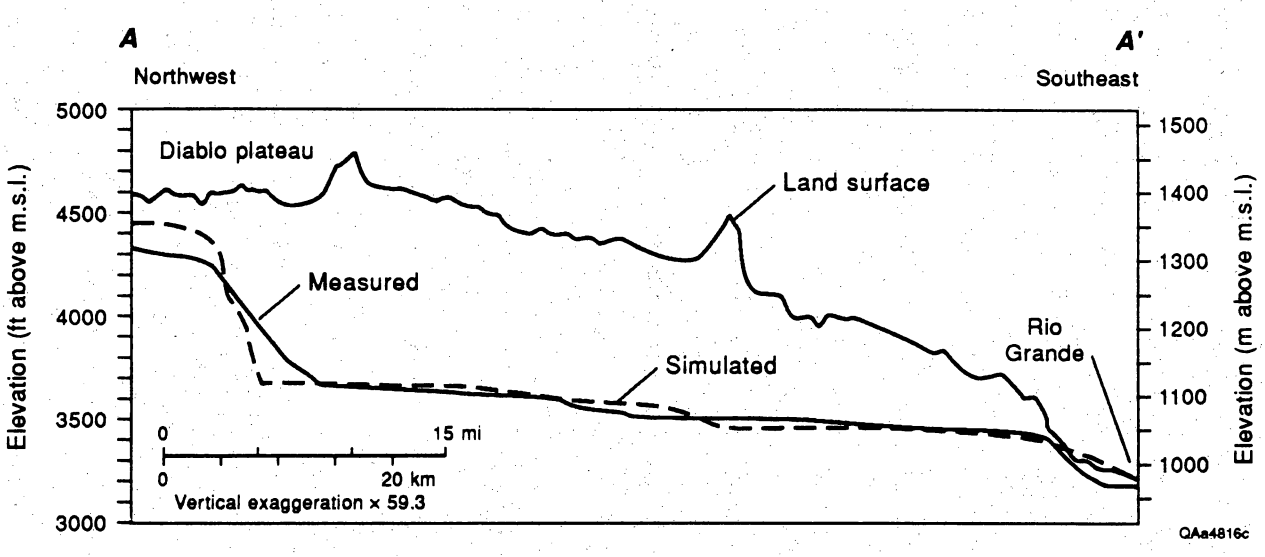

Figure 43. Comparison of measured and simulated potentiometric surface shown in cross section for model scenario 2 (horizontal to vertical anisotropy = 100:1). Simulated potentiometric surface obtained by using the simulated head value in the uppermost saturated cell in each column of the model.

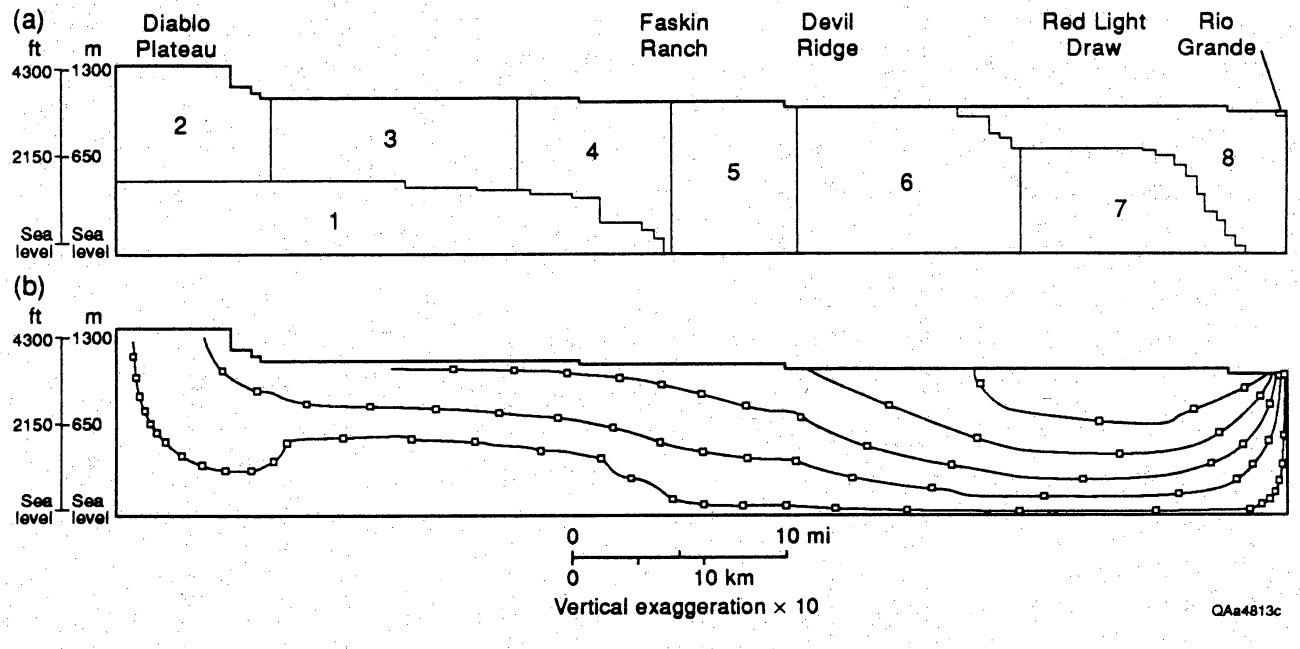

Figure 44. Particle-tracking simulations showing pathlines moving underneath the Red Light Draw bolson; model scenario 2; heterogeneous, anisotropic units (horizontal to vertical anisotropy = 100:1). Each pathline marker indicates a travel time of 4,000 years.

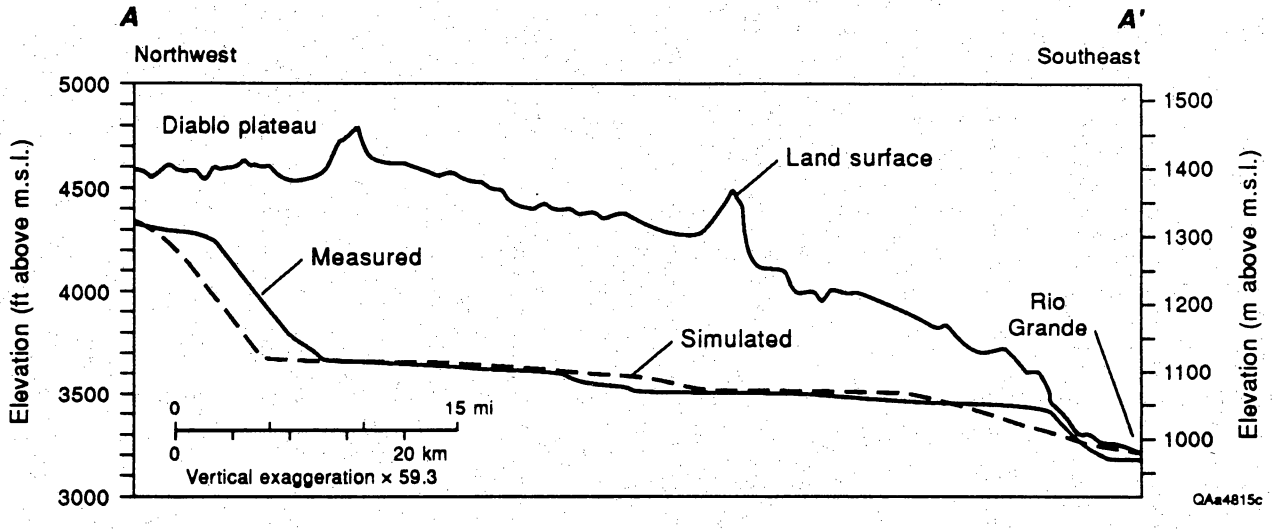

Figure 45. Comparison of measured and simulated potentiometric surface shown in cross section for model scenario 3. Simulated potentiometric surface obtained by using the simulated head value in the uppermost saturated cell in each column of the model.

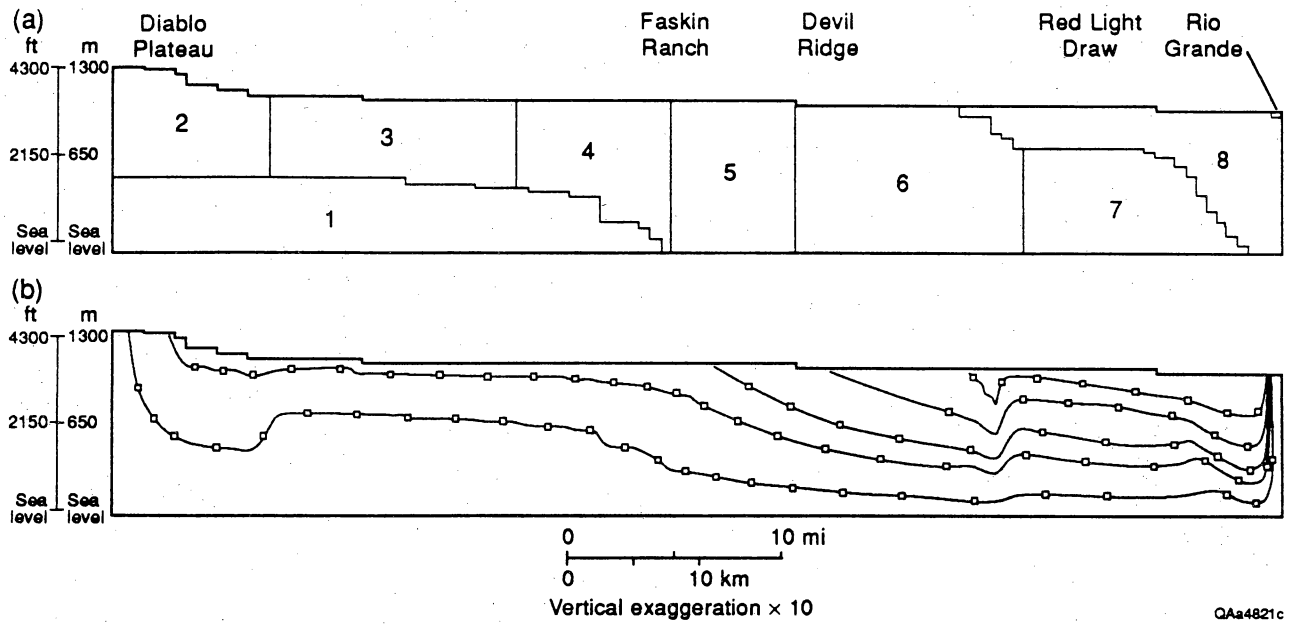

Figure 46. Particle-tracking simulations showing selected pathlines moving underneath Red Light Draw; model scenario 3; heterogeneous, isotropic units. Hydraulic conductivity was decreased one order of magnitude in zone 7 for this simulation. Each pathline marker indicates a travel time of 4,000 years.

hydraulic conductivities. These higher velocities are compared with ground-water ages inferred by ground-water isotopes. Horizontal and vertical hydraulic conductivities used in model scenario 1 were increased by one order of magnitude in the final simulation (table 8).

The recharge rate in the Diablo Plateau was increased to 1.231 inches/yr (3.127 cm/yr; or 10.26% mean annual precipitation) to provide the match between the simulated and measured hydraulic gradient (table 9 and fig. 47). A total travel time of 8,054 years is shown for particles tracked from the Diablo Plateau to the Rio Grande (table 10 and fig. 48). The simulated travel time between Faskin Ranch and the Rio Grande is 2,995 years. Ground-water in northwest Eagle Flat again moves laterally underneath the Red Light Draw bolson and discharge by vertical upwelling beneath the Rio Grande discharge boundary in the final model scenario.

Discussion and Model Limitations

Recharge rates to the Diablo Plateau in model scenarios 1, 2 and 3 vary between 0.66 and 1.02 percent mean annual precipitation (table 9) and are consistent with estimated recharge rates of between 0.5 and 3 percent of the available precipitation falling on mountain drainage areas in Trans-Pecos Texas (Kelly and Hearne, 1976; Orr and Risser, 1992). The recharge rate of 10.26 percent mean annual precipitation in model scenario 4 (table 8) is considerably higher than recharge rates estimated in other Trans-Pecos investigations. The higher recharge rate needed to match the measured and simulated hydraulic gradient is a direct consequence of higher hydraulic conductivity values specified in the model. The short residence times estimated in model scenario 4 are inconsistent with ground-water ages determined by ground-water isotopes. These results probably imply that hydraulic conductivities are too high in model scenario 4. True hydraulic conductivities and ground-water velocities are probably much closer to hydraulic conductivities specified in model scenarios 1 through 3.

Overall, the model results agree with the hydrochemical segregation hypothesis formulated earlier. These results are a simple consequence of the tendency of the flowpaths to refract and move downward when a zone of higher permeability is encountered as waters move from zone 6 to zone 7. This is a realistic scenario because extensive fracturing and jointing in thrust belts tend to

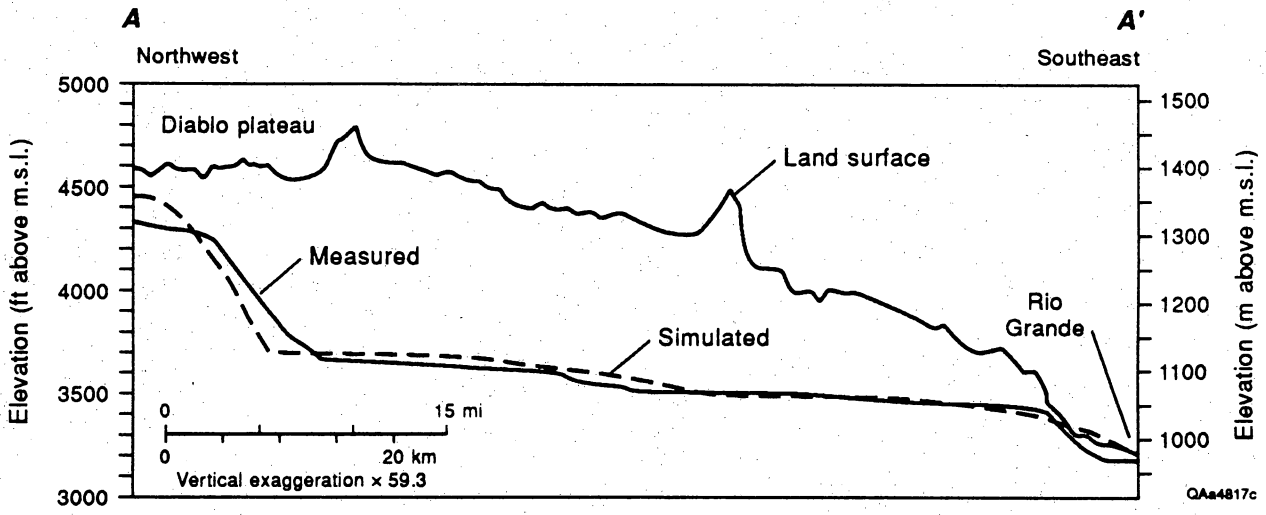

Figure 47. Comparison of measured and simulated potentiometric surface shown in cross section for model scenario 4. Simulated potentiometric surface obtained by using the simulated head value in the uppermost saturated cell in each column of the model.

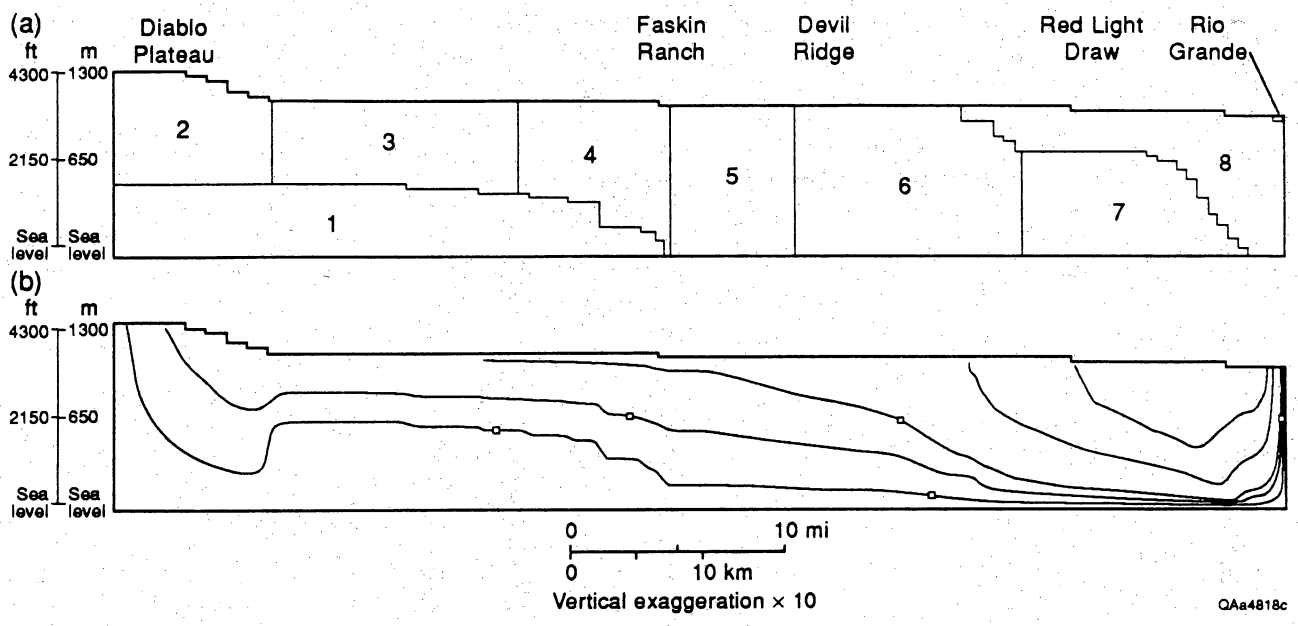

Figure 48. Particle-tracking simulations showing selected pathlines moving underneath Red Light Draw; model scenario 4; heterogeneous, isotropic units. Horizontal and vertical hydraulic conductivity was increased one order of magnitude in all zones for this simulation. Each pathline marker indicates a travel time of 4,000 years.

increase rock permeability. The geochemical data and model results provide reasonable evidence for segregation of waters.

A semiconfining layer of tuffs and pyroclastic flows that probably underlies sediment fills in Red Light Draw (Gates and White, 1976; Gates and others, 1980) was not simulated in the present version of the model. These types of rocks usually are low permeability, even when slightly-to-moderately fractured (e.g., 0.001 ft/day [0.0003 m/day]; Bedinger and others, 1986). Volcanic tuffs and pyroclastic flows usually have hydraulic conductivities that are lower than slightly-to-moderately fractured carbonate rocks (Bedinger and others, 1986). A low-permeability layer of tuffs and pyroclastic flows simulated between zones 7 and 8 would accentuate model results.

The paucity of data along the model profile limits the use of the model beyond that of an interpretive tool for estimating specific ground-water flowpaths and velocities. The model presents a simplified picture of the hydrostratigraphy of the area, as defined by major structural and geologic features such as the Red Hills and Devils Ridge thrust belt (zone 6). The simulated hydraulic gradient was fairly well matched with the measured hydraulic gradient in every model scenario, but the model's reliability is limited by the lack of information on vertical and horizontal hydraulic conductivity, effective porosity, and hydrostratigraphy. The limiting factors that are most pertinent to this modeling effort include the assumptions that

- fractured rock, at large scales, is equivalent to a porous medium
- ground-water flow is restricted to the plane of the profile model
- each of the zones has a constant vertical and horizontal hydraulic conductivity and effective porosity.

Of these, the most limiting is the last assumption. It is certain that rock units in any particular zone are laterally and vertically heterogeneous. These zones, in most cases were defined by the boundaries between rock and sediment types. Within Permian and Cretaceous rocks for example, a few aquifer tests along with structural attributes and transitions in the potentiometric surface were used to separate the water-bearing unit into zones. The simplistic definition of zones that have uniform hydrogeologic properties is required because

borehole and aquifer test data are unavailable at most depths simulated in the model.

CONCLUSIONS

This report presents the results of local hydrogeologic and hydrochemical investigations at Faskin Ranch and vicinity, and regional ground-water studies in a 1,200 mi^2 (3,110 km^2) area of southern Hudspeth County, Texas. Faskin Ranch is a proposed repository site for storage of low-level radioactive waste. The regional study area is bounded to the south and southwest by the Rio Grande and Quitman Mountains, to the east by the Van Horn and Carrizo Mountains, and to the north by the Diablo Plateau.

Aquifer tests results from five well tests in northwest Eagle Flat indicate a leaky confined aquifer with transmissivity values that vary from 2.4 to 68 ft^2/day (0.2 to 6.3 m^2/day). At Faskin Ranch transmissivity values are between 2.4 and 10.2 ft^2/day (0.2 to 0.95 m^2/day). Depths to water typically vary between 667 and 920 ft (203.5 and 280.5 m) in northwest Eagle Flat and between 667 and 751 ft (203.5 and 229 m) at Faskin Ranch. Ground water beneath Faskin Ranch is primarily Na-Cl to Na-SO_4-Cl in composition with total dissolved solids between 1500 to 4000 mg/L. The slightly to moderately saline ground-water moves to the northwest beneath Faskin Ranch at an estimated flow rate of about 1.6 ft/year (0.5 m/year), where it merges with ground water that flows along the southeasterly sloping regional hydraulic gradient.

In the regional flow system, recharge is limited to areas with exposures of bedrock, or where bedrock is covered by thin basin fill. Recharge waters have low total dissolved solids, ^{14}C signatures between 60 to 100 PMC, and tritium ranging from 1 to 8 TU. The most significant recharge zone is in the Streeruwitz, Bean, and Millican Hills, south of the Diablo Plateau escarpment. The Eagle Mountains constitute a second major area of recharge.

Southeast Eagle Flat is separated from ground-water in the northwest Eagle Flat area by a hydrologic divide approximately 6 miles (9.5 km) east of Grayton Lake. Ground-water in southeast Eagle Flat drains toward the south-southeast, mixing with other, more dilute water from the Eagle Mountains to the south and the Carrizo Mountains to the east. In northwest Eagle Flat, west of the Eagle Flat ground-water divide, regional ground-water flow paths are oriented along a ground-water trough, northwest-southeast from the Diablo Plateau,

across northwest Eagle Flat and Red Light Draw where ground water probably discharges in very small amounts to low-lying areas along the Rio Grande. Carbon 14 values less than 8 PMC and numerical modeling indicate that ground-water flow rates along this regional flow path are extremely low (e.g., 1 to 3 ft/yr).

Along the regional hydraulic gradient, slightly saline water flows southeast across northwest Eagle Flat and Red Light Draw, via circuitous routing along pathways controlled by stratigraphy and fractures adjacent to Devil Ridge. The slightly saline waters later disappear in the Red Light Draw bolson, probably as a result of either mixing with of dilute waters in the bolson, or by movement underneath the Red Light Draw bolson along northwest-striking bedrock formations. In the latter hypothesis, the slightly saline waters eventually discharge to the Rio Grande by vertical upwelling.

Higher salinities and elevated chloride/bromide ratios in lower Red Light Draw, a geochemical signature that could not develop by evaporation of bolson water in upgradient areas, support the second hypothesis. Numerical simulations in several model scenarios suggest that ground-water in northwest Eagle Flat moves underneath the Red Light Draw bolson and discharges by vertical upwelling near the Rio Grande, providing some support for hypothesis two. Ground-water travel times between Faskin Ranch and the Rio Grande estimated by numerical simulations vary between 19,134 years and 43,619 years in what are considered to be the most plausible model scenarios.

ACKNOWLEDGMENTS

This report was prepared for the Texas Low-Level Radioactive Waste Disposal Authority under Interagency Contract No. (92-93)-0910. The conclusions of the authors are neither approved nor endorsed by the Authority. Illustrations were drafted by Richard L. Dillon, Michele Bailey, William Bergquist, Randy Hitt, Susan Krepps, Joel Lardon, and Maria Saenz. Word processing was by Susan Lloyd, editing by Amanda R. Masterson, and layout by Margaret L. Evans. We also thank T. Warren, I. Jones, and R. Boghici for their technical assistance. Finally, we are grateful to the landowners of southern Hudspeth County for granting us access to their property.

REFERENCES

Albritton, C. C., Jr., and Smith, J. F., Jr., 1965, Geology of the Sierra Blanca area, Hudspeth County, Texas: U.S. Geological Survey Professional Paper 479, 131 p.

Alvarez, H. J., and Buckner, A. W., 1980, Ground-water development in the El Paso region with emphasis on the resources of the lower El Paso Valley, Texas: Texas Department of Water Resources, Report 246, 350 p.

Antevs, E., 1948, Climatic changes and pre-white man, *in* The Great Basin, with emphasis on glacial and post-glacial times: University of Utah Bulletin, v. 38, no. 20, p. 168–191.

Axelrod, D. I., and Baily, H. D., 1976, Tertiary vegetation, climate and altitude of the Rio Grande depression, New Mexico-Colorado: Paleobiology, v. 2, p. 235–254.

Banner, J. L., and Hanson, G. N., 1990, Calculation of simultaneous isotopic and trace element variations during water-rock interaction with applications to carbonate diagenesis: Geochimica et Cosmochimica Acta, v. 54, p. 3123–3137.

Bedinger, M. S., Langer, W. H., and Reed, J. E., 1986, Synthesis of hydraulic properties of rocks with reference to the basin and range province, southwestern United States, in Selected papers in the hydrologic sciences: U.S. Geological Survey Water-Supply Paper 2310, 142 p.

Bedinger, M. S., Sargent, K. A., and Langer, W. H., 1984, Studies of geology and hydrology in the Basin and Range Province, southwestern United States, for isolation of high-level radioactive waste: U.S. Geological Survey Open-File Report 84-739, 122 p.

Brace, W. F., 1980, Permeability of crystalline and argillaceous rocks: International Journal of Rock Mechanics and Mining Sciences and Geomechanics Abstracts, v. 17, no. 5, p. 241–251.

Bureau of Economic Geology, 1989, Collection, determination of unstable properties, and field treatment of water samples for isotopic and ionic analyses: Technical Program Manual, Specific Work Instruction 3.1, 13 p.

Chapman, J. B., 1986, Stable isotopes in southeastern New Mexico groundwater: implications for dating recharge in the WIPP area: New Mexico Environmental Evaluation Group, EEG-35, 76 p.

Chapman, J. B., Ingraham, N. L., and Hess, J. W., 1992, Isotopic investigation of infiltration and unsaturated zone flow processes at Carlsbad Cavern, New Mexico: Journal of Hydrology, v. 133, p. 343–363.

Collins, E. W., and Raney, J. A., 1993, Late Cenozoic faults of the region surrounding the Eagle Flat study area, northwestern Trans-Pecos Texas: The University of Texas at Austin, Bureau of Economic Geology final contract report, prepared for Texas Low-Level Radioactive Waste Disposal Authority under Interagency Contract IAC(92-93)-0910, 74 p.

Cooper, H. H., and Jacob, C. E., 1946, A generalized graphical method for evaluating formation constants and summarizing well field history: American Geophysical Union Transections, v. 27, p. 526–534.

Craig, H., 1961a, Isotopic variations in meteoric waters: Science, v. 133, p. 1701–1703.

Craig, H., 1961b, Standard for reporting concentrations of deuterium and oxygen-18 in natural waters: Science, v. 133, p. 1833–1834.

Dansgaard, W., 1964, Stable isotopes in precipitation: Tellus, v. 16, p. 436–469.

Davis, S. N., 1969, Porosity and permeability of natural materials, in DeWiest, R.J.M., ed., Flow through porous media: New York, Academic Press, p. 54–89.

DeFord, R. K., and Haenggi, W. T., 1970, Stratigraphic nomenclature of Cretaceous rocks in northeastern Chihuahua, *in* The geologic framework of the Chihuahua tectonic belt: West Texas Geological Society, p. 175–196.

Dorfman, M., and Kehle, R. O., 1974, Potential geothermal resources of Texas: The University of Texas at Austin, Bureau of Economic Geology Geological Circular 74-4, 33 p.

Duffield, G. M., and Rumbaugh, J. O., III, 1989, Geraghty & Miller's AQTESOLV Aquifer Test Solver, Version 1.00, 135 p.

Dutton, A. R., 1993, Sources and ages of ground water in unconfined and confined aquifers beneath the U.S. High Plains: The University of Texas at Austin, Bureau of Economic Geology Technical Rept., draft prepared for U.S. Geological Survey under award 14-08-0001-G-1885.

Dutton, A. R., and Simpkins, W. W., 1989, Isotopic evidence for paleohydrologic evolution of ground-water flow paths, southern Great Plains, U.S.A.: Geology, v. 17, no. 7, p. 653–656.

Elliot, R. D., 1949, Forecasting the weather—the weather types of North America: Weatherwise, v. 2, p. 15–18.

Evans, G. V., Otlet, R. L., Downing, R. A., Monkhouse, R. A., and Rae, G., 1979, Some problems in the interpretation of isotope measurements in United Kingdom aquifers, *in* Proceedings of the International Symposium of Isotope Hydrology, v. 2: International Atomic Energy Agency, p. 679–706.

Faure, G., 1986, Principles of isotope geology: New York, John Wiley & Sons, 589 p.

Fisher, R. S., and Mullican, W. F. III, 1990, Integration of ground-water and vadose-zone geochemistry to investigate hydrochemical evolution: a case study in arid lands of the northern Chihuahuan Desert, Trans-Pecos Texas: The University of Texas at Austin Bureau of Economic Geology Geological Circular 90-5, 36 p.

Fontes, J.-Ch., and Garnier, J.-M., 1979, Determination of the initial 14C activity of the total dissolved carbon: a review of existing models and a new approach: Water Resources Research, v. 15, no. 2, p. 399–413.

Freeman, C. E., 1972, Pollen study of some Holocene alluvial deposits in Dona Ana County, southern New Mexico: The Texas Journal of Science, v. 24, p. 203–220.

Freeze, R. A., and Cherry, J. A., 1979, Groundwater: Englewood Cliffs, NJ, Prentice-Hall, Inc., 604 p.

Frenzel and Kaehler, 1992, Geohydrology and simulation of ground-water flow in the Mesilla Basin, Dona Ana County, New Mexico, and El Paso County, Texas: U.S. Geological Survey Professional Paper 1407-C, 105 p.

Gates, J. S., and White, D. E., 1976, Test drilling for ground water in Hudspeth, Culberson and Presidio Counties in westernmost Texas : U.S. Geological Survey Open-File Report 76-338, 76 p.

Gates, J. S., White, D. E., Stanley, W. D., and Ackermann, H. D., 1980, Availability of fresh and slightly saline ground water in the basins of westernmost Texas : Texas Department of Water Resources Report 256, 108 p.

Geyh, M. A., 1990, Absolute age determination—physical and chemical dating methods and their application: New York, Springer, 503 p.

Gile, L. H., Hawley, J. W., and Grossman, R. B., 1981, Soils and geomorphology in the Basin and Range area of Southern New Mexico—Guidebook to the Desert Project: New Mexico Bureau of Mines and Mineral Resources, Memoir 39, 222 p.

Gonfiantini, R., Dincer, T., and Derekoy, A. M., 1974, Environmental isotope hydrology in the Hodna region, Algeria, *in* Isotope techniques in groundwater hydrology 1974: International Atomic Energy Agency, v. 1, p. 293–316.

Groat, C. G., 1972, Presidio Bolson, Trans-Pecos Texas and adjacent Mexico, geology of a desert basin aquifer system: The University of Texas at Austin, Bureau of Economic Geology Report of Investigations No. 76, 46 p.

Gustavson, T. C., 1991, Arid basin depositional systems and paleosols: Fort Hancock and Camp Rice Formations (Pliocene-Pleistocene), Hueco Bolson, west Texas and adjacent Mexico: The University of Texas at Austin, Bureau of Economic Geology Report of Investigations No. 198, 49 p.

Hall, S. A., 1977, Late Quaternary sedimentation and paleoecological history of Chaco Canyon, New Mexico: Geological Society of America Bulletin, v. 88, p. 1593–1618.

Hall, S. A., 1985, Quaternary pollen analysis and vegetational history of the southwest, *in* Pollen records of Lake-Quaternary North America: Bryant, V.M., Jr., and Holloway, R.G., eds., Dallas, Texas, American Association of Stratigraphic Palynologists, p. 95–123.

Hantush, M. S., and Jacob, C. E., 1955, Non-steady radial flow in an infinite leaky aquifer: American Geophysical Union Transactions, v.36, p. 95–100.

Hantush, M. S., 1960, Modification of the theory of leaky aquifers: Journal of Geophysical Research, v. 65, no. 11, p. 3713–3725.

Hearne, G. A., and Dewey, J. D., 1988, Hydrologic analysis of the Rio Grande basin north of Embudo, New Mexico, Colorado and New Mexico: U.S. Geological Survey Water-Resources Investigations Report 86-4113, 244 p.

Hem, J. D., 1985, Study and interpretation of the chemical characteristics of natural water: U.S. Geological Survey Water-Supply Paper 2254, 263 p.

Henry, C. D., 1979, Geologic setting and geochemistry of thermal water and geothermal assessment, Trans-Pecos Texas: The University of Texas at Austin, Bureau of Economic Geology Report of Investigations No. 96, 48 p.

Henry, C. D., Price, J. G., and Hutchins, M. F., 1983, Mineral resources areas of the Basin and Range Province of Texas : U.S. Geological Survey Open-File Report 83-709, 7 p.

Hill, M. C., 1990, Preconditioned conjugate-gradient 2 (PCG2), a computer program for solving ground-water flow equations: U.S. Geological Survey Water-Resources Investigations Report 87-4091, 34 p.

Hoffer, J. M., 1978, Thermal water occurrences in Trans-Pecos Texas: The Texas Journal of Science, v. 30, no. 4, p. 309–319.

Holser, W. T., 1979, Trace elements and isotopes in evaporites, *in* Marine Minerals: Mineral Society of America, p. 295–346.

Horowitz, A., Gerald, R. E., and Chaiffetz, M. S., 1981, Preliminary paleoenvironmental implications of pollen analyzed from Archaid, Formative and Historic sites near El Paso, Texas: The Texas Journal of Science, v. 33, no. 1, p. 61–72.

Hoy, R. N., and Gross, G. W., 1982, A baseline study of oxygen-18 and deuterium in the Roswell, New Mexico groundwater basin: New Mexico Water Resources Research Institute Report 44, 95 p.

Jackson, M. L. W., Langford, R. P., and Whitlaw, M., 1993, Quaternary history, basin-fill stratigraphy, and paleomagnetics, fissures, and pseudofissures of the Eagle Flat study area: The University of Texas at Austin, Bureau of Economic Geology final contract report prepared for Texas Low-Level Radioactive Waste Disposal Authority under Interagency Contract IAC(92-93)-0910.

Jones, B. R., and Reaser, D. F., 1970, Geology of southern Quitman Mountains, Hudspeth County, Texas: The University of Texas at Austin, Bureau of Economic Geology Geologic Quadrangle Map No. 39, scale 1:48,000, 24-p. text.

Kelly, T. E., and Hearne, G. A., 1976, The effects of ground-water development on the water supply in the Post Headquarters area, White Sands Missile Range, New Mexico: U.S. Geological Survey Open-File Report 76-277, 97 p.

Kernodle, J. M., 1992, Summary of U.S. Geological Survey ground-water flow models of basin-fill aquifers in the southwestern alluvial basins region, Colorado, New Mexico, and Texas: U.S. Geological Survey Open-File Report 90-361, 81 p.

King, P. B., and Flawn, P. T., 1953, Geology and mineral deposits of Precambrian rocks of the Van Horn area, Texas: The University of Texas at Austin, Bureau of Economic Geology Publication 5301, 218 p.

Kreitler, C. W., Mullican, W. F., III, and Nativ, R., 1990, Hydrogeology of the Diablo Plateau, Trans-Pecos Texas, *in* Kreitler, C. W., and Sharp, J. M., Jr., eds., The University of Texas at Austin, Bureau of Economic Geology Guidebook 25, p. 49-58.

Kreitler, C. W., Raney, J. A., Nativ, R., Collins, E. W., Mullican, W. F., III, Gustavson, T. C., and Henry, C. D., 1986, Preliminary geologic and hydrologic studies of selected areas in Culberson and Hudspeth counties, Texas, final report for the Texas Low-Level Radioactive Waste Disposal Authority under contract no. IAC(86-87)0818, 184 p.

Kruseman, G. P., and De Ridder, N. A., 1979, Analysis and evaluation of pumping test data: Bulletin 11, International institute for Land Reclamation and Improvements, Wageningen, Netherlands, 200 p.

Lambert, S. J., 1987, Feasibility study: applicability of geochronologic methods involving radiocarbon and other nuclides to the groundwater hydrology of the Rustler Formation, southeastern New Mexico: Sandia National Laboratories, 72 p.

Lambert, S. J., and Harvey, D. M., 1987, Stable-isotope geochemistry of groundwaters in the Delaware Basin of southeastern New Mexico: Sandia National Laboratories, Albuquerque, New Mexico, prepared for U.S. Department of Energy under contract DE-ACO4-76DP00789, 218 p.

Langford, R. P., 1993, Landscape evolution of Eagle Flat and Red Light basins, Chihuahuan Desert, South-Central Trans-Pecos Texas: The University of Texas at Austin, Bureau of Economic Geology contract report, prepared for Texas Low-Level Radioactive Waste Disposal Authority under Interagency Contract IAC(92-93)-0910.

Larkin, T. J., and Bomar, G.W., 1983, Climatic atlas of Texas : Texas Dept. of Water Resources Publication LP-192, 151 p.

Lohman, S. W., 1972, Ground-water hydraulics: U.S. Geological Survey Professional Paper 708, 80 p.

Mann, W. B., Unterweger, M. P., and Coursey, B. M., Comments on the NBS tritiated-water standards and their use: International Journal of Applied Radiation Isotopes, v. 33, p. 383–386.

Markgraf, V., Bradbury, J. P., Forrester, R. M., Singh, G., and Sternberg, R. S., 1984, San Augustin Plains, New Mexico: age and environmental potential reassessed: Quaternary Research, v. 22, p. 336–343.

Mazor, E., 1991, Applied chemical and isotopic groundwater hydrology: Halsted Press, 274 p.

Mazor, E., Drever, J. I., Finley, J., Huntoon, P. W., and Lundy, D. A., 1993, Hydrochemical implications of groundwater mixing: an example from the southern Laramie Basin, Wyoming: Water Resources Research, v. 29, no. 1, p. 193–205.

McDonald, M. G., and Harbaugh, A. W., 1988, A modular three-dimensional finite difference ground-water flow model: U.S. Geological Survey Techniques of Water-Resources Investigations, Book 6, Chapter A1, 586 p.

McDonald, M. G., Harbaugh, A. W., Orr, B. R., and Ackerman, D. J., 1991, A method of converting no-flow cells to variable-head cells for the U.S. Geological Survey modular finite-difference ground-water flow model: U.S. Geological Survey Open-File Report 91-536, 99 p.

Mook, W. G., 1980, Carbon-14 in hydrogeological studies, *in* Fritz, P. and Fontes: Elsevier, J.Ch., eds., Handbook of environmental isotope geochemistry: v. 1, p. 49–74.

Motts, W. S., 1965, Hydrologic types of playas and closed valleys and some relations of hydrology to playa geology, *in* Geology, mineralogy, and hydrology of U.S. playas, ed. J. T. Neal: Air Force Cambridge Research Laboratory, Environmental Research Paper 96, p. 73–104.

Muller, A. B., and Mayo, A. L., 1986, ^{13}C variation in limestone on an aquifer-wide scale and its effects on groundwater ^{14}C dating models: Radiocarbon, v. 28, no. 3, p. 1041–1054.

Mullican, W. F. III, and Senger, R. K., 1992, Hydrogeologic investigations of deep ground-water flow in the Chihuahuan Desert, Texas: The University of Texas at Austin, Bureau of Economic Geology, Report of Investigations No. 205, 60 p.

Musgrove, M., 1993, Origin, evolution, and mixing of saline and dilute groundwaters in three regional flow systems, midcontinent, U.S.A.: The University of Texas at Austin, Master's thesis, 225 p.

Nativ, R., and Gutierrez, R. N., 1988, Hydrogeology and hydrochemistry of Cretaceous aquifers, Texas panhandle and eastern New Mexico: The University of Texas at Austin, Bureau of Economic Geology Geological Circular 88-3, 32 p.

Nativ, R., and Riggio, R., 1990, Precipitation the southern High Plains: Meteorologic and Isotopic Features: Journal Geophysical Research, v. 95, D13, p. 22,559–22,564.

Orr, B. R., and Risser, D. W., 1992, Geohydrology and potential effects of development of freshwater resources in the northern part of the Hueco Bolson, Dona Ana and Otero Counties, New Mexico, and El Paso County, Texas: U.S. Geological Survey Water Resources Investigations Report 91-4082, 92 p.

Payne, B. R., and Yurtsever, Y., 1974, Environmental isotopes as a hydrogeological tool in Nicaragua, in Isotopes in groundwater hydrology 1974: International Atomic Energy Agency, v. 1, p. 193–202.

Plummer, L. N., Prestemon, E. C., and Parkhurst, D. L., 1991, An interactive code (NETPATH) for modeling net geochemical reactions along a flow path: U.S. Geol. Survey Water-Resources Investigations Report 91-4078, 227 p.

Pollock, D. W., 1989a, Documentation of computer programs to compute and display pathlines using results from the U.S. Geological Survey modular three-dimensional finite-difference ground-water flow model: U.S. Geological Survey Open-File Report 89-381, various pagination.

Pollock, D. W., 1989b, A graphical kernel system (GKS) version of computer program MODPATH-PLOT for displaying path lines generated from the U.S. Geological Survey three-dimensional ground-water flow model: U.S. Geological Survey Open-File Report 89-622, 49 p.

Raney, J. A., and Collins, E., 1993, Regional geologic setting of the Eagle Flat study area, Hudspeth County, Texas: The University of Texas at Austin, Bureau of Economic Geology contract report, prepared for Texas Low-Level Radioactive Waste Disposal Authority under Interagency Contract IAC(92-93)-0910, 53 p.

Richardson, G. B., 1904, Report of a reconnaissance in Trans-Pecos Texas north of the Texas and Pacific Railway: The University of Texas Mineral Survey, 119 p.

Sami, K., 1992, Recharge mechanisms and geochemical processes in a semi-arid sedimentary basin, Eastern Cape, South Africa: Journal of Hydrology, v. 139, p. 27–48.

Scanlon, B. R., Wang, F. P., and Richter, B. C., 1991, Field studies and numerical modeling of unsaturated flow in the Chihuahuan Desert, Texas: The University of Texas at Austin, Bureau of Economic Geology Report of Investigations No. 199, 56 p.

Schoch-Fischer, H., Rozanki, K., Jacob, H. J., Sonntag, C., Jouzel, I., Oustlund, G., and Geyh, M. A., 1983, Hydrometerological factors controlling the time variation of D, ^{18}O and ^{3}H in atmospheric water vapor and precipitation in the northern westwind belt, *in* Isotope Hydrology 1983: International Atomic Energy Agency, p. 3–30.

Siegenthaler, U., and Oeschger, H., 1980, Correlation of ^{18}O in precipitation with temperature and altitude: Nature, p. 314–317.

Sofer, Z., and Gat, J. R., 1972, Activities and concentrations of oxygen-18 in concentrated aqueous salt solutions: analytical and geophysical implications: Earth and Planetary Science Letters, v. 15, p. 232–238.

Sonntag, C., Klitzsch, E., Lohnert, E. P., Ee-Shazly, E. M., Munich, K. O., Junghans, Ch., Thorweihe, U., Weistroffer, K., and Swailem, F. M., 1979, Paleoclimatic information from deuterium and oxygen-18 in carbon-14 dated north Saharan groundwaters, *in* Isotope hydrology 1978: International Atomic Energy Agency, v. 2, p. 569–581.

Taylor, C. B., and Roether, W., 1982, A uniform scale for reporting low-level tritium measurements in water: International Journal of Applied Radiation Isotopes, v. 33, p. 377–382.

Theis, C. V., 1935, The relation between the lowering of the piezometric surface and the rate and duration of discharge of a well using groundwater storage: American Geophysical Union Transactions, v. 16, p. 519–524.

Todd, D. K., 1980, Groundwater hydrology: New York, John Wiley and Sons, 535 p.

Toth, J., 1963, A theoretical analysis of groundwater flow in small drainage basins: Journal of Geophysical Research, v. 67, p. 4795–4812.

Underwood, J. R., Jr., 1962, Geology of the Eagle Mountains and vicinity, Trans-Pecos, Texas: The University of Texas at Austin, Ph.D. dissertation, 560 p.

Van Devender, T. R., and Spaulding, W. G., 1979, Development of vegetation and climate in the southwestern United States: Science, v. 204, p. 701–710.

Walton, W. C., 1962, Selected analytical methods for well and aquifer evaluation: Illinois State Water Survey Bulletin 49, 81 p.

Water Analysis Handbook, 1989: Loveland, Colorado, Hach Company, 691 p.

Wells, S. G., Bullard, T. F., and Smith, L. N., 1982, Origin and evolution of deserts in the Basin and Range and Colorado Plateau Provinces of western North America, *in* The geological story of the world's deserts: Stria, v. 17, p. 101–111.

White, D. E., Gates, J. S., Smith, J. T., and Fry, B. J., 1980, Ground-water data for the Salt Basin, Eagle Flat, Red Light Draw, Green River Valley, and Presidio Bolson in westernmost Texas: Texas Department of Water Resources Report 259, 97 p.

Wolff, R. C., 1982, Physical properties of rocks—porosity, permeability, distribution coefficients, and dispersivity: U.S. Geological Survey Open-File Report 82-166, 118 p.

Wood, W. W., 1976, Guidelines for collection and field analysis of ground-water samples for selected unstable constituents: U.S. Geological Survey Water-Resources Investigations, Chapter D2, 24 p.